

MAGNETIC RESONANCE IMAGING ASSESSMENT OF
TUMOR MICROVESSELS AND RESPONSE TO
ANTIANGIOGENESIS THERAPY

ANDA PREDA

Lay-out: Dirk Verver
Cover: Karin ten Wolde

Printed by Ridderprint B.V. Ridderkerk

MAGNETIC RESONANCE IMAGING ASSESSMENT OF
TUMOR MICROVESSELS AND RESPONSE TO
ANTIANGIOGENESIS THERAPY

EVALUATIE VAN TUMOR MICROBLOEDVATEN EN DE REACTIE
OP ANTI-ANGIOGENESE BEHANDELING MET BEHULP VAN
KERNSPINTOMOGRAFIE

PROEFSCHRIFT

TER VERKRIJGING VAN DE GRAAD VAN DOCTOR AAN DE
ERASMUS UNIVERSITEIT ROTTERDAM
OP GEZAG VAN DE
RECTOR MAGNIFICUS

PROF.DR. S.W.J. LAMBERTS

EN VOLGENS BESLUIT VAN HET COLLEGE VOOR PROMOTIES

DE OPENBARE VERDEDIGING ZAL PLAATSVINDEN OP
VRIJDAG 2 SEPTEMBER 2005 OM 16.00 UUR
DOOR

ANDA PREDA

GEBOREN TE BOEKAREST - ROEMENIË

Promotiecommissie

Promotoren: Prof. dr. G.P. Krestin
Prof. dr. R.C. Brasch

Overige leden: Prof. dr. A.M.M. Eggermont
Prof. dr. J.O. Barentsz
Prof. dr. J.W. Oosterhuis

Copromotor: Dr. C.F. van Dijke

Financial support by department of Radiology, Erasmus MC-University Medical Center Rotterdam, the “Drie Lichten” and the “Johannes Vermeij” Foundations, The Netherlands, for the publication of this thesis is gratefully acknowledged.

To the memory of my father
To mama, Ruud and Alexandru

CONTENTS

Chapter 1	Introduction	11
Chapter 2	MR macromolecular contrast agents for monitoring tumor angiogenesis and angiogenesis inhibition	23
Chapter 3	The choice of region of interest measures in contrast-enhanced MRI characterization of experimental breast tumors	39
Chapter 4	Assessment of a rapid clearance blood pool MR contrast medium (P792) for assays of microvascular characteristics in experimental breast tumors with correlations to histopathology	51
Chapter 5	MR characterization of tumor microvessels in experimental breast tumors using a slow clearance blood pool contrast agent (carboxymethyldextran-A2-Gd-DOTA) with histopathologic correlation	67
Chapter 6	Tumor microvascular characterization using ultrasmall superparamagnetic iron oxide particles (USPIO) in an experimental breast cancer model	83
Chapter 7	MRI monitoring of tumor response following angiogenesis inhibition in an experimental human breast cancer model	101
Chapter 8	Tumor microvascular changes in antiangiogenic treatment: assessment by magnetic resonance contrast media of different molecular weights	117
Chapter 9	MRI monitoring of Avastin™ antiangiogenesis therapy using B22956/1, a new blood pool contrast agent, in an experimental model of human cancer	133
Chapter 10	Dynamic contrast-enhanced MRI using macromolecular contrast media for monitoring the response to isolated limb perfusion in experimental soft-tissue sarcomas	153
Chapter 11	Summary and conclusions	167
	Samenvatting en conclusies	171
Curriculum Vitae		175
Publications		177
Acknowledgements		179

CHAPTER 1

INTRODUCTION

General introduction

Magnetic resonance imaging (MRI) is a diagnostic modality with high inherent contrast resolution and multiplanar imaging capability. Advances in MR technology and image processing have increased the utility and availability of this technique in the past two decades. MRI has become one of the leading modalities in current diagnostic imaging, combining soft tissue contrast with high anatomic and temporal resolution. MRI is now a widely employed diagnostic method for the clinical evaluation of tumors.

One of the most recent applications of MRI is the investigation of angiogenesis using dynamic contrast-enhanced magnetic resonance imaging (DCE-MRI). DCE-MRI represents the acquisition of serial MR images before, during, and after the administration of an intravenous contrast agent. The use of contrast enhancement in conjunction with magnetic resonance imaging provides a means to evaluate tissue function, as well as morphology. Tissue blood volume, blood flow, perfusion and capillary permeability represent indicators of the status of the vasculature that can be investigated with DCE-MRI. Use of such quantitation potentially allows tumors to be characterized in terms of pathophysiology and to be monitored over time, during the course of therapeutic interventions. The understanding of the angiogenesis process and the evaluation of new drugs that inhibit or stimulate angiogenesis are directly related to the development of an imaging assay of angiogenic activity. This method should provide functionally relevant and quantitative images, should be high in spatial resolution, should sample the entire tumor and could be repeated at frequent intervals.

DCE-MRI has grown in importance with the development of antiangiogenic and neoadjuvant strategies for tumor therapy. Dedicated software makes it possible to interpret imaging pharmacokinetics and aid the assessment of physiological parameters such as capillary permeability and tissue perfusion. For instance, the permeability of functional tumor microvessels can be assessed noninvasively by dynamic MRI of contrast agent uptake in the tumor tissue (1-4). The analysis of contrast kinetics can be applied to differentiate between a malignant and a benign lesion and to determine whether a tumor is responding to treatment (5). It has been demonstrated that the permeability of blood vessels correlates with the ability of the tumor to metastasize, and with its response to treatment (6, 7). Thus, information concerning the status of vascular permeability might help assessing the metastatic potential of tumors and predict the sensitivity to chemotherapy or to antiangiogenic treatment.

MRI enhanced with low molecular contrast media has been used to estimate permeability and perfusion (8-11). However, the standard low molecular contrast agents for MR imaging, such as gadopentetate dimeglumine, extravasate nonselectively to the interstitium of nearly any extracerebral organ (12, 13). High transendothelial permeability of small molecular contrast media has been observed in both normal and tumor microvessels; thus, reliable differentiation of normal and diseased tissue may be problematic (4, 14). In order to assess tissue permeability and perfusion, the search for contrast agents with prolonged vascular residence time has been extensive (15). Macromolecular contrast media (MMCM) represent a new class of diagnostic drugs that can be applied with dynamic MRI to obtain physiologic

and morphologic information on tissue properties. MMCM distribute predominantly in the blood volume of the healthy tissues (16-18). In addition, they extravasate in conditions with pathologically increased microvascular permeability and thus may be helpful in evaluation of neoplasia, inflammation and ischemia (15, 19-22). MMCM may also be more specific for distinguishing benign from malignant tumor tissue, since they extravasate across the discontinuous capillaries of malignant tumors, but not, or to a substantial lower extent, across the intact endothelium of benign lesions (4).

Purpose and outline of this thesis

The purpose of this thesis was to evaluate the role of dynamic MRI enhanced with MMCM for the assessment of the tumor microvessels and for the monitoring of response to therapy with various antiangiogenesis drugs. In the first part, several new developed MMCM have been investigated with respect to the potential for differentiation of benign from malignant tumors, or for tumor grading. The capability of DCE-MRI enhanced with MMCM for defining changes in the microvascular characteristics as a result of antiangiogenesis therapy and for monitoring the effect of treatment was evaluated in the second part of this thesis.

Several macromolecular contrast agents with molecular weight between 10 kDa and 100 kDa are under development and have been tested experimentally, some clinically, over the past years. Several macromolecular contrast media are at the moment in clinical trials or in the registration process. **Chapter 2** gives an overview of the potential applications and limitations of various MMCM for the evaluation of tumor microvessels.

DCE-MRI has become an increasingly used method for evaluation of tumors. The choice of the area (region of interest-ROI) to be analyzed within the tumor margins may have a substantial influence on accuracy of MRI predictors on tumor status. At present, there is no standardized method for ROI assignment in DCE-MRI. The goal of the study described in **chapter 3** was to analyze whether the choice of ROI in which contrast kinetics are determined with DCE-MRI has an effect on the outcome of the kinetic analysis. For this purpose we analyzed MRI microvascular characteristics obtained from the kinetic analysis of DCE-MRI image data from the whole tumor and compared it with microvascular characteristics derived from data obtained from the tumor periphery. The study was based on a meta-analysis of 98 quantitative MRI breast tumor characterizations, acquired in three separate experimental studies using identical methods for tumor induction and contrast enhancement. The specific MRI-derived measures for comparison to histologic grade were the tumor fractional plasma volume and the endothelial transfer coefficient K^{PS} , reflecting the endothelial leakiness of the tumor vessels.

Currently, a major research goal is to identify one or more MMCM that can safely be used clinically for tumor characterization and monitoring treatment response. Albumin-(Gd-DTPA)₃₀ is a prototype MMCM that has been used successfully to quantitatively define the characteristics of tumor microvessels in experimental studies (3, 4, 21-26). However, albumin-(Gd-DTPA)₃₀ is considered an unlikely candidate for human use due to its potential

immunogenic properties and its prolonged partial retention in the body (27, 28). New MMCM candidates must be examined for their potential as MRI probes for assaying tumor microvessels. Three novel contrast agents (P792, carboxymethyl-dextran-A2-Gd-DOTA and SHU555C) were tested to define their ability to noninvasively characterize tumor microvessels and to differentiate between a malignant and a benign lesion. In **chapter 4**, a new rapid clearance blood pool contrast medium, P792, was compared to albumin-(Gd-DTPA)₃₀ in chemically induced rat breast tumors, based on quantitative estimates of microvascular permeability and fractional plasma volume of tumor tissue using a two-compartment model. The MR-derived estimates of microvascular characteristics using each contrast agent were correlated to the histologic tumor grade and microvascular density counts.

Chapter 5 describes a study designed to analyze the role of carboxymethyl-dextran-A2-Gd-DOTA, a slow clearance blood pool contrast agent, for characterization and differentiation of the microvessels of malignant and benign breast tumors. DCE-MRI was undertaken in rats with a chemically induced mammary tumor. The endothelial transfer coefficient K^{ps} and fractional plasma volume of the breast tumors were estimated from the DCE-MRI data, using a two-compartment model of tumor tissue. The MRI microvascular characteristics were correlated with the histopathologic tumor grade.

Recently, the capability of ultrasmall superparamagnetic iron oxide particles (USPIO) to characterize tumor microvessels has been demonstrated in an experimental study performed in a rodent breast cancer model (24). However, one limitation of the study was the minimal enhancement of the tumors after intravenous administration of contrast medium, probably due to a low-dose USPIO (1 mg Fe/kg). For this reason, the objective of the study described in **chapter 6** was to investigate if the use of a different USPIO with a higher dose (5 mg of Fe/kg) in the same tumor model could improve the tumor enhancement. Additionally possible dose dependencies of USPIO for characterization of tumor microvessels were assessed. The values of the transendothelial permeability and fractional plasma volume of the tumors derived from kinetic analysis of dynamic MRI data were compared to albumin-(Gd-DTPA)₃₀, a prototype macromolecular contrast medium standard and correlated with tumor histopathology and microvascular density counts.

In the second part of this thesis, the ability of DCE-MRI used in combination with MMCM to monitor changes in the tumor microvasculature following therapeutic interventions with antiangiogenic drugs was investigated. The aim of the study described in **chapter 7** was to evaluate the potential of dynamic MRI enhanced by macromolecular contrast agents to monitor noninvasively the therapeutic effect of an antiangiogenesis VEGF receptor kinase inhibitor in an experimental human breast cancer model. Dynamic MRI was performed at baseline using albumin-(Gd-DTPA)₃₀ and ultrasmall superparamagnetic iron oxide particles (USPIO). Subjects were treated for 1 week either with PTK787/ZK222584, a VEGF receptor tyrosine kinase inhibitor or with saline, followed by repeat MRI examinations serially using each contrast agent. Tumor microvessel characteristics including fractional plasma volume and transendothelial permeability were estimated for each contrast medium employing a kinetic model comprising the plasma and interstitial water compartments. Tumor growth and the microvascular density, a histologic surrogate of angiogenesis, were also measured.

Chapter 8 presents a study conducted with the purpose of testing several MR contrast media of different molecular weights for their potential to noninvasively characterize microvascular changes in an experimental treatment model. The study was performed in a human breast cancer xenograft, implanted in athymic rats. The animals were assigned randomly to a control (saline) or drug treatment group (anti-VEGF antibody). In both groups, DCE-MRI was performed in each animal using six different contrast media on sequential days at baseline and follow-up examination. The molecular weights of the used contrast media ranged from 557 Da to 92 kDa. Using a bidirectional kinetic model, tumor microvascular characteristics, including fractional plasma volume and transendothelial permeability, were estimated for each contrast medium. These microvascular characteristics were compared between drug and control groups and between contrast media of different molecular weights.

Chapter 9 investigates the diagnostic and prognostic potential of a novel protein-binding MR contrast medium, B22956/1, for quantitative characterization of tumor microvessels by DCE-MRI and for monitoring the tumor response to antiangiogenic therapy with Avastin™, a humanized anti-vascular endothelial growth factor antibody (anti-VEGF). DCE-MRI was performed in an experimental human breast cancer model, using B22956/1, a low molecular contrast agent (ProHance™), and a prototype macromolecular contrast medium, albumin-(Gd-DTPA). The animals, assigned randomly to a control (saline) or drug-treated group (Avastin™), were imaged at baseline and after nine days of treatment. The transendothelial permeability and the fractional blood volume of the tumors were estimated from the kinetic analysis of the dynamic MR data using a two-compartment tissue model. Tumor growth was also measured from volumetric MRI.

During the antitumor therapy with a combination of a cytostatic drug like melphalan and tumor necrosis factor alpha (TNF- α , a cytokine with established antitumor properties), a synergistic effect on tumor activity can be obtained. An immediate TNF- α mediated tumor-selective enhanced uptake of the cytostatic agent (29, 30), dependent of the vascularity of the tumor (31) is followed by a tumor-selective eradication of tumor-associated vasculature (32). TNF- α cannot be used systemically in doses high enough to obtain tumor response. However, in isolated limb perfusion (ILP), tumors can be exposed to local drug concentrations up to 15-20 times higher than those reached after systemic administration without major side effects (33). In **chapter 10**, the method of DCE-MRI was applied for assessment of treatment response in isolated limb perfusion with TNF- α and melphalan. DCE-MRI was performed in an experimental cancer model of soft-tissue sarcoma implanted in rats, using a macromolecular contrast medium, albumin-(Gd-DTPA)₄₅. The subjects were randomly assigned to a control (Haemaccel) or drug-treated group (TNF- α /melphalan). DCE-MRI was performed at baseline and 24 hours after isolated limb perfusion. The transendothelial permeability and the fractional plasma volume of the tumor tissue were estimated from the kinetic analysis of MR data using a two-compartment model.

A summary of this thesis and the general conclusions are presented in **chapter 11**.

References

1. Demsar F, Roberts TPL, Schwickert HC, et al. A MRI spatial mapping technique for microvascular permeability and tissue blood volume based on macromolecular contrast agent distribution. *Magn Reson Med* 1997;37:236-242
2. Roberts HC, Saeed M, Roberts TPL, et al. Comparison of albumin-(Gd-DTPA)₃₀ and Gd-DTPA-24-cascade-polymer for measurements of normal and abnormal microvascular permeability. *J Magn Reson Imaging* 1997;7:331-338
3. Su MY, Muhler A, Lao X, Nalcioğlu O. Tumor characterization with dynamic contrast enhanced MRI using MR contrast agents of various molecular weights. *Magn Reson Med* 1998;39:259-269
4. Daldrup H, Shames DM, Wendland M, et al. Correlation of dynamic contrast-enhanced MR imaging with histologic tumor grade: comparison of macromolecular and small-molecular contrast media. *Am J Roentgenol* 1998; 171:941-949
5. Padhani A, Husband JE. Dynamic contrast-enhanced MRI studies in oncology with emphasis on quantification, validation and human studies. *Clin Radiol* 2001; 56:607-620
6. Jain RK. Transport of molecules across tumor vasculature. *Cancer Metast Rev* 1987;6:559-593
7. Dvorak HF. Leaky tumor vessels: consequences for tumor stroma generation and for solid tumor therapy. In: Ragaz J, editor. *Effects of therapy on biology and kinetics of the residual tumor, part A: pre-clinical aspects*. New-York: Wiley-Liss; 1990. P.317-330
8. Barentsz JO, Engelbrecht M, Jager GJ, et al. Fast dynamic gadolinium-enhanced MR imaging of urinary bladder and prostate cancer. *J Magn Reson Imaging* 1999; 10:295-304
9. Port RE, Knopp MV, Hoffmann U, Milker-Zabel S, Brix G. Multicompartment analysis of gadolinium chelate kinetics: blood-tissue exchange in mammary tumors as monitored by dynamic MR imaging. *J Magn Reson Imaging* 1999; 10:233-241
10. Padhani AR, Gapinski CJ, Macvicar DA, et al. Dynamic contrast-enhanced MRI of prostate cancer: correlation with morphology and tumour stage, histological grade and PSA. *Clin Radiol* 2000; 55:99-109
11. Wasser K, Klein SK, Fink C, et al. Evaluation of neoadjuvant chemotherapeutic response of breast cancer using dynamic MRI with high temporal resolution. *Eur Radiol* 2003; 13:80-87
12. Weinmann H, Brasch R, Press W, Wesbey G. Characteristics of gadolinium-DTPA complex: a potential new NMR contrast agent. *AJR* 1984;142:619-624
13. Weinmann H, Laniado M, Mutzel W. Pharmacokinetics of Gd-DTPA/dimeglumine after intravenous injection in healthy volunteers. *Physiol Chem Phys Med NMR* 1984; 16:167-172
14. Helbich T, Roberts T, Gossmann A, et al. Quantitative gadopentetate-enhanced MR imaging of breast tumors: testing of different analytical methods. *Magn Res Med* 2000; 44:915-924
15. Brasch RC. New directions in the development of MR imaging contrast media. *Radiology* 1992;183:1-11
16. Schmiedl U, Ogan M, Moseley M, et al. Comparison of the contrast-enhancing properties of Albumin-(Gd-DTPA) and Gd-DTPA at 2.0 T: an experimental study in rats. *Am J Roentgenol* 1986; 147:1263-1270

17. Schmiedl U, Ogan MD, Paaajanen H, et al. Albumin labeled with Gd-DTPA as an intra-vascular, blood-pool-enhancing agent for MR imaging: biodistribution and imaging studies. *Radiology* 1987;162:205-210
18. Wikstrom M, Moseley M, White D, et al. Comparison of Gd-DTPA and a macromolecular agent. *Invest Radiol* 1989;24:609-615
19. Berthezene Y, Vexler V, Kuwatsuru R, et al. Differentiation of alveolitis and pulmonary fibrosis with a macromolecular MR imaging contrast agent. *Radiology* 1992;185:97--103
20. Kuwatsuru R, Liu T, Cohen F, et al. Acute liver transplantation rejection. Early detection of endothelial leak in a rat model using magnetic resonance imaging and a macromolecular contrast medium. *Invest Radiol* 1994;29:297-299
21. Schwickert HC, Stiskal M, Roberts TP, et al. Contrast-enhanced MR imaging assessment of tumor capillary permeability: effect of irradiation on delivery of chemotherapy. *Radiology* 1996; 198:893-898
22. Brasch R, Pham C, Shames D, et al. Assessing tumor angiogenesis using macromolecular MR imaging contrast media. *J Magn Reson Imaging* 1997;7:68-74
23. Gossman A, Okuhata Y, Shames DM, et al. Prostate cancer tumor grade differentiation with dynamic contrast-enhanced MR Imaging in the rat: comparison of macromolecular and small-molecular contrast media-preliminary experience. *Radiology* 1999; 213:265-272
24. Turetschek K, Huber S, Floyd E, et al. MRI Characterization of microvessels in experimental breast tumors using a particulate contrast agent with histopathologic correlation. *Radiology* 2001;218:562-569
25. Turetschek K, Floyd E, Shames DM, et al. Assessment of a rapid clearance blood pool MR contrast medium (P792) for assays of microvascular characteristics in experimental breast tumors with correlations to histopathology. *Magn Reson Med* 2001; 45:880-886
26. Turetschek K, Floyd E, Helbich T, et al. MRI assessment of microvascular characteristics in experimental breast tumors using a new blood pool contrast agent (MS-325) with correlation to histopathology. *J Magn Reson Imaging* 2001; 14:237-242
27. White D, Wang S-C, Aicher K, Dupon J, Engelstad B, Brasch R. Albumin-(Gd-DTPA)₁₅₋₂₀: whole body clearance, and organ distribution of gadolinium. In: *Proceedings of the Society of Magnetic Resonance in Medicine, 8th Annual Meeting, Amsterdam, 1989*, p 807.
28. Baxter AB, Melnikoff S, Stites DP, Brasch RC. Immunogenicity of gadolinium-based contrast agents for MRI. *Invest Radiol* 1991; 26:1035-1040
29. De Wilt JH, ten Hagen TL, de Boeck G, van Tiel ST, de Bruijn EA, Eggermont AM. Tumour necrosis factor alpha increases melphalan concentration in tumour tissue after isolated limb perfusion. *Br J Cancer* 2000; 82:1000-1003
30. Van der Veen AH, de Wilt JH, Eggermont AM, van Tiel ST, ten Hagen TL. TNF- α augments intratumoural concentration of doxorubicin in TNF- α -based isolated limb perfusion in rat sarcoma models and enhances antitumour effects. *Br J Cancer* 2000; 82:972-980
31. Van Etten B, de Vries M, van Ijken M, et al. Degree of tumour vascularity correlates with drug accumulation and tumour response upon TNF- α -based isolated hepatic perfusion. *Br J Cancer* 2003; 87:314-319

32. Eggermont AM, Schraffordt Koops H, Klausner JM, et al. Isolated limb perfusion with tumor necrosis factor alpha and melphalan in 186 patients with locally advanced extremity soft tissue sarcomas. The cumulative multicenter European experience. *Ann Surg* 1996; 224:754-764; discussion 764-765
33. Benckhuijsen C, Kroon BB, van Geel AN, et al. Regional perfusion treatment with melphalan for melanoma in a limb: an evaluation of drug kinetics. *Eur J Surg Oncol* 1998; 14:157-163

PART ONE

MAGNETIC RESONANCE IMAGING ASSESSMENT OF
TUMOR MICROVESSELS USING CONTRAST MEDIA OF
DIFFERENT MOLECULAR WEIGHTS

CHAPTER 2

MR MACROMOLECULAR AGENTS FOR MONITORING TUMOR MICROVESSELS AND ANGIOGENESIS INHIBITION

MR MACROMOLECULAR AGENTS FOR MONITORING TUMOR MICROVESSELS AND ANGIOGENESIS INHIBITION

2

(SUBMITTED FOR PUBLICATION)

A. Preda¹, MD; M. van Vliet¹, MD; G.P. Krestin¹, MD; R.C. Brasch², MD; C.F. van Dijke¹, MD

¹ Department of Radiology, Erasmus MC-University Medical Center, Rotterdam, The Netherlands.

² Department of Radiology, University of California San Francisco, San Francisco, California.

Abstract

Dynamic contrast-enhanced MRI (DCE-MRI) using macromolecular contrast media enables assessment of the tumor vasculature based upon the differential distribution of the contrast agent within normal and pathological tissues. Quantitative assays of both morphological and functional properties can provide useful diagnostic insights into tissue angiogenesis. The utility of MRI enhanced with macromolecular agents for the characterization of tumor microvessels has been experimentally demonstrated in a range of malignant tumor types. Kinetic analysis of DCE-MRI data can be used to estimate microvascular permeability and tumor blood volume. By measuring these functional tumor properties, an accurate, noninvasive, and quantitative description of the microcirculation of individual tumors can be acquired, improving the specificity of imaging examinations for cancer diagnosis and for treatment and follow-up. The noninvasive MRI assessment of tumor angiogenesis can be applied in the diagnostic differentiation between benign and malignant tumors and can also provide means for in vivo monitoring of anti-tumor therapy. In this review, the potential clinical applications and limitations of various macromolecular contrast agents applied for evaluations of tumor angiogenesis, with and without drug interventions will be discussed.

Introduction

Angiogenesis plays a key role in the pathogenesis of tumors and is essential to tumor growth and metastasis (1, 2). Without angiogenesis, solid tumors cannot grow beyond 2 mm in diameter due to hypoxia; angiogenically supplied new vessels derived from host tissues permit tumors to grow exponentially. Recent developments in anti-cancer therapies directed against the tumor neovasculature (3, 4) have heightened the need for angiogenesis imaging markers. Quantification of tumor angiogenesis status might serve both as a prognostic index for the specific tumor examined as a tool for monitoring the effects of antiangiogenesis treatment. Dynamic contrast-enhanced MRI can be applied to quantitatively characterize certain tumor microvascular properties including richness of vascular supply and vascular endothelial leakiness, or permeability, and thereby to assess angiogenesis. Microvascular characteristics of tumor tissue such as capillary permeability and fractional blood volume can be estimated by contrast-enhanced MRI, based on kinetic analyses of contrast agent distribution over time between the vascular and interstitial spaces within the tumor. A simple two compartment model is appropriate for this analysis and can be readily adapted to computerized analysis.

Low molecular weight gadolinium chelates used as contrast media, like Gd-DTPA (gadopentetate dimeglumine, Magnevist® molecular weight 567 Da), are now widely available, governmentally approved for humans, and have been applied to estimate permeability and perfusion (5-8). One major limitation for low molecular contrast agents is that exclusive of the brain, where the specialized blood-brain-barrier prevents contrast agent extravasation or leak, these small molecular weight probes are known to diffuse quickly from the blood into the extracellular space for both normal and pathological tissues. For tumor microvessels extravasation rates for Gd-DTPA as great as 45% for each pass

through the capillary bed have been measured (9), similarly leak rates in normal vessels can be very high. With the exception of the central nervous system, the differentiation of benign and malignant tissue might thus be problematic using small molecular weight contrast media.

Macromolecular contrast media (MMCM), with molecular sizes approximating the size of serum proteins (up to 70 kDa or 7 nm in diameter), have been shown to remain largely confined within the intravascular space of normal tissues, with single-pass extraction fractions far below 1% (10, 11). However, these agents do extravasate and accumulate interstitially within tissues with damaged or otherwise hyperpermeable microvessels (12–14). Tumor microvessels have been long recognized to be hyperpermeable to macromolecular solutes as shown for many tumor types and by a variety of invasive techniques (15). Correspondingly, published results from preclinical studies in cancer models indicate that MMCM are well suited for the detection and measurement of this characteristic macromolecular leakiness of malignant tumors (16). Macromolecular MRI contrast agents, as a class of agents, have been variably defined as paramagnetic or superparamagnetic probes with molecular weights higher than 10 kDa (17) or 30 kDa (18). Intermediate-sized molecules (molecular weight between 10 and 50 kDa) have been included by some authors in the class of MMCM. Ultrasmall superparamagnetic iron oxide (USPIO) particles have also been investigated as MMCM, although their size is considerably larger than human albumin (molecular weight 69000) or albumin-(Gd-DTPA)₃₅, (a prototype MMCM with molecular weight of 92 kDa). Recently, contrast agents with low molecular weights but high binding affinity to plasma proteins have been evaluated for potential to characterize tumor microvessels.

Dynamic magnetic resonance imaging (MRI) enhanced with MMCM has previously been used to measure specifically defined characteristics of tumor microvessels, namely the endothelial transfer coefficient, K^{PS} , (leakiness) and fractional plasma volume (fPV) (13). A dynamic series of T1-weighted images was used to generate signal enhancement data that were further analyzed using pharmacokinetic modeling techniques. The contrast agent concentration, modeled as a function of time, could be derived from MR signal intensity data, assuming that changes in longitudinal relaxation rates R_1 ($1/T_1$) after administration of contrast medium are proportional with contrast agent concentration (19). The analysis of MMCM-enhanced MRI data within this context of a mathematical two compartment model of vascular permeability provides estimates of permeability, expressed as the endothelial transfer coefficient K^{PS} (units mL min^{-1} per volume of tissue) and fPV (mL per volume of tissue), which have been assumed to closely correlate with the angiogenesis process. K^{PS} represents the rate of diffusive transfer of contrast agent from the blood to the interstitial space and it is dependent on both the permeability/leakiness of the capillaries and available surface area of the endothelium across which it can leak. Usually a two-compartment, bidirectional or for relatively slow leak rates a unidirectional kinetic model representing the blood plasma and the extravascular extracellular spaces have been used.

Several macromolecular contrast agents with molecular weight between 10 kDa and 100 kDa are under development and have been tested experimentally, some clinically. The optimal size for a contrast medium suited for the assessment of tumor microvasculature, however,

has yet to be determined. The contrast agent should be sufficiently large not to leak across the normal vascular endothelium and small enough to be eliminated through glomerular capillaries. A near-exclusive vascular distribution has been shown for large molecular tracers with sizes between 70 and 150 kDa, whereas free glomerular filtration by the kidneys was only possible for smaller molecules below 70 kDa (20). Several macromolecular contrast agents are at the moment in clinical trials or in the registration process.

Albumin-(Gd-DTPA)_n

Albumin-(Gd-DTPA)_n consisting of a human protein backbone with multiple (typically 30-35) covalently bound gadolinium chelates, is a prototype of a water-soluble macromolecular contrast medium having a molecular weight of 92 kDa (10, 11, 21). It has a distribution volume of 0.05 liter/kg (which closely approximates the body's relative blood volume indicating its vascular distribution) and a plasma half-life of three hours in rats, which produces nearly constant enhancement of normal, non-leaky tissues for 30 minutes or longer after injection (22). The T1 relaxivity (R1) of albumin-(Gd-DTPA)_n is substantially higher compared to low molecular gadolinium chelates. The R1 of albumin-(Gd-DTPA)_n is 14.8 mM⁻¹ s⁻¹ relative to gadolinium concentration (21). For comparison, the R1 value of Gd-DTPA is 4.9 mM⁻¹ s⁻¹ (23). Thus by binding it to human albumin, the molar relaxivity of each Gd-DTPA chelate is approximately three-fold increased (21).

The ability of dynamic MRI enhanced with albumin-(Gd-DTPA)₃₀ to quantitatively define the characteristics of tumor microvessels, including transendothelial permeability and fractional plasma volume has been shown in several experimental cancer models, including breast, prostate and ovarian adenocarcinomas (24-31). Experimental studies performed in chemically induced rodent mammary tumors showed a higher specificity of albumin-(Gd-DTPA)₃₀ kinetic behavior for differentiation of malignant from benign tumors with a strong correlation (R²=0.76, P<0.01) of tumor microvascular MMCM permeability (K^{ps}) with the tumor histopathologic grade as measured by the Scarff-Bloom-Richardson method (24). Similar strong correlations between tumor histopathologic grade of mammary tumors and permeability to albumin-(Gd-DTPA)₃₀ have been shown in several additional studies (27-29, 31).

Albumin-(Gd-DTPA)₃₀-enhanced MRI has also the potential to monitor the effect of antiangiogenesis therapy exemplified by anti-VEGF (vascular endothelial growth factor) antibody (30, 32-34) (AvastinTM, Genetech, South San Francisco, CA); this antibody is worldwide the first governmentally-approved angiogenesis inhibiting drug. Tumor microvascular permeability of human mammary tumors (30, 32, 33) or human ovarian carcinoma (34) decreased significant (P<0.05) after multiple anti-VEGF antibody administrations (32-34) or after only a single dose (30).

The effects of an antiangiogenesis treatment with PTK787/ZK222584, an orally administrated VEGF receptor tyrosine kinase inhibitor, have also been monitored by dynamic MMCM-enhanced MRI using albumin-(Gd-DTPA)₃₀ in a breast cancer xenograft (35). In this study endothelial transfer coefficient K^{ps} decreased in the group treated with

PTK787/ZK222584, while the control group had a significant increase in permeability values; differences between the treated and control group were also significant.

Albumin-(Gd-DTPA)_n is however considered an unlikely candidate for clinical use due to its potential immunogenic properties and its prolonged partial retention in the body, 17% at two weeks (36, 37). Additionally, MRI enhanced with albumin-(Gd-DTPA)_n with a low 0.03 mmol Gd/dose, yields a relatively low contrast to noise ratio in tumors. Relatively long scan serial times (30-45 minutes) have been chosen to resolve the progressive extravasation of albumin-(Gd-DTPA)_n molecule, but the minimum duration of scanning has not been addressed and likely is considerably shorter.

Macromolecular gadolinium chelates

Macromolecular gadolinium chelates are typically based on a polymeric backbone, such as a polypeptide or polysaccharide to which are bound multiple gadolinium chelates such as Gd-DTPA or Gd-DOTA; other types of polymers including dendrimers have been considered as candidates for this class of agents. The compounds with a molecular weight of more than 69 kDa, the weight of human albumin, that cannot be eliminated by glomerular filtration have been classified as “slow-clearance blood pool contrast agents” (38). Contrast agents that can be included in this group are polylysine polymers of varying lengths, to which multiple gadolinium chelates have been bound (29, 39). Other large molecules that are used for binding of gadolinium chelates include polysaccharides (40), polyglycol polyethyleneimine (12) as well as paramagnetic dextrans (41). A new formulation of a slow-clearance dextran-based contrast medium with a favorable toxicity profile is carboxymethyldextran-Gd-DOTA (Guerbet Laboratories, Aulnay-Sous-Bois, France), with a molecular weight of 52.1 kDa (41). One exception to this problem are the ultrasmall superparamagnetic iron particles, approximately 30 nm in diameter, that have been applied clinically as a macromolecular probe. Polymer-based soluble macromolecular formulations will have to undergo chemical improvements to solve the problem of elimination. If these agents could be metabolized to components smaller than 50 kDa (for urinary excretion) or if they could be eliminated by other routes, they might be applied for clinical testing.

Intermediate-sized gadolinium chelates

Intermediate-sized contrast media with a molecular weight between 30 and 69 kDa, that are eliminated from the body by renal glomerular filtration, have been termed “rapid clearance blood pool agents” (38). They act as blood pool agents during the first pass. Their diffusion through the normal vascular endothelial membrane is partly limited by their size, but these compounds can still pass the glomerular membrane.

Three different intermediate sized contrast media have been under investigation recently: Gadomer 17, P792 and ZK181220. **Gadomer-17** (Schering AG, Berlin, Germany) is a dendritic gadolinium chelate containing 24 Gd ions (42) with a total molecular weight of about 17 kDa. Gadomer 17 is exclusively eliminated by the kidney through glomerular

filtration within 24 hours from intravenous administration (42). Due to the globular shape of the molecule, the apparent molecular weight is larger than the true weight, more like a 30 kDa molecule, resulting in a retarded diffusion into the extravascular compartment. Gadomer 17 provides a high R1 relaxivity, approximately five times higher than that of gadopentetate dimeglumine.

The value of Gadomer 17-enhanced MRI for differentiation between benign and malignant breast tumors was investigated in two studies performed in a chemically induced rodent mammary tumor model (43, 44). Both reports revealed a limited capability for tumor characterization. Su et al (43) showed that Gadomer 17-enhanced MRI was able to distinguish low-grade from high-grade cancers based on fractional vascular volume (v_v) and extravascular and whole tumor kinetics (derived from pharmacokinetic analysis of the relative contrast agent concentration curves), but unable to differentiate benign tumors from low-grade carcinomas, because of permeability range overlap. In the study of Daldrup-Link et al (44) the mean values for transendothelial permeability and fractional plasma volume estimated from Gadomer 17-enhanced MRI data were significantly higher in malignant than in benign tumors. However, none of the quantitative microvascular parameters was significantly correlated with histopathologic tumor grade. In dog tumor models, Gadomer 17 provided a higher specificity for breast tumor characterization as compared with gadopentetate dimeglumine (45-47).

The potential of dynamic MRI enhanced with Gadomer 17 to monitor the therapeutic effects of an anti-VEGF antibody on microvascular characteristics has been recently demonstrated using a human breast cancer line implanted in rats (33). Gadomer 17 revealed a statistically significant difference in permeability and fractional plasma volume between pre- and post-treatment examinations. This high specificity for the differentiation of responders from non-responders was also shown after therapy with Mytomicin C in a rodent R3230 AC mammary adenocarcinoma model (48). In a different study performed in the same rodent R3230 AC mammary adenocarcinoma model, Gadomer 17 revealed significant changes in vascular properties, specifically vascular volume index and out-flux transport rate K (2) of the tumors treated with chemotherapy (Taxotere®, docetaxel, Aventis Pharmaceutical Inc.; Bridgewater, NJ) (49).

P792 (Vistarem, Guerbet, Aulnay-Sous-Bois, France) is a rapid-clearance contrast agent with a molecular weight of 6.47 kDa (50). It contains a single gadolinium ion in a four-armed gadolinium chelate. P792 has a plasma half-life in rats of approximately 20 minutes and a R1 relaxivity of $39 \text{ mM}^{-1} \text{ s}^{-1}$ at 20 MHz and 37 °C.

Using P792 and Gd-DTPA in a rodent prostate tumor model it was shown to be possible to differentiate metastatic from nonmetastatic tumors based on contrast agent wash-out rates, when the concentration vs. time curves were analyzed employing an empirical mathematical model to improve fitting of the DCE-MRI data (51). However, when analyzing the DCE-MRI data using a two-compartment kinetic model, it was not possible to reliably discriminate between metastatic and nonmetastatic tumors. In an experimental model of human prostate tumors using P792, significant reductions in this agent's tumor vascular

permeability, tumor blood volume and tumor blood flow were demonstrated following treatment with ZD4190, a VEGF receptor tyrosine kinase inhibitor (52). In a different experimental study performed in chemically induced rodent mammary tumor, P792 showed a lack of feasibility for the differentiation of benign from malignant tumors, based on estimates of permeability or tumor blood volume (28).

ZK181220 (Schering AG, Berlin, Germany) is a prototype MR contrast agent with an intermediate size (molecular weight of 25.9 kDa). In an experimental study performed in a human breast cancer xenograft, the microvascular permeability and the fPV derived from ZK181220-enhanced MRI data decreased significantly ($P < 0.05$) after therapy with anti-VEGF antibody compared with the control group (33). Although the values of K^{ps} and fPV were generally higher compared to the estimated values for the two larger agents investigated in the same study, USPIO SHU555C (Schering AG, Berlin, Germany) and albumin-(Gd-DTPA)₃₀, MR-based monitoring of anti-VEGF drug effect was still feasible.

Low molecular weight gadolinium chelates with reversible binding to plasma proteins

Small molecular gadolinium chelates with high binding affinity for plasma proteins represent a new class of MR contrast agents that undergo reversible interactions with circulating albumin. The contrast medium becomes associated with a macromolecular carrier. The bound form assumes the macromolecular attributes of albumin and remains intravascular, while the non-bound minor component (with the low relaxivity typical of small Gd-chelates) is free in the plasma and extravasates readily. These molecules have been recently extensively studied, and their blood persistence has been demonstrated in experimental models (31, 53-58). The long intravascular residence of the albumin-bound contrast media serves as an aid in delineating abnormal vascular beds and increased vascularization associated with fast-growing tumors.

B22956/1, a new protein-binding contrast agent (Bracco S.p.A., Milan, Italy) is a Gd-chelate with a low molecular weight (1059 Da). B22956/1 is the trisodium salt of a polyaminocarboxylate Gd complex linked to deoxycholic acid (58). It has a high affinity for serum proteins (94% for a 0.5mM solution in Seronorm® for human serum albumin, and 84% for rat serum albumin). The relaxivity of B22956/1 is 27 mM⁻¹ s⁻¹ at 20 MHz in human serum, which is almost six-fold higher than that of conventional extravascular contrast agents. Experimental studies performed in human mammary tumors demonstrated the effects of an antiangiogenesis therapy with anti-VEGF monoclonal antibody (59). The microvascular permeability K^{ps} estimated from B22956/1-MRI data decreased significantly in the drug-treated group compared to baseline and progressed significantly in the control group. B22956/1 demonstrated a number of favorable imaging characteristics. In a short examination time, substantial progressive enhancement of the tumors was observed, allowing clear visualization of the effects of anti-VEGF therapy on the permeability of tumor blood vessels. The dynamic range of observed permeability changes spanned a wide range, rendering observation of progressive disease and the permeability reducing effects of successful antiangiogenic therapy readily resolved.

MS-325 (Angiomark, Schering AG, Berlin, Germany) is a non-covalent protein-bound small molecular gadolinium chelate (MW 957 Da) with a relaxivity of $35 \text{ mM}^{-1} \text{ s}^{-1}$. After intravenous administration, this agent binds reversibly to plasma albumin to form a MS-325-albumin complex with a molecular weight of roughly 70 kDa. This macromolecular complex acts as a blood pool-enhancing agent with a plasma half-life of 2-3 hours in humans (60). The bound form is in equilibrium with a small amount of free form, which is eliminated by glomerular filtration. The affinity of MS-325 binding for albumin varies with species: it is approximately 95% in humans and 75% in rats (31, 54, 57). The prolonged half-life of MS-325 provides excellent properties for use as a MR angiography agent (58, 61).

Initial studies performed in chemically induced rodent mammary tumors (31) did not show a significant correlation between MS-325-enhanced microvascular assays with either tumor histopathologic grade or microvascular counts, a surrogate of angiogenesis. A likely explanation for the lack of feasibility for tumor microvessel characterization, at least in this specific animal tumor model, was the inability to extract the particular pharmacokinetics of the macromolecular protein-bound component from MR data, since both the bound and unbound form of MS-325 are present in plasma at all times diffusing through vessel endothelium independently.

MP-2269 is another protein-binding small molecular gadolinium chelate of potential clinical significance. MP-2269 (Mallinckrodt Inc., St. Louis, MO) is an experimental monomeric Gd-DTPA –derived blood pool agent which binds non-covalently and reversibly (80%) to human serum albumin (53, 62). A recent study performed in an intracranial mouse glioma model using MP-2269, MS 325 and extracellular contrast agent OptiMARK (Mallinckrodt, Inc., St Louis, MO) demonstrated that the blood pool contrast agents had an approximately threefold increased dose-effectiveness and a lengthened window of contrast enhancement in comparison to extracellular agent (62).

Macromolecular iron oxide compounds

Superparamagnetic iron oxide particles (SPIO; > 100 nm diameters), which are currently clinically applied for imaging the reticuloendothelial system, specifically the liver and spleen, are cleared too rapidly from the blood stream (plasma half-life of 8 minutes) and thus are not well-suited for characterization of tumor microvessels. On the other hand, the ultrasmall superparamagnetic iron oxide particles (USPIO; < 30 nm diameters), initially developed for MR lymphography, have an intravascular half-life of approximately 1-3 hours, allowing maintenance of a high blood concentration and a strong enhancement of the blood pool. These nanoparticles decrease T1 and T2 relaxation times of tissues, and thus they can act either as positive or negative contrast agents, according to their concentration (63).

The strong T2 and T2* relaxivity when compared to the T1 relaxivity of USPIO results in the fact that positive enhancement due to T1 shortening effect is limited to relatively low tissue concentrations and that this positive T1 enhancement is overwhelmed at higher

doses by a strong T2* effect (64). Thus, the evaluation of for instance perfusion alterations could theoretically be performed with either small doses/concentrations, which shorten T1 relaxation times, or with higher doses, that predominantly shorten the T2 relaxation times. Recently reported experimental studies indicate that USPIO are well suited for the characterization of tumor microvessels, including abnormal macromolecular permeability (27, 65, 66).

NC100150 (Feruglose, Clariscan, Nycomed Amersham, Oslo, Norway) and albumin-(Gd-DTPA)₃₀ were compared at MR imaging on sequential days in the same rats with a chemically induced mammary tumor (27). NC100150 consists of USPIO particles composed of single crystals (4-7 nm diameter core), stabilized with a carbohydrate polyethylene glycol coat. The final diameter of the USPIO particles is approximately 20 nm. The R1 relaxivity of this agent is 20 mmol/L/sec, and the R2 is 35 mmol/L/sec at 37 °C and 0.5 T. The mean plasma half-life in rats is about 3.3 hours. The tumor vascular permeability estimated with either contrast agents correlated significantly with the histopathologic tumor grade. Clariscan was administrated at a low dose of 1 mg Fe/kg. This low dose was specifically chosen to minimize the confounding T2* effects. However, one disadvantages of the low dose was low signal-to-noise ratio due to a low level of tumor signal enhancement.

The value of the USPIO Clariscan in differentiating and grading of human benign and malignant breast tumors on the basis of microvascular characteristics has been recently evaluated in a multi-center clinical trial (66). In this study, a moderate and statistically significant correlation was found between the transendothelial permeability and the pathologic tumor grade ($r=0.496$, $P<0.001$). The probability of breast tumor microvascular hyperpermeability to be associated with malignancy was 79%. Normal, non-neoplastic and mastopathic tissue did not enhance with Clariscan. Benign fibroadenomas could be accurately differentiated from high-grade carcinomas, but demonstrated a considerable overlap with the enhancement patterns of low-grade cancers. Another clinical study evaluating the role of Clariscan in grading human breast cancer (67) also demonstrated a statistically significant correlation between the transendothelial permeability estimated from dynamic Clariscan-enhanced MR data and the tumor histopathologic grade.

A different study (65) performed in a chemically induced rodent mammary tumor model investigated the diagnostic potential of a different USPIO, **SHU555C** (Resovist S, Schering AG, Berlin, Germany) for quantitative tumor microvessel characterization. SHU555C is an USPIO with a mean core size of 3-4 nm and a hydrodynamic size of < 25 nm. The R1 of the agent is 22 mM⁻¹ s⁻¹ of Fe, and the R2 is 65 mM⁻¹ s⁻¹ of Fe (at 20 MHz and 37 °C). The mean plasma half-life in rats is about 1 hour. SHU555C was injected at a dose of 5 mg Fe/kg. The tumor microvascular characteristics estimated with SHU555C were compared to albumin-(Gd-DTPA)₃₀. The transendothelial permeability K^{PS} correlated significantly with the tumor malignancy grade for the USPIO as well as for the albumin-(Gd-DTPA)₃₀. The higher dose of 5 mg Fe/kg provided increased T2* effects, that probably were responsible for the observed lower correlation ($r=0.36$, $P<0.05$) of the K^{PS} value with the tumor histopathologic grade, compared to the lower dose of 1 mg Fe/kg ($r=0.82$, $P<0.001$) used in the study reported by Turetschek (27). The potential of dynamic MRI enhanced with USPIO (SHU555C) to monitor the therapeutic effects of an anti-VEGF antibody on microvascular characteristics has also

recently been demonstrated using a human breast cancer xenograft (33). The kinetic analysis of dynamic MRI enhanced with SHU555C revealed a statistically significant difference in permeability and fractional plasma volume between examinations performed prior to and after treatment with anti-VEGF antibody.

Conclusion

Experimental and some early clinical studies have shown the potential of MMCM-enhanced MRI for characterizing tumor angiogenesis, based on the ability to assay microvessel permeability and fractional plasma volume. Several xenograft studies have suggested that MMCM enhanced MRI can monitor antiangiogenesis cancer therapies including direct inhibitors of VEGF, antagonists of VEGF receptors, and inhibitors of matrix metalloproteases. The immediate challenge is to design a contrast agent with a sufficiently high molecular weight and size that is tolerated in humans, interacts minimally with tissue, and is stable in vivo and completely cleared from the body. Intermediate size MMCM and low molecular weight agents with reversible binding to plasma proteins have the advantage of providing images with a good signal to noise ratio in a relatively short imaging time. These contrast agents can be successfully applied in DCE-MRI monitoring of the effects of antiangiogenic therapies, as indicated in several experimental studies (what may be sacrificed by their use is the specificity for cancer/diseased microvessels.) MMCM, currently in various stages of development, offer considerable promise for quantitative, physiologically based imaging evaluation of the tumor microvessels and antiangiogenesis therapy. The anticipated availability of a MMCM approved for human use should allow the future translation of these noninvasive MRI monitoring techniques from experimental to wide scale clinical implementation.

Acknowledgements

Anda Preda was supported in part by the “Drie Lichten” and the “Johan Vermeij” Foundations, the Netherlands

References

1. Plate KH, Breier G, Risau W. Molecular mechanisms of developmental and tumor angiogenesis. *Brain Pathol* 1994; 4:207-218
2. Hanahan D, Folkman J. Patterns and emerging mechanisms of the angiogenic switch during tumorigenesis. *Cell* 1996; 86:353-364
3. Li WW. Tumor angiogenesis: molecular pathology, therapeutic targeting and imaging. *Acad Radiol* 2000;7:800-811
4. Folkman J, Becker K. Angiogenesis imaging. *Acad Radiol* 2000;7:783-785
5. Barentsz JO, Engelbrecht M, Jager GJ, et al. Fast dynamic gadolinium-enhanced MR imaging of urinary bladder and prostate cancer. *J Magn Reson Imaging* 1999; 10:295-304

6. Port RE, Knopp MV, Hoffmann U, et al. Multicompartment analysis of gadolinium-chelate kinetics: blood-tissue exchange in mammary tumors as monitored by dynamic MR imaging. *J Magn Reson Imaging* 1999; 10:233-241
7. Padhani AR, Gapinski CJ, Macvicar DA, et al. Dynamic contrast-enhanced MRI of prostate cancer: correlation with morphology and tumour stage, histological grade and PSA. *Clin Radiol* 2000; 55:99-109
8. Wasser K, Klein SK, Fink C, et al. Evaluation of neoadjuvant chemotherapeutic response of breast cancer using dynamic MRI with high temporal resolution. *Eur Radiol* 2003; 13:80-87
9. Daldrup HE, Shames DM, Hussein W, et al. Quantification of the extraction fraction for gadopentetate across breast cancer capillaries. *Magn Reson Med*. 1998; 40:537-543
10. Schmiedl U, Ogan MD, Pajajani H, et al. Albumin labeled with Gd-DTPA as an intravascular, blood-pool-enhancing agent for MR imaging: biodistribution and imaging studies. *Radiology* 1987;162:205-210
11. Brasch RC. New directions in the development of MR imaging contrast media. *Radiology* 1992;183:1-11
12. Demsar F, Roberts TP, Schwickert HC, et al. A MRI spatial mapping technique for microvascular permeability and tissue volume based on macromolecular contrast agent distribution. *Magn Reson Med* 1997;37:236-242
13. Shames D, Kuwatsuru R, Vexler V, et al. Measurement of capillary permeability to macromolecules by dynamic magnetic resonance imaging: a quantitative non-invasive technique. *Magn Reson Med* 1993; 29:616-622
14. Cohen F, Kuwatsuru R, Shames D, et al. Contrast-enhanced magnetic resonance imaging estimation of altered capillary permeability in experimental mammary carcinomas after X-radiation. *Invest Radiol* 1994;29:970-977
15. Jain RK. Barriers to drug delivery in solid tumors. *Sci Am*. 1994; 271:58-65.
16. Brasch R, Turetschek K. MRI characterization of tumors and grading angiogenesis using macromolecular contrast media: status report. *Eur J Radiol* 2000;34:148-155
17. Daldrup-Link HE, Brasch RC. Macromolecular contrast agents for MR mammography: current status. *Eur Radiol* 2003; 13:354-365
18. Padhani AR. MRI for assessing antivasular cancer treatments. *The British Journal of Radiology* 2003; 76:S60-S80
19. Roberts TP. Physiologic measurements by contrast-enhanced MR imaging: expectations and limitations. *J Magn Reson Imaging* 1997 ;7:82-90.
20. Yuan F, Dellin M, Fukumura D, et al. Vascular permeability in a human tumor xenograft: molecular size dependence and cutoff size. *Cancer Res* 55:3752-3756
21. Ogan MD, Schmiedl U, Moseley ME, et al. Albumin labeled with Gd-DTPA. An intravascular contrast-enhancing agent for magnetic resonance blood pool imaging: preparation and characterization. *Invest Radiol* 1987;22:665-671.
22. Schmiedl U, Ogan M, Moseley M, et al. Comparison of the contrast-enhancing properties of Albumin-(Gd-DTPA) and Gd-DTPA at 2.0 T: an experimental study in rats. *Am J Roentgenol* 1986; 147:1263-1270
23. Weinmann H-J, Brasch RC, Press W-R, et al. Characteristics of gadolinium-DTPA complex: a potential NMR contrast agent. *AJR* 1984; 142:619-624

24. Daldrup H, Shames DM, Wendland M, et al. Correlation of dynamic contrast-enhanced MR imaging with histologic tumor grade: comparison of macromolecular and small-molecular contrast media. *Am J Roentgenol* 1998; 171:941-949
25. Schwickert HC, Stiskal M, Roberts TP, et al. Contrast-enhanced MR imaging assessment of tumor capillary permeability: effect of irradiation on delivery of chemotherapy. *Radiology* 1996; 198:893-898
26. Gossman A, Okuhata Y, Shames DM, et al. Prostate cancer tumor grade differentiation with dynamic contrast-enhanced MR Imaging in the rat: comparison of macromolecular and small-molecular contrast media-preliminary experience. *Radiology* 1999; 213:265-272
27. Turetschek K, Huber S, Floyd E, et al. MRI Characterization of microvessels in experimental breast tumors using a particulate contrast agent with histopathologic correlation. *Radiology* 2001;218:562-569
28. Turetschek K, Floyd E, Shames DM, et al. Assessment of a rapid clearance blood pool MR contrast medium (P792) for assays of microvascular characteristics in experimental breast tumors with correlations to histopathology. *Magn Reson Med* 2001;45:880-886
29. Su M, Muhler A, Lao X, et al. Tumor characterization with dynamic contrast-enhanced MRI using contrast agents of various molecular weights. *Magn Reson Med* 1998; 39:259-269
30. Brasch R, Pham C, Shames D, et al. Assessing tumor angiogenesis using macromolecular MR imaging contrast media. *J Magn Reson Imaging* 1997;7:68-74
31. Turetschek K, Floyd E, Helbich T, et al. MRI assessment of microvascular characteristics in experimental breast tumors using a new blood pool contrast agent (MS-325) with correlation to histopathology. *J Magn Reson Imaging* 2001; 14:237-242
32. Pham C, Roberts T, van Bruggen N, et al. Magnetic Resonance Imaging detects suppression of tumor vascular permeability after administration of antibody to vascular endothelial growth factor. *Cancer Invest* 1998; 6:224-230
33. Turetschek K, Preda A, Novikov V, et al. Tumor microvascular changes in antiangiogenic treatment: assessment by magnetic resonance contrast media of different molecular weights. *J Magn Reson Imaging* 2004; 20:138-144
34. Gossman A, Helbich TH, Mesiano S, et al. Magnetic resonance imaging in an experimental model of human ovarian cancer demonstrating altered microvascular permeability after inhibition of vascular endothelial growth factor. *Am J Obstet Gynecol* 2000; 183:956-963
35. Turetschek K, Preda A, Floyd E, et al. MRI monitoring of tumor response following angiogenesis inhibition in an experimental human breast cancer model. *Eur J Nucl Med* 2003; 30:448-455
36. White D, Wang S-C, Aicher K, et al. Albumin-(Gd-DTPA)₁₅₋₂₀: whole body clearance, and organ distribution of gadolinium. In: *Proceedings of the Society of Magnetic Resonance in Medicine, 8th Annual Meeting, Amsterdam, 1989*, p 807.
37. Baxter AB, Melnikoff S, Stites DP, et al. Immunogenicity of gadolinium-based contrast agents for MRI. *Invest Radiol* 1991; 26:1035-1040
38. Bourrasset F, Dencausse A, Bourrinet P, et al. Comparison of plasma and peritoneal concentrations of various categories of MRI blood pool agents in a murine experimental pharmacokinetic model. *MAGMA* 2001;12:82-87

39. Schuhmann-Giampieri G, Schmitt-Willich H, Frenzel T, et al. In vivo and in vitro evaluation of Gd-DTPA -polylysine as a macromolecular contrast agent for magnetic resonance imaging. *Invest Radiol* 1991;26:969-974
40. Helbich TH, Gossman A, Mareski PA, et al. A new polysaccharide macromolecular contrast agent for MR imaging: biodistribution and imaging characteristics. *J Magn Reson Imaging* 2000;11:694-701
41. Corot C, Schaefer M, Beaute S, et al. Physical, chemical and biologic evaluations of CMD-A2-Gd-DOTA. A new paramagnetic dextran polymer. *Acta Radiol* 1997; 412(Suppl):91-99
42. Misselwitz B, Schmitt-Willich H, Ebert W, et al. Pharmacokinetics of Gadomer 17, a new dendritic magnetic resonance contrast agent. *MAGMA* 2001;12:128-134
43. Su M-Y, Wang Z, Carpenter PM, et al. Characterization of N-ethyl-N-nitrosourea-induced malignant and benign tumors in rats by using three MR contrast agents. *J Magn Reson Imaging* 1999;9:177-186
44. Daldrup-Link H, Shames D, Wendland M, et al. Comparison of Gadomer 17 and gadopentetate for differentiation of benign from malignant breast tumors with MR imaging. *Acad Radiol* 2000;7:934-944
45. Adam G, Muhler A, Spuentrup E, et al. Differentiation of spontaneous canine breast tumors using dynamic magnetic resonance imaging with 24-gadolinium cascade polymer, a new blood-pool agent. *Invest Radiol* 1996;31:267-274
46. Adam G, Neuerburg J, Spuentrup E, et al. 24-gadolinium-cascade polymer: a potential blood-pool contrast agent for MR imaging. *J Magn Reson Imaging* 1994;4:462-466
47. Adam G, Neuerburg J, Spuentrup E, et al. Dynamic contrast enhanced MR-imaging properties of gadobutol, gadolinium-DTPA-polylysine, and Gd-DTPA cascade polymer. *Magn Reson Med* 1994;32:622-628
48. Su M, Wang Z, Nalcioğlu O. Investigation of longitudinal vascular changes in control and chemotherapy-treated tumors to serve as therapeutic efficacy predictors. *J Magn Reson Imaging* 1999;9:128-137
49. Su MY, Yu H, Chiou JY, et al. Measurement of volumetric and vascular changes with dynamic contrast enhanced MRI for cancer therapy monitoring. *Technol Cancer Res Treat* 2002;1:479-488
50. Port M, Corot C, Rousseaux O, et al. P792: a rapid clearance blood pool agent for magnetic resonance imaging: preliminary results. *MAGMA* 2001;12:121-127
51. Fan X, Medved M, River JN, et al. New model for analysis of dynamic contrast-enhanced MRI data distinguishes metastatic from nonmetastatic transplanted rodent prostate tumors. *Magn Reson Med* 2004;51:487-494
52. Clement O, Pradel C, Siauve N, et al. Assessing perfusion and capillary permeability changes induced by a VEGF inhibitor in human tumor xenografts using macromolecular MR imaging contrast media. *Acad Radiol* 2002; 9(Suppl 2):S328-S329
53. Wallace RA, Haar Jr JP, Miller DB et al. Synthesis and preliminary evaluation of MP-2269: a novel, non-aromatic small molecule blood-pool MR contrast agent. *Magn Reson Med* 1998;40:733-739
54. Lauffer RB, Parmelee DJ, Dunham SU, et al. MS-325: albumin-targeted contrast agent for MR angiography. *Radiology* 1998;207:529-538
55. Adzamli K, Toth E, Periasamy MP, et al. ¹H-NMRD and ¹⁷O-NMR assessment of water exchange and rotational dynamics of two potential MRI agents: MP-1177 (an extracellular agent) and MP-2269 (a blood pool agent). *MAGMA* 1999;8:163-171

56. Adzamli K, Haar Jr JP, Hynes MR, et al. Development of a novel nonaromatic small-molecule MR contrast agent for the blood pool. *Acad Radiol* 1998;5(Suppl 1):S210-S213
57. Grist TM, Korosec FR, Peters DC, et al. Steady-state and dynamic MR angiography with MS-325: initial experience in humans. *Radiology* 1998;207:539-544
58. Zheng J, Carr J, Harris K, et al. Three-dimensional MR pulmonary perfusion imaging and angiography with an injection of a new blood pool contrast agent B-22956/1. *J Magn Reson Imaging* 2001; 14:425-432
59. Preda A, Novikov V, Möglich M, et al. MRI monitoring of Avastin™ antiangiogenesis therapy using B22956/1, a new blood pool contrast agent, in an experimental model of human cancer. *J Magn Reson Imaging* 2004; 20:865-873
60. Parmelee DJ, Walovitch RC, Ouellet HS, et al. Preclinical evaluation of the pharmacokinetics, biodistribution, and elimination of MS-325, a blood pool agent for magnetic resonance imaging. *Invest Radiol* 1997;32:741-747
61. Prasad PV, Canillo J, Chavez DR, et al. First-pass renal perfusion imaging using MS-325, an albumin-targeted MRI contrast agent. *Invest Radiol* 1999;34:566-571
62. Adzamli K, Yablonskiy DA, Chicoine MR, et al. Albumin-binding MR blood pool agents as MRI contrast agents in an intracranial mouse glioma model. *Magn Reson Med* 2003;49:586-590
63. Chambon C, Clement O, Le Blanche A, et al. Superparamagnetic iron oxides as positive MR contrast agents: in vitro and in vivo evidence. *Magn Reson Imaging* 1993;11:509-511
64. Trillaud H, Degreze P, Combe C, et al. Evaluation of intrarenal distribution of ultrasmall iron oxide particles by magnetic resonance imaging and modification by furosemide and water restriction. *Invest Radiol* 1994;29:540-546
65. Turetschek K, Roberts TPL, Floyd E, et al. Tumor microvascular characterization using ultrasmall superparamagnetic iron oxide particles (USPIO) in an experimental breast cancer model. *J Magn Reson Imaging* 2001; 13:882-888
66. Daldrup-Link HE, Rydland J, Helbich TH, et al. Quantification of breast tumor microvascular permeability with feruglose-enhanced MR imaging: initial phase II multicenter trial. *Radiology* 2003;229:885-892
67. Rydland J, Bjornerud A, Haugen O, et al. New intravascular contrast agent applied to dynamic contrast-enhanced MR imaging of human breast cancer. *Acta Radiol* 2003;44:275-283

CHAPTER 3

THE CHOICE OF REGION OF INTEREST MEASURES IN CONTRAST-ENHANCED MRI CHARACTERIZATION OF EXPERIMENTAL BREAST TUMORS

THE CHOICE OF REGION OF INTEREST MEASURES IN CONTRAST-ENHANCED MRI CHARACTERIZATION OF EXPERIMENTAL BREAST TUMORS

3

(INVESTIGATIVE RADIOLOGY, 2005, 40:349-354)

Anda Preda^{1,2}, MD; Karl Turetschek¹, MD; Heike Daldrup¹, MD; Eugenia Floyd³, DVM;
Viktor Novikov¹, MD; David M. Shames¹, MD; Timothy PL Roberts¹, Ph.D.;
Wayne O. Carter³, DVM, Robert C. Brasch¹, MD

¹ Center for Pharmaceutical and Molecular Imaging, Department of Radiology,
University of California San Francisco, California.

² Visiting Research Scholar from the Department of Radiology, Erasmus University
Medical Center, Rotterdam, The Netherlands.

³ Pfizer Central Research, Groton, Connecticut.

Abstract

Objectives

To determine if MR estimates of quantitative tissue microvascular characteristics from regions of interest (ROI) limited to the tumor periphery provided a better correlation with tumor histologic grade than ROI defined for the whole tumor in cross-section.

Methods

A meta-analysis was based upon 98 quantitative MRI breast tumor characterizations, acquired in three separate experimental studies using identical methods for tumor induction and contrast enhancement.

Results

The endothelial transfer coefficient (K^{PS}) of albumin- (Gd-DTPA)₃₀ from the tumor periphery correlated ($r=0.784$) significantly more strongly ($p < 0.001$) with the pathologic tumor grade than K^{PS} derived from the whole tumor ($r=0.604$). K^{PS} estimates, either from the tumor periphery or from the whole tumor correlated significantly more strongly with histologic grade ($p < 0.01$) than MRI estimates of fractional plasma volume (fPV) from either tumor periphery ($r=0.368$) or whole tumor ($r=0.323$).

Conclusions

K^{PS} estimates from the tumor periphery were the best of these measurable MRI microvascular characteristics for predicting the histologic grade.

Key words

Magnetic resonance imaging, region of interest, tumor microvascular characteristics, breast tumor.

Introduction

Dynamic contrast-enhanced magnetic resonance imaging has become an increasingly used method for evaluating breast masses. Different methods have been proposed for analysis of dynamic contrast-enhanced MR data in order to characterize breast tumors and to improve the specificity of diagnosis. Several approaches involve the analysis of dynamic MR contrast-enhanced data within the context of mathematical models (1-4). Using a two compartment bidirectional model in conjunction with a macromolecular contrast medium, albumin- (Gd-DTPA)₃₀, our group has shown the potential to successfully predict tumor histologic grade based on the MRI microvascular characteristics (5).

The choice of region of interest (ROI) to be analyzed within the tumor margins may have a substantial effect on accuracy of MRI predictions of tumor status. At present, there is no standardized method for ROI assignment in dynamic breast MRI. A large ROI encompassing the entire cross-section of the tumor at its maximum diameter (henceforth termed the "whole tumor") can be drawn, from which mean signal intensity pixel values can be extracted at each time point. A large ROI has the advantage of "averaging out" random

noise contributions within and among individual pixels. However, reasonable concerns have arisen that a large ROI covering the whole tumor, particularly if the tumor is heterogeneous may yield misleading results. Such large ROI may include zones of necrosis, cysts, poor vascularization and areas subject to elevated interstitial pressures, any of which could distort the tumor contrast-enhancement profile. Our group and others have intuitively proposed a selective ROI, limited to the tumor periphery or strongest enhancing sub-region, defined by an operator, in an attempt to improve the quality of the analysis (5-7). However, to our knowledge no group has systematically and impartially compared the correlations differing ROI with a quantitative nonimaging tumor characteristic such as histologic grade.

The purpose of this study was to determine if the correlations between the tumor histologic grade and MRI microvascular characteristics obtained from the kinetic analysis of dynamic macromolecular contrast-enhanced image data from the whole tumor is significantly different from that when only the tumor periphery is analyzed. The specific MRI-derived microvascular measures for comparison to histologic grade were the tumor fractional plasma volume (fPV) and the endothelial transfer coefficient (K^{PS}), reflecting the endothelial leakiness of the tumor vessels.

Materials and Methods

This study is based on a retrospective meta-analysis of dynamic macromolecular contrast-enhanced MR data sets from three separate studies, already published, involving a total of 98 chemically induced breast tumors in rodents (5, 8, 9).

A spectrum of mammary tumors, ranging from benign (fibroadenomas) to highly malignant (anaplastic adenocarcinomas) was induced in Sprague-Dawley rats by intraperitoneal injection of N-ethyl-N-nitrosourea (ENU) (10). All tumors, both benign and malignant, were graded using the Scarf-Bloom-Richardson (SBR) histopathologic method (11). The details of animal handling, MR imaging and microscopic grading have been reported previously (5, 8, 9).

Briefly, MR imaging was performed on a Bruker Omega CSI-II System (Bruker Instruments, Fremont, CA) operating at 2 Tesla. Axial T1-weighted three-dimensional (3D)-spoiled gradient recalled (SPGR) sequences were acquired prior to and following contrast agent administration using the following settings: echo time (TE) 1.4 ms, one acquisition, field-of-view 60x60x48 mm, matrix 128x128x16 and an effective slice thickness of 3 mm. Postcontrast images were acquired over a period of at least 40 minutes with an acquisition time of 1 minute 42 seconds per volume of 16 slices. The contrast medium used in all 98 subjects was albumin-(Gd-DTPA)₃₀, 0.03 mmol Gd/kg, a prototype macromolecular contrast medium formulated for blood-pool and permeability-sensitive MR imaging having a molecular weight of 92 kDa (12).

Signal intensity values (SI) for each time point were obtained from regions of interest placed over the inferior vena cava, the whole tumor and the tumor periphery. For the tumor whole

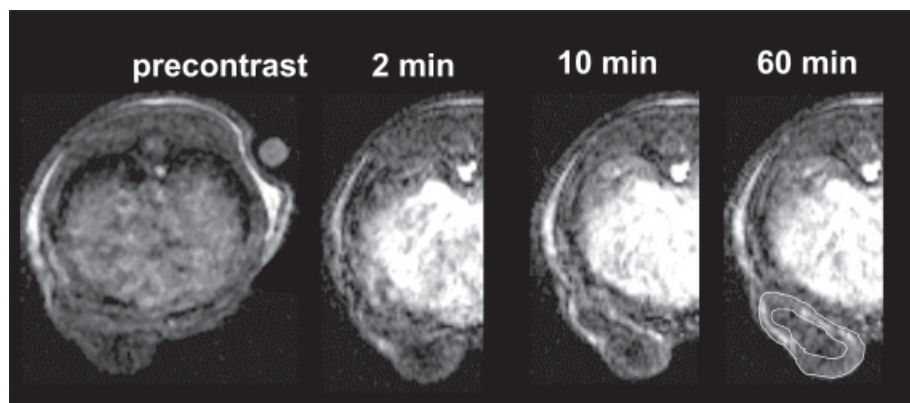


Figure 1. T1-weighted SPGR image of a mammary adenocarcinoma before and 2, 10 and 60 minutes after administration of albumin-(Gd-DTPA)₃₀ (0.03 mmol/kg). A ROI was placed in the periphery of tumor.

and tumor periphery ROIs, three separate ROIs from contiguous sections were averaged and this average was used in subsequent analyses. Based on visual inspection of late post-contrast images, the tumor periphery was defined as the peripheral strongly enhancing zone, typically with a thickness of 1-2 mm (See Figure 1 for a series of tumor enhancement images with a peripheral ROI drawn on the late post-contrast image). Tumors ranged in diameter from 1.0 to 1.5 cm. SI values from three regions of interest (each with a minimum of 30 pixels), obtained from the whole tumor and regions of peripheral tumor enhancement were averaged at each time point and the mean SI was used for calculating longitudinal relaxation rates ($R1=1/T1$). The SI data were converted to $\Delta R1$ values as previously described (5). The difference between the postcontrast $R1$ value at any time point and the precontrast $R1$, $\Delta R1(t)$ was assumed to be directly proportional to the gadolinium concentration of the tissue. The $\Delta R1$ data from blood and tumor were used for kinetic analysis to estimate the endothelial transfer coefficient, K^{PS} ($\text{ml min}^{-1} 100 \text{ cc}^{-1}$ of tissue), and fractional plasma volume fPV (ml cc^{-1} of tissue), employing a two compartment bi-directional model for tumor tissue (5). The model describes the kinetic behavior of contrast agent in tumor tissue and is composed of equilibrating pools of plasma and interstitial water spaces (the exchange between the compartments is assumed to be based on passive diffusion). In this model, a bi-exponential function fitted to the $\Delta R1$ data from blood was used as an input function for the plasma response in the tumor tissue, after scaling for fractional plasma volume.

Nonparametric Spearman correlation analyses were performed, comparing the estimated MR-derived parameters (K^{PS} and fPV) based upon kinetic analysis of data from the tumor periphery and from the whole tumor with the quantitative histologic tumor grade (SBR score). The SBR score was defined pathologically based on whole tumor microscopic interrogation for gland formation, anaplasia and mitoses in the most mitotically active areas, corresponding to the MR slices. All tumors were sectioned in the plane of the MR images. Each of these three morphologic features is score by assigning 1 to 3 points and an overall score is obtained by summation of the scores in each category. The lowest SBR score is 3 (even for a benign tumor), the highest is 9; the higher the SBR score, the more poorly differentiated and malignant the tumor. The SBR score and the pathologic diagnosis of

malignancy are somewhat independent variables and subject to the judgment of a pathologist. The statistical significance of the differences in correlations was assessed by calculating bias-corrected, accelerated bootstrap confidence intervals for each difference (13), using 2000 bootstrap iterations. The p-value was defined as one minus the largest confidence level for which the corresponding interval still excluded zero (no difference), and was reported as $p < 0.001$ if zero was excluded no matter what level was chosen.

Results

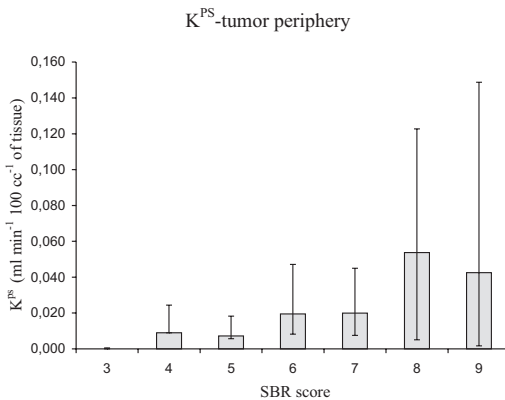


Figure 2. Bar graphs depict median (height of the box) and the 25th and the 75th quartiles of MRI-estimated endothelial transfer coefficient in tumor periphery, K^{PS} -tumor periphery (ml min⁻¹ 100 cc⁻¹ of tissue) as a function histopathologic tumor grade, assayed using Scarff-Bloom-Richardson (SBR) score.

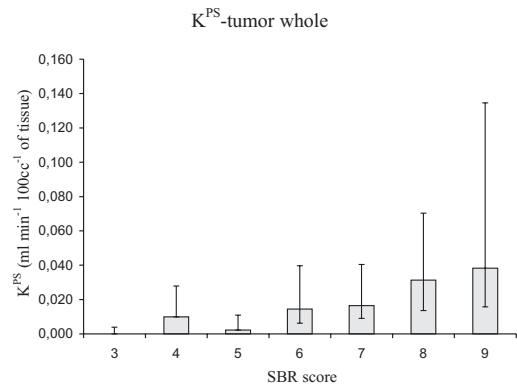


Figure 3. Bar graphs depict median (height of the box) and the 25th and the 75th quartiles of MRI-estimated endothelial transfer coefficient in tumor whole, K^{PS} -tumor whole (ml min⁻¹ 100 cc⁻¹ of tissue) as a function histopathologic tumor grade, assayed using Scarff-Bloom-Richardson (SBR) score.

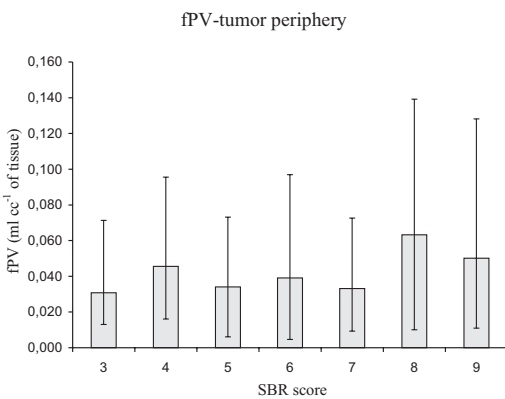


Figure 4. Bar graphs depict median (height of the box) and the 25th and the 75th quartiles of MRI-estimated fractional plasma volume in tumor periphery, fPV-tumor periphery (ml cc⁻¹ of tissue) as a function histopathologic tumor grade, assayed using Scarff-Bloom-Richardson (SBR) score.

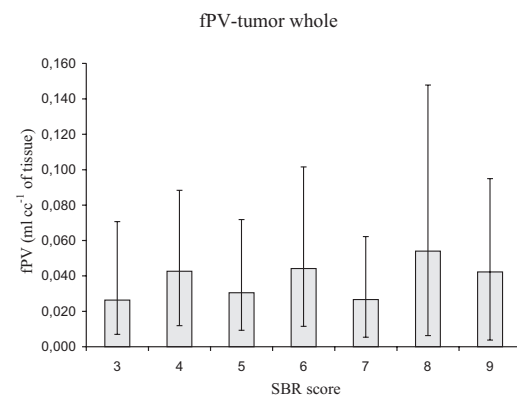


Figure 5. Bar graphs depict median (height of the box) and the 25th and the 75th quartiles of MRI-estimated fractional plasma volume in whole tumor, fPV-tumor whole (ml cc⁻¹ of tissue) as a function histopathologic tumor grade, assayed using Scarff-Bloom-Richardson (SBR) score.

	Correlation coefficient (r)	p value*
K ^{PS} -Tp with SBR	0.784	< 0.0001
K ^{PS} -Tw with SBR	0.604	< 0.0001
fPV-Tp with SBR	0.368	0.0002
fPV-Tw with SBR	0.323	0.001

* Probability of null hypothesis, i.e. $r=0$

Table 1. Correlation with the histologic tumor grade (SBR score) of MRI-derived endothelial transfer coefficient (K^{PS}) and fractional plasma volume (fPV) based on analysis of the whole tumor (Tw) or the tumor periphery (Tp).

Difference between r coefficients	p value
(K ^{PS} -Tp with SBR) versus (K ^{PS} -Tw with SBR)	< 0.001
(K ^{PS} -Tp with SBR) versus (fPV-Tp with SBR)	< 0.001
(K ^{PS} -Tw with SBR) versus (fPV-Tw with SBR)	< 0.01
(fPV-Tp with SBR) versus (fPV-Tw with SBR)	0.32

Table 2. The Differences Between Correlation Coefficients.

The tumor K^{PS} and fPV values from the tumor periphery and whole tumor for each SBR score are shown in *Figures 2 to 5*. The Spearman correlation coefficients between histologic tumor grade, quantitatively reflected in the SBR score, and the MRI-derived microvascular assays of K^{PS} and fPV from the whole tumor and from the tumor periphery are presented in *Table 1*. The differences between the correlation coefficients are shown in *Table 2*. Assays of microvascular permeability (K^{PS}) derived from the tumor periphery correlated significantly more strongly ($r=0.784$, $p < 0.001$) with the tumor histologic SBR score than did K^{PS} estimates derived from the whole tumor ($r=0.604$). Fractional plasma volume (fPV) estimated from the dynamic enhancement response correlated weakly but significantly with the tumor grade, either from regions of interest in the periphery ($r=0.368$, $p < 0.001$) or from the whole tumor ($r=0.323$, $p=0.001$); these fPV correlation coefficients did not differ significantly from each other ($p=0.32$). Both correlation coefficients between the K^{PS} and SBR score derived from the tumor periphery and from the whole tumor were significantly greater than either correlation coefficients of the fPV with the SBR score ($p < 0.01$).

Discussion

The summed experience from 98 MRI experiments gathered from three separate studies shows that MRI derived estimates of endothelial transfer coefficient (K^{PS}) provide significantly stronger correlations with histologic tumor grade than do assays of fractional plasma volume. Furthermore, K^{PS}-based correlation coefficients are improved significantly if the region of interest chosen for analysis is limited to the tumor periphery. Accordingly, MRI-based microvascular characterizations might preferentially consider data from the

tumor periphery, particularly for estimating tumor grade. Other investigators have cited a preference for analysis of the tumor periphery in their efforts to characterize pathology or drug effects, but this preference has been largely based on intuition and the qualitative observation that the rim enhances more strongly than the core of tumors. But this is the first quantitative demonstration that analysis of the tumor periphery provides a measurably superior correlation with a quantitative ex-vivo tumor property, namely, Scarff-Bloom-Richardson histologic grade. Pham and coworkers observed a larger decline in apparent permeability in the tumor periphery than in the tumor whole in xenograft human breast cancers treated with an angiogenesis inhibitor, but this observation was based on comparisons in less than 10 tumors (14). Ma and coworkers (7), in their analysis of clinical musculoskeletal masses observed that the rates of rim-to-center differential enhancement were higher in malignant than in benign lesions. However, the current study is the first to our knowledge to directly address the issue of whether any definable portion of a tumor provides an advantage for quantitative tumor characterization.

Multiple factors likely contribute to the superior correlation of K^{PS} from tumor periphery with histologic grade. The tumor enhancement pattern varies with the degree of necrosis, cell density, interstitial pressure and blood flow. Lacking good lymphatic drainage, malignant tumors consistently show a marked central elevation in the interstitial pressure, much higher than in the periphery, “where it drops precipitously” according to Jain (15). Thus, accordingly to physiological principles, the diffusion (movement of molecules from an area of high concentration to an area of lower concentration) of water and solutes through the vessel endothelial barrier into the interstitium is inhibited in the center of the tumor. Jain stated that in the inner zone of tumors, the interstitial pressure is elevated and about equal to that in the blood vessels; hence convection (transport of molecules by a stream of flowing fluid from areas of high pressure to areas of low pressure) virtually ceases. By contrast, the contribution to transendothelial transport of diffusion is not directly influenced by pressure considerations. Jain reported that the interstitial pressure in the normal breast tissue is about 0.0 mm Hg, while the mean in eight breast carcinomas was 15 mm Hg (15). Even if the volume of blood in the tumor core is not substantially different from that in the tumor rim, as suggested by our results, the transendothelial convection-driven leak of macromolecular contrast medium should be less in the center due to the higher interstitial pressure. The advancing margin of the tumor, the periphery, is also the front-line site of angiogenesis; where vessels from the host tissue, under the influence of tumor secreted angiogenic factors, sprout new vascular buds leading to an augmented vascular supply for the tumor. This zone of most active growth and angiogenic activity, and consequently vessel immaturity, may thus display the greatest leak of contrast medium.

Although the spectrum of breast tumor pathology induced by ENU is generally parallel to the pathology spectrum of human breast tumors (10), the results from an experimental subcutaneous rat breast tumor model may not translate completely to human tumors. Another limitation derives from the subjectivity and potential variability of a user-defined ROI as employed in this study for the tumor periphery. Although in the selection of ROI special care was taken to select the zone of contrast enhancement in the tumor periphery, a certain degree of observer-dependent variability can not be completely excluded. The report of Liney and coworkers (16) suggests that a semi-automated method for ROI

definition might be less subject to variability. In their study, a user-defined ROI was used to subsequently analyze the selected region on a pixel-by pixel basis to establish two additional automated ROIs (one by determining pixels within 10% of the maximum pixel intensity, the other by selecting the area of greatest enhancement using a 9-pixel square mask). Yet, another approach that could be used is the interrogation of tumors on a pixel-by-pixel basis.

Quantitatively analyzed MR data obtained from ROI limited to the tumor periphery correlated significantly better with the tumor histologic grade than did analysis from ROI covering the whole tumor cross-section. Correlations were stronger using K^{PS} than using fPV. Based on these results, future efforts to characterize tumor grade based on MRI analysis should focus on ROI confined to the tumor periphery, at least as a major component in a more complete analysis.

Acknowledgements

Supported by funds received from the National Cancer Institute, grant CA82923 and from the Cancer Research Fund, State of California, under interagency agreement 97-12013 (University of California contract 98-00924V). Anda Preda was supported in part by the “Drie Lichten” and the “Johan Vermeij” Foundations, the Netherlands.

References

1. Tofts PS, Berkowitz B, Schnall MD. Quantitative analysis of dynamic Gd-DTPA enhancement in breast tumors using a permeability model. *Magn Reson Med* 1995;33:564-568.
2. Hoffmann U, Brix G, Knopp MV, et al. Pharmacokinetic mapping of the breast - a new method for dynamic MR mammography. *Magn Reson Med* 1995;33:506-514.
3. Hulka CA, Smith BL, Sgroi DC, et al. Benign and malignant breast lesions differentiation with echo-planar MR imaging. *Radiology* 1995;197:33-38.
4. Hulka CA, Edmister WB, Smith BL, et al. Dynamic echo-planar imaging of the breast: experience in diagnosing breast carcinoma and correlation with tumor angiogenesis. *Radiology* 1997;205:837-842.
5. Daldrup H, Shames DM, Wendland M, et al. Correlation of dynamic contrast-enhanced MR imaging with histologic tumor grade: comparison of macromolecular and small-molecular contrast media. *Am J Roentgenol* 1998;171:941-949.
6. Gribbestad IS, Nilsen G, Fjosne HE, et al. Comparative signal intensity measurements in dynamic Gadolinium-enhanced MR mammography. *J Magn Reson Imaging* 1994;4:477-480.
7. Ma LD, Frassica FJ, McCarthy EF, et al. Benign and malignant musculoskeletal masses: MR imaging differentiation with rim-to-center differential enhancement ratios. *Radiology* 1997;202:739-744.
8. Turetschek K, Huber S, Floyd E, et al. MRI Characterization of microvessels in experimental breast tumors using a particulate contrast agent with histopathologic correlation. *Radiology* 2001;218:562-569

9. Turetschek K, Floyd E, Shames DM, et al. Assessment of a rapid clearance blood pool MR contrast medium (P792) for assays of microvascular characteristics in experimental breast tumors with correlations to histopathology. *Magn Reson Med* 2001;45:880-886
10. Stoica G, Koestner A, Capen CC. Neoplasms induced with high single doses of N-ethyl-N-nitrosourea in 30-day-old Sprague-Dawley rats, with special emphasis on mammary neoplasia. *Anticancer Res* 1984;4:5-12.
11. Le Doussal V, Tubiana-Hulin M, Friedman S, et al. Prognostic value of histologic grade nuclear components of Scarff-Bloom-Richardson (SBR). An improved score modification based on a multivariate analysis of 1262 invasive ductal breast carcinomas. *Cancer* 1989;64:1914-1921.
12. Ogan MD, Schmiedl U, Moseley ME, et al. Albumin labeled with Gd-DTPA. An intravascular contrast-enhancing agent for magnetic resonance blood pool imaging: preparation and characterization. *Invest Radiol* 1987;22:665-671.
13. Efron B, Tibshirani RJ. An introduction to the bootstrap. London: Chapman & Hall, Inc.; 1993. pp. 178-188, 214-218, 398-403.
14. Pham CD, Roberts TPL, van Bruggen N, et al. Magnetic resonance imaging detects suppression of tumor vascular permeability after administration of antibody to vascular endothelial growth factor. *Cancer Invest* 1998;16:225-230.
15. Jain RK. Barriers to drug delivery in solid tumors. *Sci Amer* 1994;271:58-65.
16. Liney GP, Gibbs P, Hayes C, et al. Dynamic contrast-enhanced MRI in the differentiation of breast tumors: User-defined versus semi-automated region-of-interest analysis. *J Magn Reson Imaging* 1999;10:945-949.

CHAPTER 4

ASSESSMENT OF A RAPID CLEARANCE BLOOD POOL
MR CONTRAST MEDIUM (P792) FOR ASSAYS OF
MICROVASCULAR CHARACTERISTICS IN EXPERIMENTAL
BREAST TUMORS WITH CORRELATIONS TO HISTOPATHOLOGY

ASSESSMENT OF A RAPID
CLEARANCE BLOOD POOL MR
CONTRAST MEDIUM (P792) FOR
ASSAYS OF MICROVASCULAR
CHARACTERISTICS IN
EXPERIMENTAL BREAST TUMORS
WITH CORRELATIONS TO
HISTOPATHOLOGY

(MAGNETIC RESONANCE IN MEDICINE 2001, 5:880-886)

Karl Turetschek,^{1,2} Eugenia Floyd,³ David M. Shames,¹ Timothy P.L. Roberts,¹
Anda Preda,^{1,4} Viktor Novikov,¹ Claire Corot,⁵ Wayne O. Carter,³ and Robert C. Brasch¹

¹ Center for Pharmaceutical and Molecular Imaging, Department of Radiology, University of California-San Francisco, San Francisco, California.

² Department of Radiology, University of Vienna, Vienna, Austria.

³ Pfizer Central Research, Groton, Connecticut.

⁴ Visiting Research Scholar from the Department of Radiology, Erasmus University Medical Center, Rotterdam, The Netherlands.

⁵ Guerbet Laboratories, Roissy, France.

Abstract

The diagnostic potential of a new rapid clearance blood pool contrast medium (P792; MW = 6.47 kDa) for the MR assessment of microvessel characteristics was assessed in 42 chemically-induced breast tumors, with comparisons to albumin-(Gd-DTPA). Microvessel characteristics, including the transendothelial permeability (K^{PS}) and the fractional blood volume (fPV), were estimated by using dynamic MR data fit to a bidirectional two-compartment model. The MR-derived estimates for K^{PS} and fPV using each contrast agent were compared, and assays using each contrast agent were correlated to the histologic tumor grade (SBR score) and the microvascular density (MVD) counts. Using P792-enhanced data, neither K^{PS} nor fPV showed a statistically significant correlation with the tumor grade or the MVD ($P > .05$). Conversely, using albumin-(GdDTPA)₃₀, K^{PS} values correlated significantly with the histologic tumor grade ($r = .55$; $P < .0005$) and the MVD ($r = .34$, $P < .05$), whereas no correlation was established for fPV. In conclusion, based on P792 data no correlation between tumor microvascular characteristics and histologic markers (SBR score or MVD) was found in this breast tumor model. Our analysis suggests that contrast media of relatively large (on the order of 90 kDa) molecular size, such as albumin-(GdDTPA)₃₀, are more accurate for the characterization of tumor microvessels.

Key words

Magnetic resonance imaging; breast neoplasm; contrast media; histologic tumor grade; microvascular permeability

Introduction

MRI is becoming a dominant imaging method for characterizing tumors both morphologically and functionally. Kinetic analyses of dynamic contrast-enhanced MRI data within the context of a physiologically-based mathematical model of endothelial permeability provide valuable information about tumor microvessel properties, including a measure of transendothelial permeability (K^{PS}) and fractional plasma volume (fPV). Estimates of K^{PS} and fPV serve to define the status of tumor microvasculature and quantitatively reflect the state of tumor angiogenesis (1-5), and thus offer the potential for delineation of the individual biological characteristics of any given tumor. New strategies in cancer therapy already include the inhibition of tumor angiogenesis; therefore, reliably defining tumor microvessels by contrast-enhanced MRI could represent a major improvement for the management of tumor patients. Definition of tumor biological characteristics could also have an impact on cancer therapy, particularly for treatments directed against angiogenesis. The form of therapy may hinge upon knowledge of tumor properties, and therapy response may be well reflected in MRI-defined characteristics. The definition and choice of well-designed contrast media for MRI tumor characterization remains an area of intense investigation.

Tumor microvessels consistently demonstrate impaired endothelial barrier integrity and are "leaky" to macromolecular solutes, including macromolecular contrast media (MMCM) (5-8). The capacity of MMCM-enhanced MRI to assess microvascular characteristics has

been demonstrated in a variety of disease models and tumor types (1,9-13). In several studies, albumin-(GdDTPA)₃₀ has been used successfully as a prototype MMCM, but its potential immunologic properties and its prolonged retention limits its potential for development as a clinical MRI contrast medium (14). Accordingly, there remains an unfulfilled goal for a safe MMCM capable of fulfilling pharmacologic and enhancement requirements. Some of the MR compounds now under development have potential as MRI probes for assaying endothelial permeability and plasma volume.

P792, which is representative of a rapid clearance blood pool agent (RCBPA), was tested in this study to define its potential to characterize tumor microvessels (15,16). Results were correlated with histopathology, notably tumor grade and microvascular density (MVD) counts. These correlations were then compared to results achieved in the same tumors with albumin-(GdDTPA)₃₀, which was used as a reference but is larger than most MMCMs.

Methods

Animal Model

The study was conducted under the guidelines of the Committee of Animal Care according to regulations in the Guide for the Care and Use of Laboratory Animals, DHHS Publication NIH 86-23, 1985, and the Instructions to Use Vertebrate Animals in Research (7/1/92).

Forty-two female Sprague Dawley rats, 4 - 6 weeks old, weighing 160-360 g, were purchased from Harlan (Indianapolis, IN). Breast tumors were induced chemically by intraperitoneal (ip) injection of N-ethyl-N-nitrosurea (ENU) (Isopack, St. Louis, MO) (17,18) under ether anesthesia using doses ranging from 45-250 mg/kg (45 mg: *N* = 1; 90 mg: *N* = 2; 180 mg: *N* = 9; and 250 mg: *N* = 30).

Rats were inspected daily for tumor growth and general appearance. Animals were examined by MRI when the tumors reached a size of 1.5-2 cm. Before MRI, animals were anesthetized with an ip injection of 50 mg/kg BW pentobarbital. A 23-gauge butterfly (Abbott Laboratories, Chicago, IL) was inserted into the tail vein for contrast media injection. Animals were placed supine on a heated water pad within the imaging coil; body temperature during imaging was monitored for stability with a rectal thermometer. Immediately after imaging, 2 ml of saline was injected subcutaneously to prevent dehydration effects.

MRI

Imaging was performed using a CSI-II Omega spectrometer operating at 2.0 T (Bruker Instruments, Fremont, CA) and equipped with Acustar S-150 self-shielded gradient coils (± 20 G/cm, 15-cm inner diameter). Rats were placed supine in a birdcage radiofrequency coil with a length of 7.6 cm and an inner diameter of 4.5 cm. A phantom filled with diluted 0.01 mmol/L gadopentetate dimeglumine was positioned in the field of view (FOV) to correct for potential spectrometer variation. Precontrast T1-weighted spoiled

gradient-recalled (SPGR) images were obtained for calculation of the T_1 relaxation times with the following parameters: TR = 100 ms, TE = 1.4 ms, 1 scan average, matrix = 128 X 128 X 16, FOV = 60 X 60 X 48, 3-mm slice thickness. Four different flip angles ($\alpha = 10^\circ, 30^\circ, 60^\circ$, and 90°) were used, and T1 was determined by curve fitting to the following:

$$SI = kM_0 (1 - \exp^{-TR/T_1}) \sin(\alpha) / (1 - \cos(\alpha) \exp^{-TR/T_1}) \quad [1]$$

where SI is the signal intensity, α the flip angle, TR the sequence repeat time, and kM_0 a constant related to magnetization density (19). Dynamic contrast-enhanced MRI was performed using a T1-weighted 3D-SPGR sequence with a keyhole technique consisting of three initial precontrast and 17 dynamic postcontrast images with the following parameters: TR = 50 ms, TE = 1.4 ms, $\alpha = 90^\circ$, one signal acquired, matrix = 64 x 64 x 8, FOV = 60 X 60 X 48, 3-mm slice thickness, and an acquisition time of 6 s per image. These “keyhole”-acquired images were reconstructed to high resolution using the baseline k-space data acquired in the precontrast images described above. The high temporal resolution keyhole images were immediately followed by 20 dynamic 3D-SPGR postcontrast images with a higher spatial resolution (128 x 128 x 16 matrix), acquisition time = 1 min 42 s/sequence. The total examination time was 45 min.

MR Contrast Media

P792 (research product; Fig. 1), is formulated to contain a single gadolinium ion in a four-armed organic chelate. P792 has a molecular weight of 6.47 kDa, a plasma half-life in rats of about 20 min, and an R_1 relaxivity of $39 \text{ s}^{-1}\text{mM}^{-1}$, at 20 MHz and 37°C (20). The volume of distribution is 101 ml.kg^{-1} .

P792 is well tolerated in animals (LD_{50} in rats $>1.88 \text{ mmol/kg}$, maximal injected volume) and is eliminated by glomerular filtration in the kidney. P792 (Guerbet Laboratories, Roissy, France) was administered intravenously at a dose of $15 \mu\text{mol Gd/kg}$ based on enhancement of tumors and blood evaluated in pilot studies.

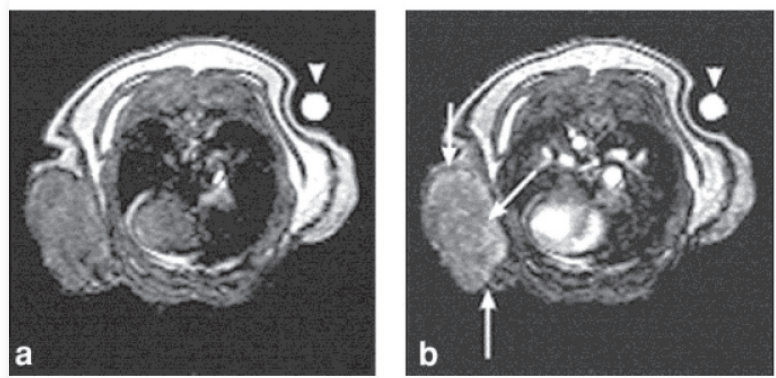


Fig. 1: Representative axial T1-weighted (TR = 50 ms, TE = 1.4 ms) SPGR images of a subcutaneous malignant mammary tumor (a) before and (b) 30 min after administration of P792 ($15 \mu\text{mol Gd/kg}$) showing a typical rim enhancement on the postcontrast image (arrow) (b). A phantom was placed in the FOV (arrowhead) to serve as an intensity reference.

One day following P792 administration, repeat MRI enhanced with albumin-(GdDTPA)₃₀ was performed. Albumin-(GdDTPA)₃₀, a prototype MMCM with a molecular weight of 92000 Daltons, was administered at a dose of 0.03 mmol Gd/kg. It demonstrates a volume of distribution that closely approximates plasma volume, 0.05 L/kg, and plasma half-life is approximately 3 hr, yielding nearly constant enhancement of blood and normal tissues for 30 min or longer after injection (14,21,22). Albumin-(GdDTPA)₃₀ has an R_1 relaxivity of $19.6 \text{ s}^{-1}\text{mM}^{-1}/\text{Gd}$ at 2 T and 37°C (21).

MRI Data and Kinetic Analysis

Imaging data were transferred, processed, and analyzed on a Sun Sparc 10 workstation (Sun Microsystems, Mountain View, CA) using an image analysis program (The MR-Vision Co, Menlo Park, CA). Signal intensity values at each time point were obtained from regions of interest (ROIs) placed in the phantom, in the inferior vena cava (IVC), and in the tumor periphery. Signal intensities (SI) from the tumor and the IVC blood were corrected for potential spectrometer variation over time by dividing the SI at each time point by the SI of the phantom. SIs from three ROIs taken when feasible from different sections of each tissue of interest were averaged, and the mean SI was used as a basis for further calculations. Postcontrast R_1 values were calculated based on the measured SI and knowledge of precontrast R_1 values according to:

$$R_{1\text{post}} = -1/\text{TR} \log[1 - S_{\text{post}}/S_{\text{pre}}(1 - \exp(-\text{TR} R_{1\text{pre}}))] \quad [2]$$

which is an approximation that ignores T_2^* effects since we used a short TE (23). Differences between the precontrast and postcontrast R_1 values (ΔR_1) at all time points were assumed to be directly proportional to the gadolinium concentration in the tissue of interest, as predicted by the Solomon-Bloembergen equations and shown in several experimental studies (24,25).

The ΔR_1 data from blood and tumor were used for kinetic analysis to estimate the coefficient of transendothelial permeability, K^{PS} ($\text{ml min}^{-1}100 \text{ cc}^{-1}$ of tissue), and the fractional plasma volume, fPV (ml cc^{-1} of tissue) employing a two-compartment bidirectional model for tumor tissue (2). In this model a monoexponential function fitted to the ΔR_1 data from blood (sufficient to describe the blood disappearance for each contrast agent for 45 min following intravenous bolus injection) was used as a forcing function for the plasma response in the tumor, after scaling for fractional plasma volume. In the analysis of the albumin (GdDTPA)₃₀ data, the reflux rate constant of the model was not resolvable, and was therefore set to zero. All data fitting was performed using the SAAM II program (SAAM Institute, Seattle, WA) employing a weighted, nonlinear least-squares parameter estimation algorithm. Measurement errors were assumed to be independent and Gaussian with zero mean and standard deviation known with a scale factor determined from the data. Weights were chosen optimally, i.e., equal to the inverse of the variance of the measurement error. The uncertainty of our estimates of fPV and K^{PS} were determined from the covariance matrix of the least-squares fit. For convenience of presentation, the K^{PS} values determined from the model were multiplied by 100 for both contrast agents.

Histologic Analysis

Immediately after the second MRI session, animals were killed by an intravenous overdose of pentobarbital and bilateral thoracotomies. Tumors were resected, fixed in 10% buffered formalin (Poly Scientific Research & Development Corp., Bay Shore, NY), processed routinely into paraffin, sectioned in the plane of the MR images at 4 μ m, and stained with hematoxylin and eosin for diagnosis and grading. Additional sections were immunostained for von Willebrand Factor/Factor VIII using an avidin-biotin peroxidase technique (Sigma rabbit antihuman polyclonal, F-3520; Vector ABC kit, PK-6100) and sent to the pathologist for further analyses. Tumors were graded according to the Scarff-Bloom-Richardson (SBR) method (26-29). This grading system has been used extensively for invasive breast adenocarcinomas by evaluating the ductoglandular formation, nuclear pleomorphism, and mitotic activity. Each of these three morphological features is scored by assigning one, two, or three points. An overall score is then obtained by summation of the individual characteristic scores. SBR scores range from 3 to 9 points; the higher the score, the more malignant and more poorly differentiated is the tumor. For microvascular count determination, all discrete, positively immunostained endothelial (brown-staining) clusters with lumina were counted in 20 400x fields (Olympus Vanox AH-2 microscope) sampled from two sections of each tumor preparation. Where possible, fields were chosen in areas of highest MVD. Stromal microvessels were included in the counts, but capsular and preexisting host small-to-medium vessels were excluded. MVD is reported as the number of vessels per 20 high-powered fields. MVD and SBR scoring were performed by the same pathologist, without knowledge of MRI findings.

Statistics

Mean values for K^{PS} and $fPV \pm SD$ for a given contrast agent were compared between fibroadenomas and carcinomas using unpaired t-tests. Nonparametric Spearman correlation analyses were performed comparing the estimated MRI-derived parameters (K^{PS} and fPV) with the histologic tumor grade (SBR score). Pearson correlation analyses were performed comparing the albumin-(GdDTPA)₃₀- and P792-derived values for K^{PS} and fPV , and for correlating these values to the MVD. A *P* value < .05 was considered statistically significant.

Results

Forty-two animals developed subcutaneous tumors within our study period: nine benign (fibroadenomas) and 32 tumors (31 adenocarcinomas, and one sarcoma arising in a fibroadenoma). After administration of ENU tumors appeared in the mammary fat pad as early as 59 days, with a mean latency of 176 ± 121 days. Benign tumors had a significantly (*P* < .05) longer latency than malignant tumors (292 ± 113 vs. 145 ± 104 days, respectively). There was a weak but statistically significant correlation between the dose of ENU and the tumor grade, as reflected in the SBR score (*r* = .13, *P* < .05). Less differentiated tumors (higher SBR score) tended to develop with larger ENU doses; however, fibroadenomas having the lowest SBR scores possible, score 3, were observed after a range of ENU doses from 45 to 250 mg/kg.

MRI examinations enhanced with both contrast agents were completed successfully in 40 animals. For two animals, only P792 data were available, but these data were still included in the analyses. The kinetic model fit the data well in all experiments, with typical fits to albumin-(GdDTPA)₃₀ and P792 data shown in Fig. 2a and b, respectively. All parameter values were obtained with good precision. The mean coefficients of variation (CV) for fPV and K^{PS} were 10% and 24%, respectively, for albumin-(GdDTPA)₃₀, and 6% and 10%, respectively, for P792. Small K^{PS} values for albumin-(GdDTPA)₃₀ with CVs greater than 100% were assumed to be not resolvable from the data, and were set equal to 0.

The tumor K^{PS} and fPV values derived using P792 and albumin-(GdDTPA)₃₀ with the corresponding SBR and MVD scores are shown in Table 1.

Using P792, no significant difference was found between the mean K^{PS} values for the carcinomas and fibroadenomas ($.539 \pm .354$ vs. $.535 \pm .271$, $P = .97$). Making the parallel comparison for fractional plasma volumes assayed with P792, the difference between

malignant and benign tumors was not significant ($.040 \pm .024$ vs. $.024 \pm .009$, $P = .07$). However, in the same tumors evaluated using albumin-(GdDTPA)₃₀, mean K^{PS} values were significantly higher in the carcinomas compared to the fibroadenomas ($.014 \pm .011$ vs. $0 \pm .001$, $P < .005$). Making the parallel comparison using fPV obtained with albumin-(GdDTPA)₃₀, the difference between carcinomas and fibroadenomas was not significant ($.038 \pm .019$ vs. $.030 \pm .013$, $P = .33$).

As shown in Table 2, fPV values assayed with P792 for both benign and malignant tumors taken together did not correlate significantly with the histologic tumor grade ($r = .25$, $P = .09$) or with the MVD ($r = .20$, $P = .20$).

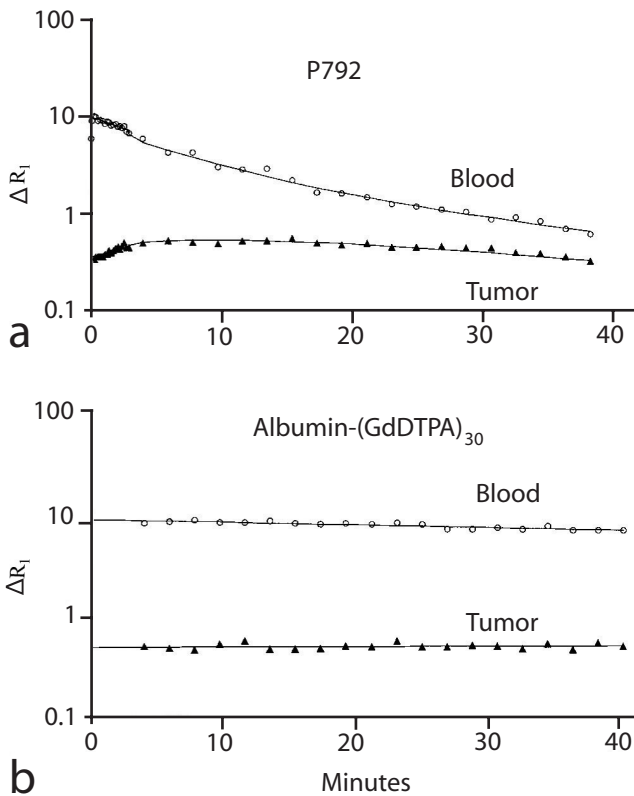


Fig. 2: Typical fits (solid lines) of dynamic mathematical model to ΔR_1 data from (O) blood and (▲) tumor using (a) P792 and (b) albumin-(GdDTPA)₃₀ contrast media.

Similarly, K^{PS} values based on P792 data did not correlate with the SBR scores ($r = .09$, $P = .46$) or the MVD ($r = .03$, $P = .86$). However, values for K^{PS} derived using albumin-(GdDTPA)₃₀ correlated significantly with the SBR score ($r = 0.55$, $P < .0005$) and the MVD ($r = .34$, $P < .05$). No significant correlations were found between albumin-(GdDTPA)₃₀-derived fPV estimates and the SBR score ($r = .08$, $P = .50$) or MVD ($r = .28$, $P = .08$). As expected, histologic MVD counts were significantly lower in the benign than in the malignant tumors (171.3 ± 112.7 vs. 341.1 ± 130 , $P < .001$). There was no significant correlation between the grade of malignant tumors, as reflected in the SBR score and tumor angiogenesis, as reflected by the MVD ($r = -.29$, $P = .18$).

Discussion

P792, a monomeric 6.47 kDa gadolinium-based contrast medium in clinical development as a rapid clearance blood pool enhancer was not shown in this experimental breast tumor model to be effective for the differentiation of benign from malignant tumors, or for tumor grading. MRI-derived microvascular characteristics (K^{PS} and fPV) estimated from P792-enhanced MRI data did not correlate significantly with pathologic tumor grade or with MVD counts, a surrogate of angiogenesis. In the same group of tumors, the previously shown utility of albumin-(Gd-DTPA)₃₀, 92 kDa, for tumor microvascular grading and characterization was reconfirmed.

Methods to better characterize tumors by noninvasive MRI are being developed on the premise that noninvasive imaging methods can be used effectively to discriminate between tumors of varying biology. Also, tumor imaging characteristics should be useful for guiding the choice of therapy as well as for better evaluating the effects of various therapeutic interventions. Although many characteristics of tumors might reasonably be evaluated by imaging, tumor microvascular properties are of particular interest, and may be uniquely well suited for defining tumor biology and following the effects of therapy. Tumor angiogenesis, the recruitment of new vessels into the tumor, is essential for unrestricted tumor growth and metastases (30,31). In this study we assayed two tumor microvascular properties-specifically, the richness of tumor vascularity expressed quantitatively as the fractional plasma volume (fPV), and the leakiness or permeability of the tumor vessels expressed as the coefficient of endothelial permeability (K^{PS}). The methods and rationale for our K^{PS} and fPV assays have been described previously in detail (2,32). Inherent in the microvascular analytical approach for tumor characterization is the hypothesis that biologically more aggressive tumors, having more active angiogenesis, will have relatively more blood (fPV) and relatively greater microvascular permeability to macromolecules (K^{PS}) than benign or less aggressive tumors. These hypotheses are supported by numerous imaging and invasive studies conducted in a spectrum of tumor types (1,33-35). In fact, the hyperpermeability of malignant tumors to macromolecular solutes has been a reliable and consistent characteristic of neoplastic vessels (7). It is this special property, macromolecular hyperpermeability, that we intend to exploit in our contrast-enhanced MRI method.

Currently, a major challenge for contrast-enhanced MRI is to identify one or more MMCM that can safely be used clinically. The sought-after compounds must be well tolerated, have appropriate pharmacologic properties, and be efficacious for tumor vessel characterization. Albumin-(GdDTPA)₃₀ is a prototype molecule that was previously shown to be effective for tumor microvascular characterizations, but which was never intended for clinical use. It has a relatively high and long retention within the body, and there is also a potential for immunologic reactivity (21). New MMCM candidates must be examined for their diagnostic potential.

SBR scores	Tumor type	MVD	P792		Albumin-(GdDTPA) ₃₀	
			fPV	K ^{PS}	fPV	K ^{PS}
Benign						
3	Fibroadenoma	113	.022	.476	.019	.000
3	Fibroadenoma	195	.034	.322	—	—
3	Fibroadenoma	83	.030	.974	.043	.000
3	Fibroadenoma	448	.029	.553	.046	.000
3	Fibroadenoma	78	.010	.458	.015	.000
3	Fibroadenoma	205	.030	.421	.037	.000
3	Fibroadenoma	152	.011	.081	.034	.001
3	Fibroadenoma	147	.031	.674	.017	.001
4	Fibroadenoma	121	.025	.854	—	—
	Mean	171.3	0.024	0.535	0.030	0.000
	SD	112.7	0.009	0.271	0.013	0.001
Malignant						
3	Carcinoma	309	.017	.319	.032	.010
3	Carcinoma	419	.057	.674	.025	.000
3	Carcinoma ^a	478	.013	.321	.031	.008
4	Carcinoma	590	.038	.451	.036	.009
4	Carcinoma	202	.022	.346	.020	.007
4	Carcinoma ^a	532	.021	.214	.021	.018
4	Carcinoma	427	.032	.399	.038	.012
4	Carcinoma	125	.076	.573	.065	.000
4	Carcinoma	b	.063	.956	.048	.016
4	Carcinoma	393	.031	.180	.049	.009
4	Carcinoma	398	.010	.391	.024	.031
5	Carcinoma	345	.063	.781	.034	.018
5	Carcinoma	414	.038	.452	.034	.011
5	Carcinoma	347	.086	1.261	.065	.000
5	Carcinoma	201	.045	.290	.051	.000
5	Carcinoma	140	.034	.455	.040	.012
5	Carcinoma	459	.037	.613	.036	.029
5	Carcinoma	559	.027	.319	.036	.006
5	Carcinoma	309	.016	.336	.029	.007
6	Carcinoma	193	.023	.141	.021	.014
6	Carcinoma	198	.023	.098	.035	.009
6	Carcinoma	306	.030	.367	.020	.009
6	Carcinoma	206	.019	.463	.031	.022
6	Carcinoma	423	.060	.865	.047	.010
6	Carcinoma	438	.022	.179	.038	.000
6	Carcinoma	231	.027	.478	.025	.013
6	Carcinoma	293	.102	1.163	.034	.025
6	Carcinoma	310	.052	.657	.039	.029
6	Carcinoma	473	.093	1.704	.119	.050
6	Carcinoma	441	.067	.571	.052	.014
7	Carcinoma	418	.031	.315	.040	.028
7	Carcinoma	226	.036	.986	.020	.014
7	Sarcoma ^a	112	.013	.480	.011	.011
	Mean	341.1 ^c	0.040	0.539	0.038	0.014 ^c
	SD	130.0	0.024	0.354	0.019	0.011

SBR, Scarff Bloom Richardson score; MVD, microvascular counts (microvessels per high powered field); fPV, fractional plasma volume (ml cc⁻¹ of tissue); K^{PS}, coefficient of endothelial permeability (ml min⁻¹ 100 cc⁻¹ of tissue).

^aMalignant tumor arising in a fibroadenoma.

^bNo MVD because of autolysis of the sample.

^cStatistically different from benign tumor group; $P < .05$.

Table 1. Tumor Pathology and MRI-Derived Microvessel Characteristics Arranged by Ascending SBR Score.

P792 is a new monodispersed contrast media with a molecular weight of 6.47 kDa, which allows for a relatively rapid blood clearance by glomerular filtration. This rapid clearance from the plasma is reflected in the blood enhancement curve shown in Fig. 2a. Although blood clearance is more rapid and complete than for albumin-(GdDTPA)₃₀, we hypothesized that the P792 macromolecular configuration (approximately 10 times heavier than a molecule of GdDTPA; MW = 557) would prove useful for tumor microvascular characterization. The results obtained in this model did not support this hypothesis, and no significant correlations with SBR and MVD were found using P792. However, fractional plasma volumes using albumin-(GdDTPA)₃₀ and P792 were not significantly different, suggesting that this microvascular property can be monitored with equal success with either contrast agent. P792 may still prove diagnostically useful for certain enhancement applications, such as angiography or evaluations of non-neoplastic lesions. First-pass kinetic analysis using this compound may also have clinical utility. For assessment of tumor microvessel hyperpermeability, our analysis shows a mean K^{PS} value for P792 in malignant tumors that is approximately 39 times greater than the mean K^{PS} values observed in the same tumors for the albumin-based contrast agent. This notably greater permeability of P792 is likely due to its smaller molecular weight and size.

Since P792 is now under clinical investigation, comparison of these experimental data with the results obtained in patients for tumor characterization will be interesting to assess, taking into account that the pharmacokinetics are likely different between rat and human.

The potential clinical utility of assaying microvascular characteristics with an MMCM, specifically albumin-(GdDTPA)₃₀, has been demonstrated for multiple disease processes (neoplasia, inflammation, myocardial and renal ischemia, and reperfusion injury (11-13,36)) as well as for numerous tumor types (prostate, ovary, brain, and breast (1,34-36)). The same ENU-induced tumor model used for this study has been evaluated previously with dynamic albumin-(GdDTPA)₃₀-enhanced MRI (1,36). In all cases, a significant correlation was shown between permeability (K^{PS}) and tumor histologic features, both with MVD counts and SBR scores. The degree of correlation (r value) varies among groups of tumors but has always been statistically significant. In the current study, the observed r value of .55 is less than the .86 value shown in the Daldrup study (1). This difference in degree of correlation may be explained by the respective proportions of low-, medium-, and high-grade tumors. In the current study, there were relatively few high-grade tumors (SBR score 7-9) compared to previously studied groups of tumors. This variation in tumor SBR scores is attributed to simple biological variation in the ENU response in different animals.

Contrast agent	K ^{PS} :SBR	K ^{PS} :MVD	fPV:SBR	fPV:MVD
Albumin-(GdDTPA) ₃₀	0.55 (<i>P</i> < 0.0005) ^a	0.34 (<i>P</i> < .05) ^a	0.08 (<i>P</i> = .50)	0.28 (<i>P</i> = .08)
P792	0.09 (<i>P</i> = .46)	0.03 (<i>P</i> = .86)	0.25 (<i>P</i> = 0.09)	0.20 (<i>P</i> = .20)

^a*P* values < .05 were considered statistically significant.

Table 2: Correlations Between MRI-Estimated Coefficients of Tumor Endothelial Permeability (K^{PS}) and Fractional Plasma Volume (fPV) With Pathologic Scarff-Bloom-Richardson (SBR) Tumor Grades and Microvascular Density Counts (MVD).

There is no single “gold standard” for the biological characterization of a tumor. For this study, the SBR scoring system was selected as an appropriate measure of tumor cell morphology. SBR has been used in numerous previous studies as a breast cancer grading system. It is based upon three elements of tumor cell morphology, each scored separately (26,27). Angiogenesis is considered a distinct and independent prognostic factor from tumor cell morphology. MVD counts were selected for this study as the surrogate of angiogenesis, and have been used widely for this purpose (37-40).

Conclusions

Conclusions from this study are limited in that only one tumor type (breast) was examined, and these tumors were induced chemically in rodents. Alternative doses of P792 might have been tried, but the single dose chosen produced enhancement of the blood comparable to that achieved with albumin-(GdDTPA)₃₀. This study did not adequately examine the potential of P792 enhancement to monitor changes in tumor microvascular characteristics that might result from tumor treatment—for instance, with antiangiogenic chemotherapy. We did not evaluate the angiography properties of this contrast agent.

In summary, kinetic analysis of dynamic P792-enhanced MRI data (using a physiologically-based compartmental model of microvessel permeability) in a rodent breast tumor model showed a lack of feasibility for the differentiation of benign from malignant tumors, and for the image-based grading of tumors corresponding to either tumor cell morphology or microvascular counts. Yet, the feasibility of individually characterizing the microvessels of tumors and for tumor differentiation was confirmed in the same tumors using a larger prototype MMCM. Clinical investigations will be helpful in better defining the level of selectivity needed for tumor characterization.

Acknowledgments

Karl Turetschek was supported by the Erwin Schrodinger Auslandsstipendium, Austria, grant. Anda Preda was supported by the De Drie Lichten and Johannes Vermeij foundations, The Netherlands.

References

1. Daldrup H, Shames DM, Wendland M, Okuhata Y, Link TM, Rosenau W, Lu Y, Brasch RC. Correlation of dynamic contrast-enhanced MR imaging with histologic tumor grade: comparison of macromolecular and small-molecular contrast media. *AJR Am J Roentgenol* 1998;171: 941-949.
2. Shames DM, Kuwatsuru R, Vexler V, Muhler A, Brasch RC. Measurement of capillary permeability to macromolecules by dynamic magnetic resonance imaging-a quantitative noninvasive technique. *Magn Reson Med* 1993;29:616-622.
3. Su M-Y, Wang Z, Carpernter PM, Lao X, Muhler A, Nalcioğlu O. Characterization of N-ethyl-N-nitrosourea-induced malignant and benign breast tumors in rats by using three MR contrast agents. *J Magn Reson Imaging* 1999;9:177-186
4. Su MY, Najafi AA, Nalcioğlu O. Regional comparison of tumor vascularity and permeability parameters measured by albumin-Gd-DTPA and Gd-DTPA. *Magn Reson Med* 1995;34:402-411.
5. Brasch R, Pham C, Shames D, Roberts T, van Dijke K, van Bruggen N, Mann J, Ostrowitzki S, Melnyk O. Assessing tumor angiogenesis using macromolecular MR imaging contrast media. *J Magn Reson Imaging* 1997;7:68-74.
6. Gerlowski LE, Jain RK. Microvascular permeability of normal and neoplastic tissues. *Microvasc Res* 1986;31:288-305.
7. Dvorak H, Nagy J, Dvorak J, Dvorak A. Identification and characterization of the blood vessels of solid tumors that are leaky to circulating macromolecules. *Am J Pathol* 1988;133:95-109.
8. Jain R. Transport of molecules across tumor vasculature. *Cancer Met Rev* 1987;6:559-593.
9. Berthezène Y, Vexler V, Kuwatsuru R, Rosenau W, Mühler A, Clément O, Price DC, Brasch RC. Differentiation of alveolitis and pulmonary fibrosis with a macromolecular MR imaging contrast agent. *Radiology* 1992;185:97-103.
10. Schwickert H, Stiskal M, Roberts T, van Dijke C, Mann J, Mühler A, Shames D, Demsar F, Disston A, Brasch R. Contrast enhanced MR imaging of tumor capillary permeability: effect of irradiation on delivery of chemotherapy. *Radiology* 1996;198:893-898.
11. van Dijke CF, Kirk BA, Peterfy CG, Genant HK, Brasch RC, Kapila S. Arthritic temporomandibular joint: correlation of macromolecular contrast-enhanced MR imaging parameters and histopathologic findings. *Radiology* 1997;204:825-832.
12. Saeed M, van Dijke CF, Mann JS, Wendland MF, Rosenau W, Higgins CB, Brasch RC. Histologic confirmation of microvascular hyperpermeability to macromolecular MR contrast medium in reperfused myocardial infarction. *J Magn Reson Imaging* 1998;8:561-567.
13. Helbich T, Roberts TPL, Rollins MD, Shames DM, Turetschek K, Hopf HW, Muehler M, Hunt TK, Brasch RC. Non-invasive assessment of wound healing angiogenesis with contrast enhanced MRI. In: Bettmann MA, Brasch RC, editors. *Book of Abstracts, Contrast Media Research*. Woodstock, Vermont; 1999.
14. Schmiedl U, Brasch RC, Ogan MD, Moseley ME. Albumin labeled with Gd-DTPA. An intravascular contrast-enhancing agent for magnetic resonance blood pool and perfusion imaging. *Acta Radiologica Suppl* 1990;3 74:99-102.
15. Port M, Meyer D, Bonnemain B, Corot C, Schaefer M, Rousseaux O, Simonot C, Bourrinet P, Benderbous S, Dencausse A, Devoldere L. P760 and P775: MRI contrast agents characterized by new pharmacokinetic properties. *MAGMA* 1999;8:172-176.

16. Bourasset F, Dencausse A, Bourrinet P, Ducret M, Corot C. Comparison of plasma and peritoneal concentrations of various categories of MRI blood pool agents in a murine experimental pharmacokinetic model. *MAGMA* 2001, in press.
17. Stoica G, Koestner A. Diverse spectrum of tumors in male Sprague Dawley rats following single high doses of N-ethyl-N-nitrosurea (ENU). *Am J Pathol* 1984;319-325.
18. Stoica G, Koestner A, Capen C. Neoplasms induced with high single doses of N-ethyl-N-nitrosurea in 30 day-old Sprague Dawley rats, with special emphasis in mammary neoplasia. *Anticancer Res* 1984;4:5-12.
19. Haase A, Frahm J, Matthai D, Haenicke W, Merboldt K. FLASH imaging: rapid NMR imaging using low flip angle pulses. *J Magn Reson Imaging* 1986;76:258-266.
20. Port M, Corot C, Rousseaux O, Raynal I, Devoldere L, Idee JM, Dencausse A, Lancelot E, LeGreneur S, Bourrinet P, Bonnemain B, Meyer D, Lautrou J. Chemical, physicochemical and biological evaluation of P792: a rapid clearance blood pool agent for MRI. *MAGMA* 2001, in press.
21. Ogan M, Schmiedl U, Moseley M, Grodd W, Paaenen H, Brasch RC. Albumin labeled with Gd-DTPA: an intravascular contrast enhancing agent for magnetic resonance blood pool imaging: preparation and characterization. *Invest Radiol* 1987;22:665-671.
22. Schmiedl U, Ogan M, Moseley M, et al. Comparison of the contrast enhancing properties of albumin-(Gd-DTPA) and Gd-DTPA at 2.0 T: an experimental study in rats. *AJR Am J Roentgenol* 1986;147:1263-1270.
23. Roberts TP. Physiologic measurements by contrast-enhanced MR imaging: expectations and limitations. *J Magn Reson Imaging* 1997;7: 82-90.
24. Strich G, Hagan PL, Gerber KH, Slutsky RA. Tissue distribution and magnetic resonance spin lattice relaxation effects of gadolinium-DTPA. *Radiology* 1985;154:723-726.
25. Koenig SH, Spiller M, Brown RD, Wolf GL. Relaxation of water protons in the intra- and extracellular regions of blood containing Gd(DTPA). *Magn Reson Med* 1986;3:791-795.
26. Scarff R, Torloni H. Histological typing of breast tumors. Geneva: World Health Organization; 1968. p 13-20.
27. Bloom H, Richardson W. Histologic grading and prognosis in breast cancer. *Br J Cancer* 1957;11:359-377.
28. Jain RK. Transport of molecules in the tumor interstitium: a review. *Cancer Res* 1987;47:3039-3051.
29. Jain RK. Physiological barriers to delivery of monoclonal antibodies and other macromolecules in tumors. *Cancer Res* 1990;50:814 —819.
30. Folkman J. The role of angiogenesis in tumor growth. *Sem Cancer Biol* 1992;3:65-71.
31. Weidner N, Semple J, Welch W, Folkmann J. Tumor angiogenesis and metastasis-correlation in invasive breast carcinoma. *N Engl J Med* 1991; 324:1-8.
32. Brasch RC, Shames DM, Cohen FM, Kuwatsuru R, Neuder M, Mann JS, Vexler V, Muhler A, Rosenau W. Quantification of capillary permeability to macromolecular magnetic resonance imaging contrast media in experimental mammary adenocarcinomas. *Invest Radiol* 1994;29:S8-S11.
33. van Dijke CF, Brasch RC, Roberts TP, Weidner N, Mathur A, Shames DM, Mann JS, Demsar F, Lang P, Schwickert HC. Mammary carcinoma model: correlation of macromolecular contrast-enhanced MR imaging characterizations of tumor microvasculature and histologic capillary density. *Radiology* 1996;198:813-818.

34. Gossmann A, Okuhata Y, Shames DM, Helbich TH, Roberts TPL, Wendland MF, Huber S, Brasch RC. Prostate cancer tumor grade differentiation with dynamic contrast-enhanced MR imaging in the rat: comparison of macromolecular and small-molecular contrast media—preliminary experience. *Radiology* 1999;213:265-272.
35. Gossmann A, Helbich T, Mesiano S, Shames DM, Wendland MF, Roberts TPL, Ferrara N, Jaffe RB, Brasch RC. Magnetic resonance imaging in ovarian cancer demonstrating altered microvascular permeability following inhibition of vascular endothelial growth factor. *Am J Obstet Gynecol* 2000;183:956-963.
36. Turetschek K, Huber S, Floyd E, Helbich T, Roberts TLP, Shames DM, Tarlo K, Wendland MF, Brasch RC. MRI characterization of microvessels in experimental breast tumors using a particulate contrast agent with histopathologic correlation. *Radiology* 2001, in press.
37. Tynnninen O, Aronen H, Ruhala M, Paetau A, Von Boguslawski K, Salonen O, Jaaskelainen J, Paavonen T. MRI enhancement and microvascular density in gliomas. Correlation with tumor cell proliferation. *Invest Radiol* 1999;34:427-434.
38. Arapandoni-Dadioti P, Giatromanolaki A, Trihia H, Harris AL, Koukourakis MI. Angiogenesis in ductal breast carcinoma. Comparison of microvessel density between primary tumour and lymph node metastasis. *Cancer Lett* 1999;137:145-150.
39. Obermair A, Wanner C, Bilgi S, Speiser P, Kaider A, Reinthaller A, Leodolter S, Gitsch G. Tumor angiogenesis in stage IB cervical cancer: correlation of microvessel density with survival. *Am J Obstet Gynecol* 1998;178:314-319.
40. Offersen BV, Borre M, Overgaard J. Immunohistochemical determination of tumor angiogenesis measured by the maximal microvessel density in human prostate cancer. *APMIS* 1998;106:463-469. *Magn Reson Med* 1986;3:791-795.

CHAPTER 5

MR CHARACTERIZATION OF TUMOR MICROVESSELS IN
EXPERIMENTAL BREAST TUMORS USING A SLOW CLEARANCE
BLOOD POOL CONTRAST AGENT
(CARBOXYMETHYLDextran-A2-Gd-DOTA)
WITH HISTOPATHOLOGIC CORRELATION

MR CHARACTERIZATION OF
TUMOR MICROVESSELS IN
EXPERIMENTAL BREAST TUMORS
USING A SLOW CLEARANCE
BLOOD POOL CONTRAST AGENT
(CARBOXYMETHYLDextran-A2-
Gd-DOTA) WITH HISTOPATHOLOGIC
CORRELATION

(EUROPEAN RADIOLOGY, IN PRESS)

Anda Preda^{1,2}, MD; Viktor Novikov¹, MD; Martina Möglich¹, Eugenia Floyd³, DVM;
Karl Turetschek¹, MD; David M. Shames¹, MD; Timothy PL Roberts¹ Ph.D.;
Claire Corot⁴, Ph.D.; Wayne O. Carter³, DVM, Robert C. Brasch¹, MD

¹ Center for Pharmaceutical and Molecular Imaging, Department of Radiology, University of California San Francisco, San Francisco, California.

² Visiting Research Scholar from the Department of Radiology, Erasmus University Medical Center, Rotterdam, The Netherlands.

³ Pfizer Central Research, Groton, Connecticut.

⁴ Guerbet Laboratories, Aulnay Sous Bois, France.

Abstract

Carboxymethyldextran-A2-Gd-DOTA, a slow clearance blood pool contrast agent with a molecular weight of 52.1 kDa, designed to have intravascular residence for more than one hour, was evaluated for its potential to characterize and differentiate the microvessels of malignant and benign breast tumors.

Precontrast single-slice inversion recovery (IR) snapshot FLASH and dynamic contrast enhanced-MR imaging using an axial T1-weighted three-dimensional (3D)-spoiled gradient recalled (SPGR) sequence was performed in 30 Sprague-Dawley rats with chemically induced breast tumors. Endothelial transfer coefficient (K^{PS}) and fractional plasma volume (fPV) of the breast tumors were estimated from MRI data acquired with CMD-A2-Gd-DOTA enhancement, injected at a dose of 0.1mmol Gd/kg body weight, using a two-compartment bidirectional model of the tumor tissue. The MRI microvessel characteristics were correlated with the histopathologic tumor grade using the Scarff-Bloom-Richardson (SBR) method. Using CMD-A2-Gd-DOTA, no significant correlations were found between the MR-estimated endothelial transfer coefficient ($r = 0.09$, $P = 0.47$) or plasma volumes ($r = 0.19$, $P = 0.22$) with the histologic tumor grade. Analysis of CMD-A2-Gd-DOTA-enhanced MR kinetic data failed to demonstrate feasibility for the differentiation of benign from malignant tumors or for image-based tumor grading.

Keywords

Magnetic resonance imaging, contrast media, carboxymethyldextran-A2-Gd-DOTA, breast neoplasms, dynamic contrast enhancement

Introduction

Dynamic contrast-enhanced MRI has become an increasingly employed noninvasive imaging method for assessing the morphological and functional properties of tumor tissue. The importance of defining the physiological characteristics of tumors and their microvessels is central to imaging evaluations of therapeutic interventions. The pharmacological inhibition of tumor angiogenesis represents only one possible option for using contrast-enhanced MRI to monitor treatment [1,2]. Quantitative MRI assays of tumor microvessel characteristics could also be applied to estimate tumor grade and prognosis [3,5].

Using kinetic analysis of dynamic contrast-enhanced MR data in the context of a tissue compartmental model, transendothelial permeability estimated as the endothelial transfer coefficient (K^{PS}) and the fractional plasma volume (fPV) of the tumor tissue can be evaluated quantitatively. Numerous studies have demonstrated that the microvessels of malignant tumors have an increased permeability for macromolecular solutes, including prototype macromolecular contrast media (MMCM), attributed to tumor-related morphologic alterations of vascular endothelial lining [3, 6-8]. The clinically currently available small molecular gadolinium chelates have a limited potential in the quantitative

assessment of blood volume or abnormal permeability outside the central nervous system due to their non-selective leak through the endothelium of both normal and pathologic blood vessels. The ability of dynamic MRI enhanced with macromolecular contrast agents to quantitatively define the leakiness of tumor microvessels has been shown in several experimental models [3,6,7]. However, the reference contrast medium used in these studies, albumin-(Gd-DTPA)₃₀, is considered unsuitable for clinical use due to its potential immunogenicity and its incomplete clearance from the body [9,10].

The search for clinically applicable MR contrast agents has been expanded in recent years, with the goal to allow improved assessment of regional blood flow and tissue perfusion. Recently, several MR contrast media were studied with respect to their potential for quantitative description of tissue microvessels. These contrast media include blood pool agents such as P792 (Vistarem, Guerbet, Aulnay Sous Bois, France) [11], small molecular gadolinium chelates such as MS-325, characterized by reversible binding to human serum albumin (Angiomark, Schering AG, Berlin, Germany) [12], ultrasmall superparamagnetic iron oxide particles (USPIO) such as NC100150 (Clariscan, Nycomed Amersham, Oslo, Norway) [13] and SHU 555C (Resovist, Schering AG, Berlin, Germany) [14].

Meglumine-carboxymethyldextran-ethylenediamino-gadoterate (CMD-A2-Gd-DOTA), a product of Guerbet Group (Guerbet Laboratories, Aulnay Sous Bois, France), is a new slow clearance blood pool agent with a high paramagnetic efficacy, approximately 3 times higher than that of extracellular gadolinium-based compounds such as Gd-DOTA, and a good tolerability [15]. In previous studies CMD-A2-Gd-DOTA has been shown to be useful for MRI in demonstrating tracer kinetics for in vivo assessment of myocardial perfusion [16].

The objective of the current study was to determine if MRI assays of microvascular characteristics might provide a non-invasive insight into the biological characteristics of the tumor as reflected in the histopathologic tumor grade, specifically the Scarff-Bloom-Richardson grade. The reasons for testing this hypothesis include the previous successful demonstration of this potential application of MRI for the assay of tumor biology using a different and larger contrast agent (3) and the generally recognized connection between the degree to which a tumor can acquire a rich vascular supply and the biological aggressiveness of the tumor, as might be reflected in its histopathologic properties. Microvascular characteristics endothelial transfer coefficient and fractional plasma volume derived from the kinetic data analysis of dynamic MRI enhanced with CMD-A2-Gd-DOTA were correlated with results of pathologic analysis, namely quantitative tumor histopathologic grade.

Material and methods

Animal Model

The study has been conducted with the approval of our Committee for Animal Research, and conformed to the guidelines of the National Institutes of Health for the care and use of the laboratory animals. Mammary tumors were induced in Sprague-Dawley rats (Charles River Laboratories) by intraperitoneal injection of N-ethyl-N-nitrosurea (ENU) (ENU Isopack,

Sigma Chemicals, St. Louis, MO). ENU is an alkylating agent and a potent carcinogen that induces tumors of varying grade and location in rats, depending on the dose, the site of injection, the age and the sex of the rats [17-19]. Mammary cells are the primary target cells when ENU is administered intraperitoneally into the female rats [18,19]. For our study, ENU, purchased as a crystalline substance, was dissolved shortly before administration in 0.9% sterile saline to a solution with a concentration of 10mg/ml. ENU was injected at different doses: 90 mg/kg (n=8), 180 mg/kg (n=10) and 250 mg/kg (n= 12). The animals were checked for tumor growth every second day. The tumors were imaged when they reached a size of 1 to 1.5 cm.

Experimental procedure

Before the MRI imaging, the animals were anesthetized by intraperitoneal administration of pentobarbital sodium, 50mg/kg body weight. Analgesia was achieved by intraperitoneal injection of 0.03mg/kg buprenorphine hydrochloride (Buprenex, Reckitt & Colman Products, Hull, UK), an opiate. A 23-gauge butterfly canula (Abbott Laboratories, North Chicago, ILL. USA) was inserted into a tail vein for contrast medium injection. Immediately after the MR imaging, 0.32 mg Naloxone (Abbot Laboratories, North Chicago, ILL) was injected intraperitoneally to reverse opioid effects. In addition, 2.0 ml of saline was injected intravenously to avoid dehydration as might occur after anesthesia.

Magnetic resonance imaging

MR imaging was performed on a Bruker Omega CSI-II System (Bruker Instruments, Fremont, CA) operating at 2 Tesla. This system is equipped with Acustar S-150 (Bruker Instruments, Fremont, CA) self-shielded gradient coils (20 G/cm, 15cm inner diameter). Animals were placed supine in a birdcage radio-frequency coil with a length of 7.6 cm and an inner diameter of 4.5 cm. A phantom filled with diluted gadopentetate dimeglumine (0.01 mmol/liter) was included in the field of view, close to each animal, to allow correction for potential spectrometer variation.

Precontrast images were acquired using an single-slice inversion recovery (IR) snapshot FLASH sequence [20] with the following parameters: TR 3ms, TE 1.5 ms, one acquisition, field of view 55x55 mm, matrix 64x64, slice thickness 3 mm and a flip angle of 5 degrees. Per slice, nine images at nine different inversion recovery times $TI = 100, 400, 700, 1000, 1300, 1600, 1900, 2200$ and 2500 ms were acquired. A total of eight slices were obtained. After the inversion recovery time TI , the data were acquired using a snapshot FLASH readout scheme with centric reordering to maintain the appropriate $T1$ contrast for the center of the k space. This sequence was used to calculate baseline longitudinal relaxation rates ($R1=1/T1$) for tumor by curve fitting [21].

Dynamic contrast enhanced MR imaging was performed using an axial $T1$ -weighted three-dimensional (3D)-spoiled gradient recalled (SPGR) sequence with the following parameters: TR 30ms, TE 4.83 ms, one acquisition, field-of-view 55x55x48mm, matrix 128x128x16, an effective slice thickness of 3.6mm and flip angle of 90 degrees. To monitor enhancement response 3 initial precontrast images and 30 dynamic postcontrast images were acquired serially with an acquisition time of 1 minute 1 second per volume of 16 slices.

Magnetic Resonance Contrast Media

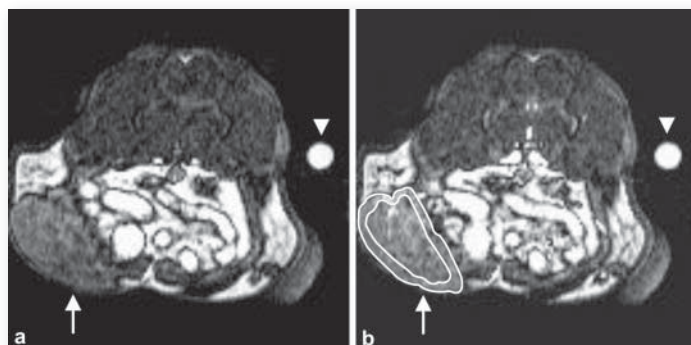


Fig. 1: Representative axial T1-weighted (TR = 30ms, TE = 4.83 ms) SPGR images of a subcutaneous malignant mammary tumor (a) before and (b) 30 min after administration of CMD-A2-Gd-DOTA (0.1 mmol Gd/kg). A phantom was placed in the field of view (arrowhead) to serve as an intensity reference.

CMD-A2-Gd-DOTA, a slow-clearance blood pool agent (*Fig.1*), is a MMCM under development (Guerbet Laboratories, Aulnay Sous Bois, France). CMD-A2-Gd-DOTA consists of a carboxymethyl dextran polymer bound to the paramagnetic macrocyclic complex Gd-DOTA using an amino spacer. The polymer is formed of 22% Gd-DOTA, 39% of carboxyl group and 39% of glucose group. The mean molecular weight of CMD-A2-Gd-DOTA is 52.1 kDa and the polydispersity index of 1.79. The r_1 relaxivity of the agent is $10.6 \text{ mmol}^{-1}\text{sec}^{-1}$ and the r_2 relaxivity is $11.1 \text{ mmol}^{-1}\text{sec}^{-1}$ (measured in water at 37°C and 20 MHz). The plasma half-life in rabbits is >180 minutes. CMD-A2-Gd-DOTA is mainly excreted by the kidneys and in a small amount by fecal elimination after hepatocyte metabolism [15]. It has a good tolerance in animals (LD50 in mice $> 5 \text{ mmol Gd/kg}$ body weight at injection rate of 2 ml/min). CMD-A2-Gd-DOTA was injected at a dose of 0.1 mmol Gd/kg body weight.

Kinetic analysis of dynamic MRI data

The MR images were transferred, processed and analyzed using a Sun SPARC 10 workstation (Sun Microsystems, Mountain View, CA) and an image analysis program (MRVision Co., Stanford, CA). Signal intensity values (SI) for each time point were obtained from multiple (three to six) operator-defined regions of interest (ROIs). Signal intensities for the blood within the inferior vena cava (IVC), the phantom, and the tumor periphery were measured in the central section of the imaging volume. The tumor periphery was defined as the peripheral zone of strong contrast enhancement, usually 1-2 mm thick. Corresponding ROI measurements were made in each of three adjacent images, each containing a minimum of 30 pixels, and were averaged. The mean signal intensities (SI) from the tumors and the blood in the vena cava were corrected for potential spectrometer variation over time by dividing the SI of each ROI by the SI from the phantom. Kinetic analysis was limited to the tumor periphery that represents the least necrotic and also the most vascularized region of the tumor [22, 23]. Precontrast longitudinal relaxation rates R_1 ($1/T_1$) estimates for tumors were obtained by curve fitting based on one set of inversion recovery snapshot FLASH images. The precontrast R_1 value for IVC blood was assumed to be 0.724 s^{-1} ($1/1.38$) on the basis of numerous previous measurements in rat blood [21]. Postcontrast R_1 values

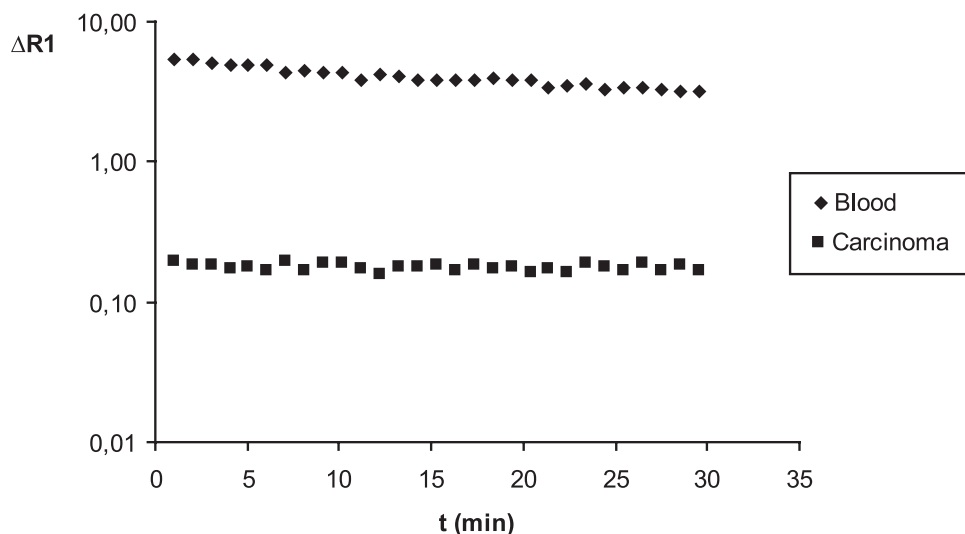


Fig 2. Representative $\Delta R1$ -vs-time curves of blood and a malignant breast tumor following intravenous administration of carboxymethyldextran-A2-Gd-DOTA (0.1mmol Gd/kg)

were calculated based on the observed signal intensities and knowledge of precontrast $R1$ values [21]. The difference between the postcontrast $R1$ value at any time point and the precontrast $R1$, $\Delta R1(t)$ is assumed to be directly proportional to the concentration of the contrast medium, either in the blood or in the tissue [24, 25]. The $\Delta R1$ data from blood and tumor (Fig 2 and Fig 3) were used for kinetic analysis to estimate leakiness expressed as the endothelial transfer coefficient (KPS, $\mu\text{l min}^{-1} 100 \text{ cc}^{-1}$ of tissue) and the fractional plasma volume of the tumor tissue (fPV, $\mu\text{l cc}^{-1}$ of tissue), using previously reported methods [3]. Briefly, a compartmental model of microvascular permeability is fitted to the $\Delta R1(t)$ data from tumor and IVC after correction for hematocrit. The $\Delta R1(t)$ from the IVC, fitted by a monoexponential function, serves as a forcing function for the tumor tissue model that has a two-compartment structure corresponding to blood plasma and tumor interstitial water spaces. The model was fitted to both IVC and tumor tissue at the same time using the SAAM II software (SAAM Institute, Seattle, WA) that employs a standard non-linear regression. The uncertainty of the estimates of fPV and KPS were derived from the covariance matrix at the least-squares fit assuming a data weighting scheme characterized by a coefficient of variation of 10 % for each point.

Histologic Analysis

After completing the second MR examination, all animals were sacrificed by an intravenous overdose of 0.3ml pentobarbital. Post-mortem, all tumors were removed, immediately fixed for 18-24 hours in 10 % buffered formalin (Poly Scientific Research & Development Corp., Bay Shore, NY, USA), embedded in paraffin, sectioned in the same plane as the MR images at 4μ , and stained with hematoxylin and eosin for diagnosis and grading. All tumors, both benign and malignant, were graded using the Scarff-Bloom-Richardson (SBR) method [26,

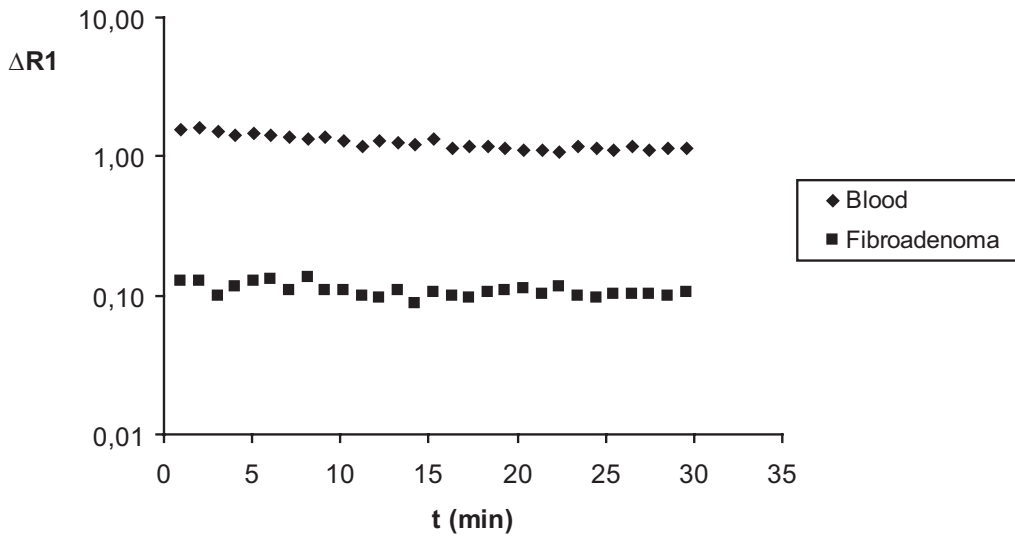


Fig 3. Representative $\Delta R1$ -vs-time curves of blood and a benign breast tumor following intravenous administration of carboxymethyl dextran-A2-Gd-DOTA (0.1 mmol Gd/kg)

27], that has been used extensively in the clinical evaluation of invasive human breast adenocarcinoma. This histopathologic grading system evaluates the ducto-glandular formation and nuclear characteristics including pleomorphism and mitotic activity. Each of these three morphological features is scored by assigning one to three points and an overall score is obtained by summation of the individual characteristic scores. The lowest SBR score possible, even for a benign tumor, is 3. The highest SBR score is 9 and it indicates a poorly differentiated tumor. The SBR score determination were performed by a single pathologist without knowledge of MR imaging findings.

Statistics

Mean values for K^{PS} and fPV were compared between fibroadenomas and carcinomas using unpaired t tests. Non-parametric Spearman correlation analyses were performed, comparing the histologic tumor grade (SBR score) with the estimated MR-derived parameters (K^{PS} and fPV). A P value of < 0.05 was considered statistically significant.

Results

Following the single intraperitoneal administration of ENU, 30 rats developed mammary tumors within our study period. Eight tumors were benign fibroadenomas and twenty-two were malignant adenocarcinomas. The overall assignment of a tumor to the benign or malignant group by the pathologist was independent of the SBR score.

CMD-A2-Gd-DOTA-enhanced dynamic images were acquired successfully in all 30 animals. The kinetic model fit the data well in all the experiments. All parameter values were obtained with good precision. The mean coefficients of variation (CV) for fPV and K^{PS} were 31% and 5%, respectively. Small K^{PS} values with CV greater than 100% were assumed not to be resolvable from the data and were set equal to 0. The K^{PS} and fPV values in all fibroadenomas and carcinomas, with their respective SBR scores for each tumor, are shown in Table 1.

Table 1: Tumor Pathology and MRI-derived Microvessel Characteristics by Ascending SBR score

SBR scores	Tumor type	fPV	K^{PS}
Benign			
3	Fibroadenoma	22	30
3	Fibroadenoma	10	9
3	Fibroadenoma	43	27
3	Fibroadenoma	129	70
3	Fibroadenoma	38	44
3	Fibroadenoma	19	19
3	Fibroadenoma	75	0
4	Fibroadenoma	52	40
	Mean	49	30
	SD	39	22
Malignant			
4	Carcinoma	42	42
4	Carcinoma	101	69
5	Carcinoma	33	36
5	Carcinoma	51	20
5	Carcinoma	90	63
5	Carcinoma	34	12
6	Carcinoma	69	33
6	Carcinoma	85	88
6	Carcinoma	76	31
6	Carcinoma	33	57
6	Carcinoma	19	28
6	Carcinoma	44	41
6	Carcinoma	32	30
6	Carcinoma	101	82
6	Carcinoma	61	65
6	Carcinoma	71	39
6	Carcinoma	67	40
6	Carcinoma	33	17
6	Carcinoma	56	91
8	Carcinoma	47	22
8	Carcinoma	104	30
9	Carcinoma	39	13
	Mean	59	43
	SD	26	24

SBR, Scarff Bloom Richardson score; fPV, fractional plasma volume ($\mu\text{l cc}^{-1}$ of tissue); K^{PS} endothelial transfer coefficient ($\mu\text{l min}^{-1} 100 \text{ cc}^{-1}$ of tissue)

The mean values for K^{PS} in carcinomas ($43 \pm 24 \mu\text{l min}^{-1} 100 \text{ cc}^{-1}$ of tissue) were not significantly different ($P = 0.18$) from the mean K^{PS} values in the fibroadenomas ($30 \pm 22 \mu\text{l min}^{-1} 100 \text{ cc}^{-1}$ of tissue). The mean values for fPV in carcinomas ($59 \pm 26 \mu\text{l cc}^{-1}$ of tissue) did not differ significantly ($P = 0.41$) from the mean fPV values in fibroadenomas ($49 \pm 39 \mu\text{l cc}^{-1}$ of tissue). No significant correlation was found between K^{PS} and SBR score ($r = 0.09$, $P = 0.47$). Also estimates of fPV did not correlate significantly with SBR scores ($r = 0.19$, $P = 0.22$).

Discussion

In this experimental breast tumor model, CMD-A2-Gd-DOTA, a slow clearance blood pool contrast agent was not shown to be effective for differentiation of benign from malignant tumors, nor for tumor grading. K^{PS} and fPV, the MRI-derived characteristics estimated from CMD-A2-Gd-DOTA-enhanced MR data, did not correlate significantly with histologic measures of tumor grade (SBR score).

The measurement of functional parameters of tumor tissue such as transendothelial leakiness and plasma volume can be achieved by contrast-enhanced MRI, analyzing the distribution kinetics of the contrast agent in the tissue. Several studies have demonstrated that the tumors with an aggressive behavior have relatively greater transendothelial leakiness to macromolecules (K^{PS}) and relatively more blood (fPV) than benign or biologically less aggressive tumors [3,7,28,29]. The quantitative assessment of these tumor properties thus makes possible an accurate noninvasive description of the microcirculation of individual tumors. Such imaging assays can be effectively used in differentiation between tumors of variable biological behavior. In addition, the follow-up of the MRI-derived estimates of microvessels properties could provide a tool for in vivo monitoring of the tumor response to therapy. These microvascular characteristics can be estimated, based on kinetic analysis of dynamic enhancement data using simple models of the tumor tissue as a compartmentalized system [30-32]. Two-compartment tissue models that represent the blood plasma and the extracellular extravascular space are typically used. The concentration of the contrast agent can be derived from signal intensity data, assuming that changes in longitudinal relaxation rates R_1 ($1/T_1$) after administration of the contrast medium are proportional with contrast agent concentration. Thus the increase in enhancement can be translated to contrast agent concentration and quantified using kinetic modeling, finally providing estimates of microvascular characteristics.

The search for a contrast agent suitable for characterization of the vessels of tumors in a clinical setting has been enthusiastic. The ideal contrast medium must be retained within the circulating plasma for at least one hour after administration, show efficacy for characterization of tumor microvessels and have an appropriate pharmacokinetic behavior. In addition, the compound should be well tolerated over a wide dose range, be completely excreted from the body and immunologically inactive. In recent years, the feasibility of several candidate contrast media to quantitatively assess the properties of tumor microvessels has been evaluated [33]. Ultrasmall superparamagnetic iron oxide (USPIO) particles such as SHU 555C (Schering AG, Berlin, Germany) and NC100150 (Clariscan, Nycomed Amersham, Oslo, Norway) have been shown feasible for defining

the tumor microvasculature in the same chemically induced breast tumor model used for this study [13, 14]. However, one limitation in the use of USPIO for tumor microvessels characterization is the negative enhancement induced by the T2* shortening, that is competitive with the positive signal enhancement caused by the T1 shortening [34].

CMD-A2-Gd-DOTA is a new paramagnetic macromolecular polymer with a mean molecular weight of 52.1 kDa, potentially large enough to differentiate the macromolecular hyper-permeability of cancer microvessels. Recent investigations have shown its potential for applications in MRI myocardial perfusion studies, due to the high relaxivity and its prolonged intravascular residence time [16]. Also CMD-A2-Gd-DOTA proved to be useful in depiction of myocardial infarction during first pass studies and in evaluating the enhancement of the infarcted zone on delayed MR imaging [35]. Another potential clinical application includes MR angiography. [36-38]. Following its intravenous administration at a dose of 0.05 mmol Gd/kg body weight in an experimental rabbit model, CMD-A2-Gd-DOTA demonstrated significant signal enhancement of abdominal organs and pelvic bone marrow, partial storage in the liver and return to baseline signal intensities after 10 days post-injection [39]. To our knowledge, CMD-A2-Gd-DOTA has not been previously tested for its potential to characterize tumor microvessels.

Urinary excretion of 45% in 24h [15] indicates that its molecular weight of 52.1 kDa may be below the threshold of urinary excretion. Since the prototype macromolecular contrast agent albumin-(Gd-DTPA)₃₀, with a molecular weight of 92kDa, seems to be unsuitable for clinical use, because its renal excretion is incomplete and slow, CMD-A2-Gd-DOTA may offer a compromise between the required renal elimination and the blood pool properties. The reported prolonged retention [15, 39] of CMD-A2-Gd-DOTA in the liver could indicate also a minor component of hepatic metabolism and fecal excretion. CMD-A2-Gd-DOTA was well tolerated in all anesthetized rats. This observation is in agreement with previous studies [15, 34, 39] that showed no toxic effects at a dose of 0.05 mmol. The hypothesis of this present study was that CMD-A2-Gd-DOTA could be used for characterization of tumor microvessels. The results obtained in this rodent model of chemically induced mammary tumors did not support this theory.

One factor that could have influenced the lack of correlation of the microvascular characteristics with the histologic tumor grade is the distribution of SBR scores in the investigated group. There were relatively few high-grade tumors (SBR score 7-9). Of the thirty tumors, seven were fibroadenoma with a SBR score of 3, while the most of the remainder of the tumors had SBR scores of 5 and 6. Only one tumor had the maximum SBR of 9 and two tumors were classified as SBR score of 8. This variation in the distribution of the tumors is subject to statistical variation, cannot be controlled and can be attributed to different biological responses to ENU administration in different animals.

Conclusions from our data are limited in several ways. The tumors investigated in this study were chemically induced in rats. Results from this rodent tumor model may not apply directly to human neoplasms. Tumors were imaged at only a single time point in their growth, at a diameter of approximately 1 to 1.5 cm, while microvascular characteristics K^{ps} and fPV may differ as a function of time and tumor size. In addition, only a single tumor type

(breast tumor) was investigated. The current study did not examine the potential of CMD-A2-Gd-DOTA enhancement to monitor the changes in the tumor microvascular assays that could result from tumor therapy. Also the “gold standard” used in this study, the histologic tumor grading by SBR score, could be subject to inter-individual variations [40]. In order to minimize the potential of bias in correlations of MR characteristics with the histology, the MR data analysis was performed completely independently of histopathologic evaluation, by a different investigator. The pathologist had no knowledge of the results of kinetic analysis and the image analyzer was blinded to the histopathologic score.

As is generally the case for a negative study, the failure to prove the hypothesis may be due to the particular model studied or to the precise methods employed and thus the negative conclusions are not necessarily generalizable to all tumors or analysis methods. Additional negative observations under different conditions would be required to confirm the results of this study. CMD-A2-Gd-DOTA, the contrast agent examined for this protocol, may yet have many and varied useful applications in the area of MRI tumor characterization.

In conclusion, kinetic analysis of dynamic CMD-A2-Gd-DOTA-enhanced MRI data in the context of a compartmental model of capillary permeability in a rodent breast tumor model failed in differentiation between benign and malignant tumors and in grading of tumors.

Acknowledgements

Supported by funds received from the National Cancer Institute, grant CA82923 and from the Cancer Research Fund, State of California, under interagency agreement 97-12013 (University of California contract 98-00924V). Anda Preda was supported in part by the “Drie Lichten” and the “Johan Vermeij” Foundations, the Netherlands

References

1. Turetschek K, Preda A, Floyd E, Shames DM, Novikov V, Roberts TPL, Wood JM, Fu Y, Carter WO, Brasch RC (2003) MRI monitoring of tumor response following angiogenesis inhibition in an experimental human breast cancer model. *Eur J Nucl Med* 30:448-455 DOI 10.1007/s00259-002-1000-5
2. Pham CD, Roberts TPL, van Bruggen N, Melnyk O, Mann J, Ferrara N, Cohen RL, Brasch RC (1998) Magnetic Resonance Imaging detects suppression of tumor vascular permeability after administration of antibody to vascular endothelial growth factor. *Cancer Invest* 6:225-230
3. Daldrup H, Shames DM, Wendland M, Okuhata Y, Link TM, Rosenau W, Lu Y, Brasch RC (1998) Correlation of dynamic contrast-enhanced MR imaging with histologic tumor grade: comparison of macromolecular and small-molecular contrast media. *Am J Roentgenol* 171:941-949
4. Brasch RC, Shames DM, Cohen FM, Kuwatsuru R, Neuder M, Mann JS, Vexler V, Muhler A, Rosenau W (1994) Quantification of capillary permeability to macromolecular magnetic resonance imaging contrast media in experimental mammary adenocarcinomas. *Invest Radiol* 29 (Suppl 2):S8-S11

5. Su MY, Wang Z, Carpenter PM, Lao X, Muhler A, Nalcioğlu O (1999) Characterization of N-ethyl-N-nitrosourea-induced malignant and benign breast tumor in rats by using three MR contrast agents. *J Magn Reson Imaging* 9:177-186
6. Schwickert HC, Stiskal M, Roberts TP, van Dijke CF, Mann J, Muhler A, Shames DM, Demsar F, Disston A, Brasch RC (1996) Contrast-enhanced MR imaging assessment of tumor capillary permeability: effect of irradiation on delivery of chemotherapy. *Radiology* 198:893-898
7. Gossmann A, Okuhata Y, Shames DM, Helbich TH, Roberts TPL, Wendland MF, Huber S, Brasch RC (1999) Prostate cancer tumor grade differentiation with dynamic contrast-enhanced MR imaging in the rat: comparison of macromolecular and small-molecular contrast media-preliminary experience. *Radiology* 213:265-272
8. Jain R. Barriers to drug delivery in solid tumors (1994) *Sci Am* 271:58-65
9. White D, Wang S-C, Aicher K, Dupon J, Engelstad B, Brasch R (1989) Albumin-(Gd-DTPA)₁₅₋₂₀: whole body clearance, and organ distribution of gadolinium. In: *Proceedings of the Society of Magnetic Resonance in Medicine, 8th Annual Meeting, Amsterdam*, p 807.
10. Baxter AB, Melnikoff S, Stites DP, Brasch RC (1991) Immunogenicity of gadolinium-based contrast agents for MRI. *Invest Radiol* 26:1035-1040
11. Turetschek K, Floyd E, Shames DM, Roberts TPL, Preda A, Novikov V, Corot C, Carter WO, Brasch RC (2001) Assessment of a rapid clearance blood pool MR contrast medium (P792) for assays of microvascular characteristics in experimental breast tumors with correlation to histopathology. *Magn Reson Med* 45:880-886
12. Turetschek K, Floyd E, Helbich T, Roberts TPL, Shames DM, Wendland MF, Carter WO, Brasch RC (2001) MRI assessment of microvascular characteristics in experimental breast tumors using a new blood pool contrast agent (MS-325) with correlation to histopathology. *J Magn Reson Imaging* 14:237-242
13. Turetschek K, Huber S, Floyd E, Helbich T, Roberts TPL, Shames DM, Tarlo KS, Wendland MF, Brasch RC (2001) MR imaging characterization of microvessels in experimental breast tumors by using a particulate contrast agent with histopathologic correlation. *Radiology* 218:562-569
14. Turetschek K, Roberts TPL, Floyd E, Preda A, Novikov V, Shames DM, Carter WO, Brasch RC (2001) Tumor microvascular characterization using ultrasmall superparamagnetic iron oxide particles (USPIO) in an experimental breast cancer model. *J Magn Reson Imaging* 13:882-888
15. Corot C, Schaffer M, Beaute S, Bourrinet P, Zehaf S, Benize V, Sabatou M, Meyer D (1997) Physical, chemical and biological evaluations of CMD-A2-Gd-DOTA. A new paramagnetic dextran polymer. *Acta Radiol* 412 (Suppl): 91-99
16. Canet EP, Casali C, Desenfant A, An MY, Corot C, Obadia JF, Revel D, Janier MF (2000) Kinetic characterization of CMD-A2-Gd-DOTA as an intravascular contrast agent for myocardial perfusion measurements with MRI. *Magn Reson Med* 43:403-409
17. Mandybur T (1985) Neural, pituitary and mammary tumors in Sprague Dawley rats treated with x-irradiation to the head and N-ethyl-N-nitrosourea (ENU) during the early postnatal period: a statistical study of tumor incidence and survival. *Radiat Res* 101:406-472
18. Stoica G, Koestner A, Capen C (1984) Neoplasms induced with high single doses of N-ethyl-N-nitrosourea in 30 day-old Sprague Dawley rats, with special emphasis on mammary neoplasia. *Anticancer Res* 4: 5-12

19. Stoica G, Jacobs R, Koestner A, O'Leary M, Welsch C (1991) ENU-induced in vitro neoplastic transformation of rat mammary epithelial cells. *Anticancer Res* 11:1783-1792
20. Haase A. Snapshot FLASH MRI (1990) Applications to T1, T2, and chemical shift imaging. *Magn Reson Med* 13:77-89
21. Schwickert HC, Roberts TP, Shames DM, van Dijke CF, Disston A, Muhler A, Mann JS, Brasch RC (1995) Quantification of liver blood volume: comparison of ultra short TI inversion recovery echo planar imaging (ULSTIR-EPI), with dynamic 3D-gradient recalled echo imaging. *Magn Reson Med* 34:845-852
22. Jain R (1987) Transport of molecules across tumor vasculature. *Cancer Metastasis Rev* 6:559-593
23. Jain RK, Baxter LT (1988) Mechanisms of heterogeneous distribution of monoclonal antibodies and other macromolecules in tumors: significance of elevated interstitial pressure. *Cancer Res* 48(24 pt 1):7022-7032
24. Wedeking P, Sotak CH, Telser J, Kumar K, Chang CA, Tweedle MF (1992) Quantitative dependence of MR signal intensity on tissue concentration of Gd(HP-DO3A) in the nephrectomized rat. *Magn Reson Imaging* 10:97-108
25. Shames DM, Kuwatsuru R, Vexler V, Muhler A, Brasch RC (1993) Measurement of capillary permeability to macromolecules by dynamic magnetic resonance imaging: a quantitative non-invasive technique. *Magn Reson Med* 29:616-622
26. Scarff R, Torloni H (1968) Histological typing of breast tumors. World Health Organization, Geneva, Switzerland: 13-20
27. Bloom H, Richardson W (1957) Histologic grading and prognosis in breast cancer. *Br J Cancer* 11:359-377
28. Gossmann A, Helbich TH, Mesiano S, Shames DM, Wendland MF, Roberts TP, Ferrara N, Jaffe RB, Brasch RC (2000) Magnetic resonance imaging in an experimental model of human ovarian cancer demonstrating altered microvascular permeability after inhibition of vascular endothelial growth factor. *Am J Obstet Gynecol* 183:956-963 DOI 10.1067/mob.2000.107092
29. Van Dijke CF, Brasch RC, Roberts TP, Weidner N, Mathur A, Shames DM, Mann JS, Demsar F, Lang P, Schwickert HC (1996) Mammary carcinoma model: correlation of macromolecular contrast-enhanced MR imaging characterizations of tumor microvasculature and histologic capillary density. *Radiology* 198:813-818
30. Tofts PS, Kernmode AG (1991) Measurement of the blood-brain barrier permeability and leakage space using dynamic MR imaging. 1. Fundamental concepts. *Magn Reson Med* 17:357-367
31. Larsson HBW, Stubgaard M, Frederiksen JL, Jenssen M, Henriksen O, Paulson OB (1990) Quantitation of blood-brain-barrier defect by magnetic resonance imaging and gadolinium-DTPA in patients with multiple sclerosis and brain tumors. *Magn Reson Med* 16:117-131
32. Brix G, Semmler W, Port R, Schad LR, Layer G, Lorenz WJ (1991) Pharmacokinetic parameters in CNS Gd-DTPA enhanced MR imaging. *J Comput Assist Tomogr* 15:621-628
33. Daldrup-Link HE, Brasch RC (2003) Macromolecular contrast agents for MR mammography: current status. *Eur Radiol* 13:354-365 DOI 10.1007/s00330-002-1719-1
34. Roberts TP (1997) Physiologic measurements by contrast-enhanced MR imaging: expectations and limitations. *J Magn Reson Imaging* 7:82-90

35. Kroft LJ, Doornbos J, van der Geest RJ, de Roos A (1999) Blood pool contrast agent CMD-A2-Gd-DOTA-enhanced MR imaging of infarcted myocardium in pigs. *J Magn Reson Imaging* 10:170-177
36. Kroft LJ, Doornbos J, Benderbous S, de Roos A (1999) Equilibrium phase MR angiography of the aortic arch and abdominal vasculature with the blood pool contrast agent CMD-A2-Gd-DOTA in pigs. *J Magn Reson Imaging* 9:777-785
37. Loubeyre P, Canet E, Zhao S, Benderbous S, Amiel M, Revel D (1996) Carboxymethyl-Dextran-Gadolinium-DTPA as a blood pool contrast agent for magnetic resonance angiography. *Invest Radiol* 31:288-293
38. Corot C, Violas X, Robert P, Port M (2000) Pharmacokinetics of three gadolinium chelates with different molecular sizes shortly after intravenous injection in rabbits. Relevance to MR angiography. *Invest Radiol* 4:213-218
39. Daldrup-Link HE, Link TM, Moller HE, Wiedermann D, Bonnemain B, Corot C, Rummeny EJ (2001) Carboxymethyl-dextran -A2-Gd-DOTA enhancement patterns in the abdomen and pelvis in an animal model. *Eur Radiol* 11:1276-1284 DOI 10.1007/s003300000699
40. Rank F, Dombernowsky P, Bang Jespersen N, Pederson B, Keiding N (1987) Histologic malignancy grading of invasive ductal breast carcinoma; a regression analysis of prognostic factors in low risk carcinomas from a multicentric trial. *Cancer* 60:1299-1305

CHAPTER 6

TUMOR MICROVASCULAR CHARACTERIZATION USING ULTRASMALL SUPERPARAMAGNETIC IRON OXIDE PARTICLES (US- PIO) IN AN EXPERIMENTAL BREAST CANCER MODEL

TUMOR MICROVASCULAR CHARACTERIZATION USING ULTRASMALL SUPERPARAMAGNETIC IRON OXIDE PARTICLES (USPIO) IN AN EXPERIMENTAL BREAST CANCER MODEL

6

(JOURNAL OF MAGNETIC RESONANCE IMAGING 2001,
13:882-888)

Karl Turetschek, MD,^{1,2} Timothy P. L. Roberts, PhD,¹ Eugenia Floyd, DVM,³
Anda Preda,^{1,4} MD,¹ Viktor Novikov, MD,¹ David M. Shames, MD,¹
Wayne O. Carter, DVM, PhD,³ and Robert C. Brasch, MD¹

¹ Center for Pharmaceutical and Molecular Imaging, Department of Radiology,
University of California San Francisco, San Francisco, California.

² Visiting Research Scholar from the Department of Radiology, University of Vienna,
Vienna, Austria.

³ Pfizer Central Research, Groton, Connecticut.

⁴ Visiting Research Scholar from the Department of Radiology, Erasmus University
Medical Center, Rotterdam, The Netherlands.

Abstract

The diagnostic potential of ultrasmall superparamagnetic iron oxide particles (USPIO) for quantitative tumor microvessel characterization was assessed by kinetic analysis of dynamic magnetic resonance imaging (MRI) in a rodent breast cancer model. Microvascular characteristics (transendothelial permeability (K^{ps}) and fractional plasma volume (fPV)) were estimated in 32 female Sprague Dawley rats, bearing breast tumors of varying malignancy. These values were compared to a prototype macromolecular contrast medium standard, albumin-(GdDTPA)₃₀. Transendothelial permeability (K^{ps}) correlated significantly ($P < 0.05$) with the tumor grade (Scarff-Bloom-Richardson (SBR) score) for the USPIO ($r = 0.36$), as well as for the reference macromolecule, albumin-(GdDTPA)₃₀ ($r = 0.54$). Estimates for the fPV did not show a statistically significant correlation with the tumor grade for either contrast medium. In conclusion, USPIO-enhanced MRI data were capable to characterize tumor microvessel properties in this breast cancer model: microvascular permeability (determined using USPIO) correlated significantly with tumor grade. Thus, quantitative estimation of microvascular characteristics in tumors could provide a surrogate of new vessel formation (angiogenesis) and thus a further important clinical indication for USPIO, in addition to MR angiography.

Key words

Magnetic resonance imaging; breast neoplasms; contrast media; microvascular density; histologic tumor grade

Introduction

Accurate characterization of individual tumors is critical for patient management, prognosis, and long-term survival, as well as selection of appropriate therapy (1). Tumor growth, as well as tumor aggressiveness/grade and the potential of setting distant metastatic sites, has shown a direct relationship to tumor neovascularization (2,3). Thus, any morphological and/or functional assessment focused on tumor microvessels might provide important additional information on the biological potential of a tumor.

Cancer microvessel characteristics, in particular fractional plasma volume (fPV) and transendothelial permeability (KPS), have been assessed by dynamic contrast-enhanced magnetic resonance imaging (MRI) using macromolecular contrast media (MMCM) and appropriate kinetic modeling (4-6) and have been compared to histopathologic tumor parameters in a number of animal models. Differences in MR-estimated microvessel properties represented a pathophysiological basis for differentiating between benign and malignant tumors, and even between various tumor grades (4,7). Albumin-(GdDTPA)₃₀ has been the reference contrast medium for characterizing tumor vessel properties in several studies (7-9), but its prolonged elimination and its immunologic potential impede its clinical use. Recently, ultrasmall superparamagnetic iron oxide particles (USPIO), which also demonstrate positive enhancement on T1-weighted imaging, have been tested and

compared to albumin-(GdDTPA)₃₀ for tumor microvessel characterization (7). The correlation coefficient between these two media for defining transendothelial permeability was high ($r = 0.81$, $P < 0.0001$), and correlations between both contrast media and the histopathological tumor grade were statistically significant ($P < 0.05$). Thus, assuming their approval for clinical use, USPIO are likely to be the first large-size contrast medium on the market that are capable of characterizing tumor microvessels.

However, one major limitation reported in this study was the minimal enhancement of the tumors after intravenous injection of low-dose USPIO; contrast differences compared to precontrast images were barely detectable. The most likely and obvious reason for this minimal enhancement effect was the dose chosen in that study, 1 mg of Fe/kg of body weight. Thus, the goal of this study was to use in the same tumor model a different USPIO with a higher dose (in this case, 5 mg of Fe/kg) to improve conspicuity of tumor enhancement, to test the reproducibility of previous results, and to assess and discuss possible dose dependencies of USPIO for tumor microvessel characterization. MR-derived estimates (fPV and K^{PS}) were correlated to histopathological tumor grade and microvascular density (MVD) counts.

Materials and methods

Animal Model

The study was performed with the approval of the Institutional Committee for Animal Research and in accordance with the guidelines of the National Institutes of Health for the care and use of laboratory animals.

Breast tumors were induced in 32 4- to 6-week-old female Sprague Dawley rats, weighing 210-340 g, by intraperitoneal injection of the carcinogen N-ethyl-N-nitrosurea (ENU) (ENU Isopack, Sigma Chemicals, St. Louis, MO) (10,11). The rats were sedated with ether, and ENU was injected at different doses (90-250 mg); tumors appeared as early as 61 days thereafter. Animals were visually checked for tumor growth every second day. Tumors were imaged as soon as they reached a size of 2 cm.

Before MRI, anesthesia was induced by intraperitoneal injection of 50 mg/kg of sodium pentobarbital. A 23-gauge butterfly catheter (Abbott Laboratories, North Chicago, IL) was inserted into the tail vein for contrast media injection. Immediately after the MRI examination, 2 mL of saline was injected subcutaneously to avoid dehydration effects.

MRI

MRI was performed on animals using a 2 Tesla Omega CSI-II superconducting system (Bruker Instruments, Fremont, CA). This system is equipped with Acustar S-150 self-shielded gradient coils (± 20 G/cm, 15-cm inner diameter). The rats were placed supine within a birdcage radio-frequency coil (inner diameter, 4.5 cm; length, 7.6 cm). A phantom filled with diluted gadopentetate dimeglumine (0.01 mmol/liter) was positioned in the field of view to correct for potential spectrometer variation.

Dynamic contrast-enhanced MRI was performed using an axial T1-weighted 3D spoiled gradient-recalled (SPGR) sequence with the following parameters: TR = 50 msec, TE = 1.4 msec, 1 NEX, 128 X 128 X 16 matrix, 60 X 60 X 48-mm field of view, 3-mm slice thickness, and an acquisition time of 1 minute, 42 seconds. That such a temporal resolution can be considered dynamic reflects the low extraction rate of the larger contrast media, and is based on considerable prior experience with protein-sized macromolecules and ultrasmall particles (4,7,9). Precontrast T1-weighted images with varying flip angles ($\alpha = 10^\circ, 30^\circ, 60^\circ$, and 90°) were obtained to calculate baseline relaxation rates ($R1 = 1/T1$) for blood and tumor by curve fitting (12). Twenty-five dynamic postcontrast 3D image sets were acquired serially at 2-minute intervals for 50 minutes with the parameters described above, except TR was fixed at 50 msec with the flip angle, α , fixed at 90° .

MR Contrast Media

Albumin-(GdDTPA)₃₀ is a 92-kDa prototype of a water-soluble MMCM with a 6-nm diameter, synthesized in our laboratory following the method of Ogan et al (13). Albumin-(GdDTPA)₃₀ has a distribution volume of 0.05 liters/kg (which closely approximates the blood volume) and a plasma half-life of 3 hours in rats, which produces nearly constant enhancement of normal tissues for 30 minutes or longer after injection (14). Albumin-(GdDTPA)₃₀ was injected on imaging day 1 at a dose of 0.03 mmol Gd/kg. SHU555C (Schering AG, Berlin, Germany) consists of USPIO with a mean core size of 3-4 nm in diameter and a hydrodynamic size of < 25 nm. The distribution volume of SHU555C is 0.04 liters/kg, the acute tolerance (in mice, i.v.) is > 10 mmol/kg. The $R1$ ($1/T1$) of the agent in plasma is $22 \text{ sec}^{-1}\text{mM}^{-1}$ of Fe, and the $R2$ ($1/T2$) is $65 \text{ sec}^{-1}\text{mM}^{-1}$ of Fe (at 20 MHz, 37°C). The mean plasma half-life in rats is about 1 hour, and the particles are taken up by the mononuclear phagocyte system and distributed mainly to the liver and spleen. SHU555C was injected 24-30 hours after the first examination at a dose of 5 mg of Fe/kg.

MRI Data and Kinetic Analysis

Images were transferred to, processed, qualitatively examined, and quantitatively analyzed on a Sun Sparc 10 workstation (Sun Microsystems, Mountain View, CA) using the MR-Vision Software package (MR-Vision Co., Menlo Park, CA). In each rat and at each time point, regions of interest were defined by a semiautomated threshold-based method, in which the strongly contrast-enhancing pixels on a late postcontrast image were selected to represent the tumor periphery. Regions of interest (ROIs) were also drawn in the phantom and in the inferior vena cava (IVC). The dynamic signal responses were corrected for potential temporal spectrometer variation by dividing by the signal intensity (SI) of the phantom. Postcontrast $R1$ values were calculated based on the SI and knowledge of precontrast values for each ROI (12). Differences between the precontrast and postcontrast $R1$ values at any time ($\Delta R1$) were assumed to be proportional to the concentration of the contrast medium, either in the blood or in the tissue of interest (12,15). This method of $\Delta R1$ determination is limited by the inherent assumption that the fully relaxed SI did not vary significantly on pre- and postcontrast SPGR images. The $\Delta R1$ data from the blood and tumor were used for kinetic analysis to estimate the coefficient of endothelial permeability, K^{PS} ($\text{mL min}^{-1} 100 \text{ cc}^{-1}$ of tissue), and the fPV (mL cc^{-1} of tissue) using a two compartment, bidirectional model for tumor tissue as previously described in detail (4,16). In this model, a monoexponential function fitted to the $\Delta R1$ data from the blood was used as a forcing function (input function) for the plasma response in the

tumor after correction for hematocrit and after scaling for the fPV. The K^{PS} values determined from the model were multiplied by 100, thereby scaling our permeability measure for 100 cc of tissue. All data fitting was performed with the commercially available SAAM II computer program (SAAM Institute, Seattle, WA), which employs standard variance-weighted nonlinear regression. The uncertainty of the estimates of the model parameters was determined from the covariance matrix at the least-squares fit.

Histologic Analysis

All animals were sacrificed after the second MR examination by an intravenous overdose of 0.3 mL of pentobarbital. Tumors were excised, immediately fixed for 18-24 hours in 10% buffered formalin (Poly Scientific Research & Development Corp., Bay Shore, NY), processed routinely into paraffin, sectioned approximately in the plane of the MR images at 4 μ m, and stained with hematoxylin and eosin for diagnosis and grading. Additional sections were immunostained for von Willebrand Factor and Factor VIII using an avidin-biotin peroxidase technique (Sigma rabbit anti-human poly-clonal, F-3520; Vector ABC kit, PK-6100, Sigma Chemicals, St. Louis, MO).

The Scarff-Bloom-Richardson (SBR) method was applied for tumor grading (17,18). This grading system evaluates (i) the ductoglandular formation and the nuclear characteristics, including (ii) pleomorphism and (iii) the mitotic activity of the tumors. Each of these three morphological features is scored by assigning one to three points; an overall score is obtained then by summation of the individual characteristic scores. SBR scores range from 3 to 9 points; the higher the score, the more malignant and more poorly differentiated is the tumor. For MVD count determination, all discrete, positively immunostained endothelial (brown-staining) clusters with lumina were counted in 20 400 X fields (Olympus Vanox AH-2 microscope) sampled from two sections of each tumor. Where possible, fields were chosen in areas of highest MVD. Stromal microvessels were included in the counts, but capsular and preexisting host small-to-medium vessels were excluded.

MVD is reported as the number of vessels per high-power field. MVD and SBR scoring were performed by the same pathologist without knowledge of MRI findings.

Statistics

Mean values for K^{PS} and fPV for a given contrast agent were compared between fibroadenomas and carcinomas using unpaired t-tests. The paired two-tailed Student's t-test was used to compare mean values of K^{PS} and fPV in the same tumors between albumin-(Gd-DTPA)₃₀ and USPIO. Spearman correlation analyses were performed comparing the estimated MRI-derived parameters (K^{PS} and fPV) with the histologic tumor grade (SBR score) and the MVD. Pearson correlation analyses were performed, comparing the albumin-(Gd-DTPA)₃₀- and the USPIO-derived values for K^{PS} and fPV in the same tumors. A *P* value of < .05 was considered statistically significant.

Results

Thirty-two rats developed mammary tumors as early as 61 days and within 430 days after ENU injection with a mean latent period of 177 ± 114 days. In general,

the latent period for benign tumors was significantly longer (mean, 309 ± 108 days) than for malignant tumors (mean, 143 ± 94 days). Six tumors were benign fibroadenomas, and 26 were malignant tumors (24 adenocarcinomas, 1 sarcoma arising in a fibroadenoma) showing a clear trend toward higher SBR scores with a higher injected ENU dose. However, fibroadenomas were found after injection of 90 ($N = 2$), 180 ($N = 2$), and 250 ($N = 2$) mg of ENU/kg. All six fibroadenomas had the lowest possible SBR score, 3; the malignant tumors spanned a range from 3 to 7; none of the malignant tumors in this study had the highest SBR score possible (8 or 9). (Table 1).

There was a statistical significant difference between the MVD counts in the benign fibroadenomas (187.0 ± 154.5), compared to the malignant tumors (355.8 ± 128.9 , $P < 0.05$). No statistically significant correlation between the SBR score and the MVD was found ($r = 0.13$, $P = 0.41$).

Both albumin-(GdDTPA)₃₀ and USPIO-enhanced MR examinations could be completed successfully in all 32 animals. The kinetic model fit the data well in all experiments. In none of the experiments was a reflux rate constant resolvable from the data using our bidirectional model. Consequently, each data set was refit subject to the constraint that the reflux rate constant was zero. Under

Tumor Type	SBR Score	MVD	Albumin-(GdDTPA) ₃₀		SHU555C	
			fPV	K ^{PS}	fPV	K ^{PS}
benign						
fibroadenoma	3	83	.043	0	.023	0
fibroadenoma	3	**	.038	0	.027	0
fibroadenoma	3	448	.046	0	.030	0
fibroadenoma	3	78	.015	0	.022	0
fibroadenoma	3	205	.037	0	.025	0
fibroadenoma	3	121	.020	0	.022	0
	mean	187.0	.033	0	.025	0
	SD	154.5	.013	0	.003	0
malignant						
carcinoma**	3	532	.021	.018	.021	.020
carcinoma	4	590	.036	.009	.030	.015
carcinoma	4	125	.065	0	.033	.000
carcinoma	4	393	.049	.009	.016	.000
carcinoma	4	358	.024	.014	.033	.006
carcinoma	4	370	.075	.045	.073	.093
carcinoma	5	345	.034	.018	.018	.015
carcinoma	5	206	.031	.022	.019	.016
carcinoma	5	347	.065	.004	.040	0
carcinoma	5	140	.040	.012	.017	.005
carcinoma	5	459	.036	.029	.023	.013
carcinoma	5	386	.017	.006	.013	.003
carcinoma	6	423	.047	.010	.027	.018
carcinoma	6	438	.044	.011	.012	.000
carcinoma	6	231	.025	.013	.039	.018
carcinoma	6	293	.034	.025	.050	.044
carcinoma	6	310	.039	.029	.014	.036
carcinoma	6	473	.119	.050	.011	.000
carcinoma	6	441	.052	.014	.019	.006
carcinoma	6	352	.043	.011	.015	.000
carcinoma	6	464	.036	.006	.034	.000
carcinoma	6	555	.084	.027	.067	.000
carcinoma	7	418	.040	.028	.028	.016
carcinoma	7	226	.020	.014	.030	.019
sarcoma***	7	112	.011	.011	.023	.008
carcinoma	7	263	.049	.015	.019	.016
	mean	355.8	.044	.017*	.028	.014*
	SD	128.9	.023	.012	.016	.020

SBR Score = Scarff Bloom Richardson Score; MVD = Microvascular Density Count; fPV = fractional Plasma Volume; K^{PS} = Trans-endothelial Permeability.

* = statistically significant different from benign group.

** = MVD unavailable (autolysis of the issue).

*** = malignant tumor arising in a fibroadenoma.

Table 1. Histopathologic Results and MR-derived Microvessel Characteristics (fPV, K^{PS}) Sorted by Ascending SBR Score

these conditions all coefficients of variation for the estimated parameter values were acceptable, being less than 50%. A tabulation of K^{PS} and fPV values for albumin-(GdDTPA)₃₀ and USPIO in the fibroadenomas and carcinomas with their respective SBR and MVD scores for each experiment is shown in Table 1.

The mean values for K^{PS} were significantly larger in the carcinomas than in the fibroadenomas for both albumin-(GdDTPA)₃₀ (0.017 ± 0.012 vs. 0, $P < 0.05$) and USPIO (0.014 ± 0.020 vs. 0, $P < 0.05$). Making the same comparisons for fPV, no significant differences were found between carcinomas and fibroadenomas using albumin-(GdDTPA)₃₀ (0.044 ± 0.023 vs. 0.033 ± 0.013 , $P = 0.15$) or USPIO (0.028 ± 0.016 vs. 0.025 ± 0.003 , $P = 0.39$). Furthermore, no significant differences were found comparing mean K^{PS} values between albumin-(GdDTPA)₃₀ and USPIO for either fibroadenomas (0 vs. 0) or carcinomas (0.017 ± 0.012 vs. 0.014 ± 0.020 , respectively, $P = 0.49$). No significant differences were found for mean values of fPV between albumin-(Gd-DTPA)₃₀ and USPIO for fibroadenomas (0.033 ± 0.013 vs. 0.025 ± 0.03 , $P = 0.15$). However, a statistically significant difference was observed for the mean values of fPV in the malignant tumor group between albumin-(GdDTPA)₃₀ and USPIO (0.044 ± 0.023 vs. 0.028 ± 0.016 , $P < 0.05$).

Nonparametric correlation values between K^{PS} (derived with albumin-(GdDTPA)₃₀ and USPIO) and the SBR scores were moderate ($r = 0.54$ and 0.36 , respectively) but nonetheless statistically significant ($P < 0.05$). Correlations between the fPV values and the histologic tumor grades were poor for both contrast media ($r = 0.11$ for albumin-(GdDTPA)₃₀, $r = -0.06$ for USPIO) and did not reach statistical significance.

Weak but still significant ($P < 0.05$) correlations were found for K^{PS} and fPV values between albumin-(Gd-DTPA)₃₀ and MVD ($r = 0.39$ and 0.36 , respectively). MR estimates of K^{PS} and fPV derived with USPIO did not correlate significantly with MVD ($r = 0.08$ and 0.15 , $P > 0.05$). Results of Pearson correlation analyses between albumin-(GdDTPA)₃₀ and USPIO for K^{PS} values in all 32 tumors (fibroadenomas and carcinomas grouped together) in the same animals showed a strong and significant correlation ($r = 0.60$, $P < 0.0005$). Making the same comparison for fPV values, correlations were weak and did not reach statistical significance ($r = 0.27$, $P = 0.13$).

Discussion

The current study shows that USPIO are capable of differentiating various tumor grades by characterizing their microvascular characteristics in a rodent breast cancer model. The transendothelial permeability of cancer microvessels, as expressed by K^{PS} , correlated significantly ($P < 0.05$) with the histologic tumor grade (SBR score) for both contrast media, albumin-(Gd-DTPA)₃₀ ($r = 0.54$) and USPIO ($r = 0.36$). None of the benign tumors revealed any measurable leak to the two MMCM; all tumors with measurable hyperpermeability were malignant.

These results might have important diagnostic consequences for breast cancer patients because USPIO, unlike albumin-(GdDTPA)₃₀, are already used in clinical trials as an angiographic agent and their approval for clinical use is pending (19,20).

SHU555C, as a representative of these contrast media class, is an insoluble iron oxide particle with an average size of $< 25\text{nm}$. Thus, SHU555C has a considerably smaller size than the already clinically available SPIO (200-400nm), which is reflected by prolonged plasma half-life (approximately 3 hours in rats), because the uptake of iron oxide particles by the mononuclear phagocytic system (MPS) is known to be basically a function of their size (21). Consequently, MR angiography has been considered to be the primary indication for USPIO so far; but the shown potential of USPIO to also characterize tumor microvessels will extend its range of clinical indications: USPIO could be used to grade noninvasively individual tumors and, subsequently, could guide therapeutic decisions. USPIO-enhanced MR estimates of tumor endothelial permeability might influence the choice of the optimal therapy (antiangiogenic, cytotoxic, radiation etc.) and, furthermore, could be used for monitoring these therapeutic effects.

The capability of USPIO to characterize tumor microvessels has recently been demonstrated in another animal study (7). Turetschek et al could show, using a different USPIO with slightly different paramagnetic properties than the one used in the current study, that USPIO-enhanced estimates of tumor microvessel hyperpermeability are capable of differentiating various tumor grades (7). The reported correlations between the MR estimates and the SBR scores were high and statistically significant ($r = 0.88$ for albumin-(GdDTPA)₃₀ and $r = 0.82$ for USPIO, $P < 0.05$). However, one limitation of this study was the poor tumor enhancement, which was interpreted to be due to the low dose of USPIO (1 mg of Fe/kg). Although kinetic analyses of their MR data could retrieve sufficient measurable differences between pre- and postcontrast images, in daily clinical routine clear postcontrast enhancement of tumors is a desired morphologic feature for reading and interpreting the films. For this reason, in our study we have chosen to use a rather high dose of USPIO (5 mg/kg), which is still considered to be safe and well tolerated in clinical practice and, moreover, provides an increased signal-to-noise ratio after contrast media injection (Fig. 1).

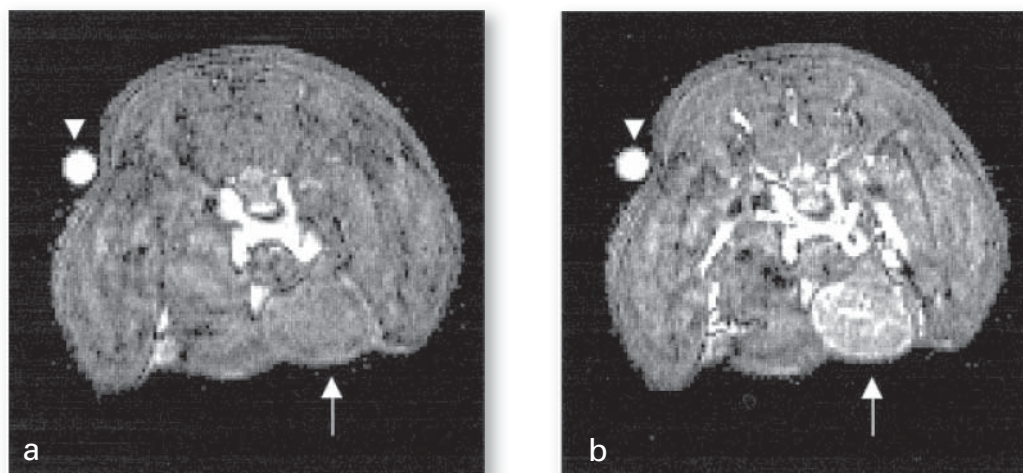


Figure 1. Representative axial T1-weighted (TR = 50 msec, TE = 1.4 msec) SPGR images of a subcutaneous malignant mammary tumor before (a) and 10 minutes after (b) administration of SHU (5 mg of Fe/kg), showing a typical rim enhancement on the postcontrast image (arrow) (b). A phantom was placed in the field of view (arrowhead).

An intrinsic property of USPIO is the reduction of T1 and T2* relaxation times; the magnitude of these effects are dose and MR parameter dependent. The key MR parameter for avoiding confounding T2* effects is the echo time (TE), which, in both studies, was kept as low as possible (1.4 msec).

Two factors compromise the use of USPIO for quantitative descriptions of the tissue microvasculature, primarily, the fact that the positive signal enhancement associated with T1 shortening is accompanied by a negative enhancement associated with T2* shortening. Especially at higher doses, the T2* shortening effects can be severe and may even overwhelm the positive enhancement (15,22). The second is the capricious dependence of the T2* shortening on compartmentalization of the superparamagnetic particle—in short the microgeometry of the microvascular organization. In homogeneous distribution the T2* effects of such contrast agents are less pronounced than when compartmentalized, as in tissue. To a certain extent, leakage of the contrast medium reduces the heterogeneity of compartmentalization, further complicating the scenario.

Our results demonstrate that, using USPIO at a dose of 5 mg/kg, the contrast-to-noise ratio is excellent and correlations between tumor grades and cancer microvessel permeability are still statistically significant. However, the trade-off is a decrease in the correlation values (compared to the results in reference 7), which are interpreted to be caused by technical (higher dose of USPIO) and partly by biological factors.

Unlike Gd-based macromolecules, such as albumin-(GdDTPA)₃₀, the magnetic field disruption and T2* shortening associated with iron oxide particles is considerable, compared to their positive enhancing or T1 shortening effects. Indeed, both large and small iron oxide particles have been considered as T2* shortening agents for studies of the liver and lymph nodes (primary sites of accumulation) (23-25).

The effect of concomitant T2* shortening is a further nonlinearity in the relationship between signal enhancement on T1-weighted MRI and contrast agent concentration. As previously stated, at high concentrations or long TEs, T2* effects may overwhelm T1 shortening and lead to paradoxical isointensity or even hypointensity. To ameliorate this, a short TE is critical, such that the effects of T2* shortening on SI are minimized. As reported by Bremerich et al, a difference in TE between 1.1 and 4.2 msec can dramatically reverse vessel/tissue contrast at high doses of USPIO administration (at 1.5 T). In principle, if changes in T2* can be related to changes in T1, as a function of tracer concentration, these confounding effects could at least in theory be addressed and compensated for (22). However, unlike the relationship between T2 and T1, associated with a contrast medium, the relationship between T2* and T1 depends additionally on the compartmentalization and microgeometry of distribution of the T2* shortening moiety. Water proton spins in the gradient of magnetic field caused by heterogeneous iron distribution dephase, leading to signal loss. In a homogeneous distribution, this gradient vanishes and the dephasing mechanism is averted.

Thus, the relative error in contrast agent concentration determination in a reference, large blood vessel and the tumor tissue, cannot be determined due to the different fractional blood volumes and microvessel distributions. One might argue that the lower fractional blood volume of tissue leads to a lower pixel concentration of iron and thus a lesser T2* shortening—this would lead to a relative hyperintensity on T1-weighted images in

tissue compared to blood and consequent fPV overestimation. On the other hand, one might argue that large vessel pixels contain a homogeneous distribution of iron and do not suffer the confounding distribution heterogeneities that lead to pronounced T2* shortening in tissue voxels. This would lead to an underestimation of tissue fPV (based on positive enhancement). The truth must be presumed to lie somewhere between these two arguments, a function of the specific microvascular geometry and biased by the sensitivity of the pulse sequence, primarily the length of the TE. By choosing a short TE, we attempted to minimize the significance of the above debate. However, the systematic, albeit small, underestimation of fPV using USPIO compared to albumin-(GdDTPA)₃₀ forces us to conclude that the latter argument carries more weight and that tissue heterogeneous distribution of contrast media leads to a more pronounced T2* shortening effect per pixel, compared to a pixel containing 100% blood.

An interesting ray of light may be shone upon the above discussion by the direct comparison of fPV determined by albumin-(GdDTPA)₃₀ and USPIO in a rat-by-rat basis.

Dividing the rats into upper and lower 50 percentiles in terms of their albumin-(GdDTPA)₃₀-based fPV (independent of histopathological findings) (cutoff = 3.8%) reveals that the lower fPV group shows no difference in fPV between albumin-(GdDTPA)₃₀ and USPIO (2.7 vs. 2.7). Interestingly, the group defined by albumin-(GdDTPA)₃₀ as having higher fPV (3.9%-11.9%; mean, 5.6%) has a mean USPIO-derived fPV of 2.8%, no different for the other 50 percentile group. That is to say that differences between albumin-(GdDTPA)₃₀- and USPIO-derived fPV determination differ only when the albumin-(GdDTPA)₃₀-derived values are high (in this case, > 3.8%). Does this mean that in some cases albumin-(GdDTPA)₃₀ overestimates fPV, or does it suggest that at high fPVs the underestimation of fPV associated with the T2* shortening effects of USPIO becomes significant?

Hypothesizing why albumin-based fPV estimates are too high in the more vascular group might introduce arguments about temporal resolution and the leakage of contrast media before the first postcontrast imaging point. In particular, in aggressive tumors with higher permeabilities, this might have some impact.

On the other hand, arguments for the underestimation of USPIO-derived fPV have been made based on the heterogeneous distribution of the agent. Which of these positions is correct is not yet clear. Arguing for albumin-(GdDTPA)₃₀-based accuracy of fPV is the correlation with the MVD (which was absent in the USPIO-derived fPV calculations).

On the other hand, arguing in favor of USPIO, one might expect the larger particle to better remain intravascular (even in malignant hyperpermeable tumor vessels) and not suffer the leak before the first postcontrast imaging time point.

In general, pursuit of yet shorter TEs will render the confounding effects of T2* shortening decreasingly relevant.

The SBR score has been used as our pathologic gold standard for assessing different tumor grades. This grading method evaluates tumor cell morphology, and each tumor is assigned a score between 3 and 9. It has been shown in previous studies that SBR scores correlate strongly with tumor hyperpermeability to macromolecules (4,5). From a statistical point

of view, the scores of the graded tumors should ideally be distributed equally to the different groups in order to ensure maximal statistical power. This, unfortunately, cannot be determined a priori. Any inhomogeneous distribution of tumor grades (i.e., in our study we did not have the highest possible grades, 8 and 9) will influence the results in terms of lower correlation values. We see this as a major explanation for the different correlation values in this study, compared to previously reported values.

Another commonly used biomarker to evaluate tumor microvessels quantitatively is the MVD count. MVD determines quantitatively the vascular status of a given tissue and has been shown to be a marker for patient prognosis and outcome. High MVDs are considered to be linked to the degree of tumor malignancy; the higher the MVD, usually the more malignant or less differentiated a tumor is (26). In this study, using albumin-(GdDTPA)_{30'}, we observed a statistical significance ($P < 0.05$) between MVD and K^{PS} and fPV. In our current tumor model, higher counts of tumor microvessels correlated with higher permeability values and a higher fPV. However, no statistical significant correlation was found between these microvascular characteristics (K^{PS} and fPV) and MVD using USPIO. We interpret these particular results to be the consequence of the higher USPIO dose used in this study because the apparent T2* effects obviously lead to an underestimation of fPV and K^{PS} values.

In summary, our study shows that USPIO can be used for quantitative characterization of tumor microvessels. Estimates of transendothelial permeability, as expressed by K^{PS} , correlate with histologic tumor grade and therefore seem to be better indicators than fPV for assessing cancer microvessel characteristics. Furthermore, we have demonstrated that quantitative MR estimates of microvessels are influenced by intrinsic properties of USPIO, requiring careful considerations of the dose and MR parameters used in any clinical study.

Acknowledgments

Karl Turetschek was supported by the grant: Erwin Schroedinger Auslandsstipendium, Austria. Anda Preda was supported by the “De Drie Lichten” and the “Johannes Vermeij” Foundations, The Netherlands.

References

1. Le Doussal V, Tubiana-Hulin M, Friedman S, Hacene K, Spyrtos F, Brunet M. Prognostic value of histologic grade nuclear components of Scarff-Bloom-Richardson (SBR). An improved score modification based on a multivariate analysis of 1262 invasive ductal breast carcinomas. *Cancer* 1989;64:1914-1921.
2. Harris AL, Zhang H, Moghaddam A, et al. Breast cancer angiogenesis—new approaches to therapy via antiangiogenesis, hypoxic activated drugs, and vascular targeting. *Breast Cancer Res Treat* 1996;38:97-108.
3. Goede V, Fleckenstein G, Dietrich M, Osmers RG, Kuhn W, Augustin HG. Prognostic value of angiogenesis in mammary tumors. *Anticancer Res* 1998;18:2199-2202.

4. Daldrup H, Shames DM, Wendland M, et al. Correlation of dynamic contrast-enhanced MR imaging with histologic tumor grade: comparison of macromolecular and small-molecular contrast media. *Am J Roentgenol* 1998;171:941-949.
5. Su MY, Najafi AA, Nalcioğlu O. Regional comparison of tumor vascularity and permeability parameters measured by albumin-Gd-DTPA and Gd-DTPA. *Magn Reson Med* 1995;34:402-411.
6. Gossmann A, Okuhata Y, Shames DM, et al. Prostate cancer tumor grade differentiation with dynamic contrast-enhanced MR imaging in the rat: comparison of macromolecular and small-molecular contrast media—preliminary experience. *Radiology* 1999;213:265-272.
7. Turetschek K, Huber S, Floyd E, et al. MRI characterization of microvessels in experimental breast tumors using a particulate contrast agent with histopathologic correlation. *Radiology* 2001; 218:562-569.
8. Schwickert HC, Stiskal M, van Dijke CF, et al. Tumor angiography using high-resolution, three-dimensional magnetic resonance imaging: comparison of gadopentetate dimeglumine and a macromolecular blood-pool contrast agent. *Acad Radiol* 1995;2:851-858.
9. Brasch R, Pham C, Shames D, et al. Assessing tumor angiogenesis using macromolecular MR imaging contrast media. *J Magn Reson Imaging* 1997;7:68-74.
10. Stoica G, Koestner A, Capen C. Neoplasms induced with high single doses of N-ethyl-N-nitrosurea in 30 day-old sprague dawley rats, with special emphasis in mammary neoplasia. *Anticancer Res* 1984;4:5-12.
11. Stoica G, Koestner A. Diverse spectrum of tumors in male sprague dawley rats following single high doses of N-ethyl-N-nitrosurea (ENU). *Am J Path* 1984;319-325.
12. Schwickert HC, Roberts TP, Shames DM, et al. Quantification of liver blood volume: comparison of ultra short TI inversion recovery echo planar imaging (ULSTIR-EPI), with dynamic 3D-gradient recalled echo imaging. *Magn Reson Med* 1995;34:845-852.
13. Ogan M, Schmiedl U, Moseley M, Grodd W, Pajenen H, Brasch RC. Albumin labeled with Gd-DTPA: an intravascular contrast enhancing agent for magnetic resonance blood pool imaging: preparation and characterization. *Invest Radiol* 1987;22:665-671.
14. Schmiedl U, Ogan M, Moseley M, et al. Comparison of the contrast-enhancing properties of Albumin-(Gd-DTPA) and Gd-DTPA at 2.0 T: an experimental study in rats. *Am J Roentgenol* 1986; 147:1263-1270.
15. Roberts TP. Physiologic measurements by contrast-enhanced MR imaging: expectations and limitations. *J Magn Reson Imaging* 1997;7:82-90.
16. Shames DM, Kuwatsuru R, Vexler V, Muhler A, Brasch RC. Measurement of capillary permeability to macromolecules by dynamic magnetic resonance imaging—a quantitative noninvasive technique. *Magn Reson Med* 1993;29:616-622.
17. Scarff R, Torloni H. Histological typing of breast tumors. World Health Organization, Geneva, Switzerland. 1968:13-20.
18. Bloom H, Richardson W. Histologic grading and prognosis in breast cancer. *Br J Cancer* 1957;11:359-377.
19. Anzai Y, Prince MR, Chenevert TL, et al. MR angiography with an ultrasmall superparamagnetic iron oxide blood pool agent. *J Magn Reson Imaging* 1997;7:209-214.
20. Engelbrecht MR, Saeed M, Wendland MF, Canet E, Oksendal AN, Higgins CB. Contrast-enhanced 3D-TOFMRA of peripheral vessels: intravascular versus extracellular MR contrast media. *J Magn Reson Imaging* 1998;8:616-621.

21. Weissleder R, Elizondo G, Wittenberg J, Rabito CA, Bengele HH, Josephson L. Ultra-small superparamagnetic iron oxide: characterization of a new class of contrast agents for MR imaging. *Radiology* 1990;175:489-493.
22. Bremerich J, Roberts TPL, Wendland M, et al. Three-dimensional MR imaging of pulmonary vessels and parenchyma with NC100150 (Clariscan). *J Magn Reson Imaging* 2000;11:622-628.
23. Reimer P, Tombach B. Hepatic MRI with SPIO: detection and characterization of focal liver lesions. *Eur Radiol* 1998;8:1198-1204.
24. Harisinghani MG, Saini S, Weissleder R, et al. MR lymphangiography using ultrasmall superparamagnetic iron oxide in patients with primary abdominal and pelvic malignancies: radiographic/pathologic correlation. *Am J Roentgenol* 1999;172:1347-1351.
25. Weissleder R, Elizondo G, Wittenberg J, Lee AS, Josephson L, Brady TJ. Ultrasmall superparamagnetic iron oxide: an intravenous contrast agent for assessing lymph nodes with MR imaging. *Radiology* 1990;175:494-498.
26. de Jong JS, van Diest PJ, Baak JP. Hot spot microvessel density and the mitotic activity index are strong additional prognostic indicators in invasive breast cancer. *Histopathology* 2000;36:306-312.

PART TWO

MAGNETIC RESONANCE IMAGING ASSESSMENT OF ANTIANGIOGENESIS THERAPY

CHAPTER 7

MRI MONITORING OF TUMOR RESPONSE FOLLOWING ANGIOGENESIS INHIBITION IN AN EXPERIMENTAL HUMAN BREAST CANCER MODEL

MRI MONITORING OF TUMOR RESPONSE FOLLOWING ANGIOGENESIS INHIBITION IN AN EXPERIMENTAL HUMAN BREAST CANCER MODEL

7

(EUROPEAN JOURNAL OF NUCLEAR MEDICINE AND
MOLECULAR IMAGING 2003, 3:448-455)

Karl Turetschek^{1,2}, Anda Preda^{1,3}, Eugenia Floyd⁴, David M. Shames¹, Viktor Novikov¹, Timothy P. L. Roberts¹, Jeanette M. Wood⁵, Yanjun Fu¹, Wayne O. Carter⁴, Robert C. Brasch¹

¹ Center for Pharmaceutical and Molecular Imaging, Department of Radiology, University of California San Francisco, San Francisco, California.

² Department of Radiology, University of Vienna, Austria.

³ Visiting Research Scholar from the Department of Radiology, Erasmus University Medical Center, Rotterdam, The Netherlands.

⁴ Pfizer Central Research, Groton, Connecticut.

⁵ Oncology Research, Novartis Pharma AG, Ltd., Basel, Switzerland.

Abstract

The aim of this study was to evaluate the potential of dynamic magnetic resonance imaging (MRI) enhanced by macromolecular contrast agents to monitor noninvasively the therapeutic effect of an anti-angiogenesis VEGF receptor kinase inhibitor in an experimental cancer model. MDA-MB-435, a poorly differentiated human breast cancer cell line, was implanted into the mammary fat pad in 20 female homozygous athymic rats. Animals were assigned randomly to a control ($n=10$) or drug treatment group ($n=10$). Baseline dynamic MRI was performed on sequential days using albumin-(GdDTPA)₃₀ (6.0 nm diameter) and ultrasmall superparamagnetic iron oxide (USPIO) particles (~30 nm diameter). Subjects were treated either with PTK787/ZK 222584, a VEGF receptor tyrosine kinase inhibitor, or saline given orally twice daily for 1 week followed by repeat MRI examinations serially using each contrast agent. Employing a unidirectional kinetic model comprising the plasma and interstitial water compartments, tumor microvessel characteristics including fractional plasma volume and transendothelial permeability (K^{PS}) were estimated for each contrast medium. Tumor growth and the microvascular density, a histologic surrogate of angiogenesis, were also measured. Control tumors significantly increased ($P<0.05$) in size and in microvascular permeability (K^{PS}) based on MRI assays using both macromolecular contrast media. In contrast, tumor growth was significantly reduced ($P<0.05$) in rats treated with PTK787/ZK 222584 and K^{PS} values declined slightly. Estimated values for the fractional plasma volume did not differ significantly between treatment groups or contrast agents. Microvascular density counts correlated fairly with the tumor growth rate ($r=0.64$) and were statistically significant higher ($P<0.05$) in the control than in the drug-treated group. MRI measurements of tumor microvascular response, particularly transendothelial permeability (K^{PS}), using either of two macromolecular contrast media, were able to detect effects of treatment with a VEGF receptor tyrosine kinase inhibitor on tumor vascular permeability. In a clinical setting such quantitative MRI measurements could be used to monitor tumor anti-angiogenesis therapy.

Keywords

Magnetic resonance imaging - Breast cancer - Vascular endothelial growth factor receptor tyrosine kinase - Contrast media

Introduction

Neovascularization by angiogenesis is crucial for tumor development, growth, and metastasis [1]. A high level of vascularization, considered a negative prognostic marker, is associated with higher tumor aggressiveness and increased potential for metastasis [2, 3, 4]. Thus, inhibition of tumor angiogenesis has become a primary target of numerous therapeutic anticancer schemes [5, 6, 7, 8, 9, 10, 11].

Tumor cells and/or tumor-associated inflammatory cells produce a range of growth factors that have become targets for suppression as a therapeutic approach to slow, stop, or even reverse tumor growth [5, 6, 7, 8, 9, 10, 11]. One of these growth factors, vascular

endothelial growth factor (VEGF), also termed vascular permeability factor (VPF), is a well-studied multifunctional cytokine considered to play a pivotal role in the induction of tumor angiogenesis. Expression of VEGF and its receptors correlates with the degree of tumor vascularization and has been proposed as a prognostic factor for assessing patient survival [12]. Current approaches to inhibit tumor neovascularization by attacking the VEGF pathway include (a) a direct inhibition of VEGF itself, (b) blockade of VEGF receptors, (c) blockade of the intracellular molecular cascade triggered by the VEGF-receptor complex, and (d) blockade of VEGF-receptor associated adhesion molecules [13, 14, 15]. In the current study, an orally administered inhibitor of VEGF receptor tyrosine kinase (PTK787/ZK 222584, Novartis, Basel, Switzerland) was used to block the intracellular receptor phosphorylation and signal transduction triggered by the VEGF-receptor complex.

Dynamic magnetic resonance imaging (MRI) enhanced by macromolecular contrast media (MMCM) combined with kinetic modeling has shown a potential for the detection of drug-induced (IL-2 and anti-VEGF antibodies) [16, 17] changes in tumor microvascular status, particularly transendothelial permeability [16, 18]. However, the prototype MMCM used in these previous studies, albumin-(GdDTPA)₃₀, is considered ill-suited for clinical development based on potential immunologic responses and incomplete, prolonged elimination of gadolinium [19, 20]. As alternative MMCM, like ultrasmall superparamagnetic iron oxide (USPIO), are identified as having potential for clinical use [21], these should be evaluated in tumor models as probes for the definition of microvascular characteristics with the final goal of translation to clinical practice.

Thus, in the current study, two macromolecular contrast media, USPIO particles (~30 nm diameter) and albumin-(GdDTPA)₃₀ (~6 nm diameter), were compared in the MRI assessments of tumor microvessel status in an experimental human breast cancer model. Furthermore, the potential use of each contrast medium to detect and measure hypothesized changes in the tumor microvasculature, as well as accompanying changes in fractional plasma volume (fPV) and permeability to the macromolecules, was evaluated 1 week after initiation of anti-angiogenesis therapy with PTK787/ZK 222584. Measures of the dynamic MRI data, including fPV and transendothelial permeability (K^{PS}), obtained with each contrast medium were compared and correlated to tumor growth and to microvascular density, a biomarker of angiogenesis.

Materials and methods

Animal model

The study was performed with the approval of the institutional Committee for Animal Research and in accordance with the guidelines of the National Institutes of Health for the care and use of laboratory animals.

Twenty 4-week-old female homozygous athymic rats (Harlan, Indianapolis, Ind.) were implanted in mammary fat pad with 5×10^6 human breast cancer cells, MDA-MB-435 (Cell Culture Facility of the University of California, San Francisco), suspended in a total volume of 0.3 ml (1:1 mixed with Matrigel), using a 25G needle. This cell line represents a poorly differentiated adenocarcinoma with high expression of VEGF. Animals were

visually checked for tumor growth every second day. Tumors were imaged the first time when they reached a diameter of 1.0-1.5 cm. Before MRI, anesthesia was induced by intraperitoneal injection of 50 mg/kg sodium pentobarbital. A 25-gauge butterfly catheter (Abbott Laboratories, North Chicago, Ill.) was inserted into the tail vein for contrast medium injection. Rats were placed on a heated water pad to keep the body temperature at physiological levels. Immediately after the MRI examination, 2 ml saline was injected subcutaneously to avoid potential dehydration.

MR imaging

MRI was performed on animals using a 2-Tesla Omega CSI-II superconducting system (Bruker Instruments; Fremont, Calif.). This system is equipped with Acustar S-150 self-shielded gradient coils (± 20 G/cm, 15 cm inner diameter). The rats were placed supine within a birdcage radiofrequency coil (inner diameter 4.5 cm, length 7.6 cm). A phantom filled with diluted 0.01 mmol/l gadopentetate dimeglumine was positioned in the field of view to correct for temporal spectrometer variation. A series of precontrast images were acquired using an axial T1-weighted 3D-SPGR (spoiled gradient-recalled) sequence with varying repetition times between 30 and 1,000 ms. Other parameters were: TE 1.4 ms, one NEX (number of excitations), 128x128x16 matrix, 60x60x48 mm, 3 mm slice thickness, flip angle (α) = 90°. These sequences were used to calculate baseline relaxation rates ($R1=1/T1$) for blood and tumor by monoexponential curve fitting. Subsequently dynamic images (precontrast, n=3; postcontrast, n=20) were acquired serially at 2-min intervals for 46 min with the parameters described above, except TR was fixed at 30 ms.

MR contrast media

Albumin-(GdDTPA)₃₀. Albumin-(GdDTPA)₃₀ is a 92-kDa prototype of a water-soluble macromolecular contrast medium with 6 nm hydrodynamic diameter, synthesized in our laboratory following the method of Ogan [22]. Albumin-(GdDTPA)₃₀ has a distribution volume of 0.05 l/kg (which closely approximates the blood volume) and a plasma half-life of approximately 3 h in rats, which produces nearly constant enhancement of normal tissues for 30 min or longer after injection. Albumin-(GdDTPA)₃₀ was injected on imaging day 1 at a dose of 0.03 mmol Gd/kg.

SHU555C. SHU555C (Schering AG, Berlin, Germany) consists of USPIO particles with a mean core size of 3-4 nm diameter and a total hydrodynamic diameter of ~30 nm. The distribution volume of SHU555C is 0.04 l/kg, and the acute tolerance (in mice, i.v.) is >10 mmol/kg. The $R1$ ($=1/T1$) of the agent in plasma is $22\text{ s}^{-1}\text{ mM}^{-1}\text{ Fe}$, and the $R2$ ($=1/T2$) is $65\text{ s}^{-1}\text{ mM}^{-1}\text{ Fe}$ (at 20 MHz, 37°C). The mean plasma half-life in rats is about 1 h, and the particles are ultimately degraded by the mononuclear phagocyte system. SHU555C was injected on day 2, 24 h after the albumin-(GdDTPA)₃₀ injection at a dose of 2.5 mg Fe/kg. At the time the SHU555C was injected, the tumor signal, potentially influenced by the previous day's injection of albumin (Gd-DTPA)₃₀, had returned to baseline values.

Tumor volumes were calculated by summation of the measured tumor area on each slice, adjusted by the slice thickness (3 mm).

Experimental protocol

After the baseline MR examinations, animals were randomly assigned to either the drug treatment or the control group. The control group was fed by gavage with saline; the drug group was treated, also by gavage, with a novel tyrosine kinase inhibitor drug, PTK787/ZK 222584.

PTK787/ZK 222584 is a potent VEGF receptor tyrosine kinase inhibitor [23] that has not been observed to have harmful effects on physiological neovascularization such as wound healing. PTK787/ZK 222584 suppresses VEGF-mediated endothelial cell proliferation, migration, and cell survival. PTK787/ZK 222584 was prepared as follows for oral administration: the succinate salt was suspended in a vehicle containing 5% DMSO and 1% Tween 80 in distilled water. PTK787/ZK 222584 was administered orally by gavage twice daily (morning and evening) at a dose of 50 mg/kg per feeding.

On the day following the seventh day of gavage treatment, all animals were imaged a second time using the identical protocol applied for pretreatment assessment.

MRI data and kinetic analysis

Images were transferred to, processed, qualitatively examined and quantitatively analyzed on a Sun Spark 10 workstation (Sun Microsystems, Mountain View, Calif.) using the MR-Vision Software package (The MR-Vision Co, Menlo Park, Calif.). In each rat and at each time point, regions of interest were defined by a semiautomated threshold-based method in which the strongly contrast-enhancing pixels on a late postcontrast image were selected to represent the tumor periphery. Regions of interest (ROIs) were also drawn in the phantom and in the inferior vena cava (IVC). The dynamic signal responses were corrected for potential temporal spectrometer variation by dividing by the signal intensity (SI) of the phantom. Postcontrast R1 values were calculated based on the SI and knowledge of precontrast R1 values for each ROI as previously described [24]. Differences between the precontrast and postcontrast R1 values at any time ($\Delta R1$) were assumed to be proportional to the concentration of the contrast medium, either in the blood or in the tissue of interest [25, 26, 27]. This method of $\Delta R1$ determination is limited by the inherent assumption that the fully relaxed SI did not vary significantly on pre- and postcontrast SPGR images [27]. The $\Delta R1$ data from blood and tumor were used for kinetic analysis to estimate the coefficient of endothelial permeability, K^{PS} ($\mu\text{l min}^{-1} 100 \text{ cc}^{-1}$ of tissue), and the fractional plasma volume, fPV ($\mu\text{l cc}^{-1}$ of tissue) using a two-compartment, unidirectional model for tumor tissue as previously described in detail [18, 24]. In this model, a monoexponential function fitted to the $\Delta R1$ data from blood was used as a forcing function for the plasma response in the tumor after correction for hematocrit and after scaling for fractional plasma volume. The K^{PS} values determined from the model were multiplied by 100, thereby scaling our permeability measure for 100 cc of tissue. All data fitting was performed with the commercially available SAAM II computer program (SAAM Institute, Seattle, Wash.), which employs standard variance-weighted nonlinear regression. The uncertainty of the estimates of the model parameters was determined from the covariance matrix at the least squares fit.

Histologic analysis

All animals were sacrificed after the second, post-treatment MR examination by an intravenous overdose of pentobarbital and thoracotomy. Tumors were excised, immediately fixed in 70% ethanol and stored at 4°C for 24 h. Tumor sections were processed routinely into paraffin, sectioned in the plane of the MR images at 4 μ m, and immunostained with anti-CD31 antibodies for microvascular density (MVD) counts. All discrete, positively immunostained endothelial clusters were counted in twenty 200X fields (Olympus Vanox AH-2 microscope). Areas containing the highest number of stained vessels were chosen. Stromal microvessels were included in the counts, but capsular and preexisting host small-to-medium vessels were excluded. MVD is reported as the number of vessels per high-power field. The same pathologist, without knowledge of MRI findings, performed all MVD counting.

Statistics

The paired two-tailed Student's *t* test was used to compare mean values of K^{PS} and fPV values in the same tumors pre and post intervention (drug or control) for each contrast medium. This statistical test was also used to compare changes in tumor volume over time in each rat. The unpaired two-tailed Student's *t* test was used to compare mean values for K^{PS} and fPV between the control and the treated group. Pearson correlation analyses were performed comparing the K^{PS} and fPV values for each contrast agent to MVD for both control and treatment studies. A *P* value <0.05 was considered statistically significant.

Results

Tumors grew in all implanted animals and obtained a diameter of approximately 1.5 cm within 14 days (Fig. 1). MR imaging was completed successfully in 23 animals; however, MR-derived data from three rats (all assigned to the control group) were excluded from group analysis because of unacceptably high noise, attributable to subject motion during data acquisition. Thus, the final study population consisted of 20 animals (ten controls and ten treated).

There was no significant difference (*P*=0.52) between groups with respect to tumor volume at baseline: $1,701 \pm 957$ mm³ (mean \pm SD) in the drug treatment group and $1,813 \pm 769$ mm³ in the control group. At the second MRI examination following 7 days of treatment, mean tumor volume had increased significantly in both groups (*P*<0.005), to $3,444 \pm 2,321$ mm³ in the PTK787/ZK 222584-treated group and to $5,610 \pm 1,604$ mm³ in the control group. The calculated tumor volume growth ratio between baseline and follow-up examinations was significantly higher (*P*<0.01) in the control group (3.5 ± 1.4) than in the drug-treated (2.1 ± 0.9) group.

The model provided good fits to the data from all four studies (one baseline and one perturbed experiment for each contrast agent) for each rat. The uncertainty estimates (coefficient of variation in %) for all model measures were within acceptable limits (<50% with means of 7% and 30% for fPV and K^{PS} , respectively). The mean values for fPV and K^{PS} obtained from the model in the pre- and postdrug studies for each contrast agent are shown in *Table 1*.

Using albumin-(GdDTPA)₃₀, the mean K^{PS} values at baseline were $19 \pm 15 \mu\text{l min}^{-1} 100 \text{ cc}^{-1}$ tissue for the drug group and $20 \pm 12 \mu\text{l min}^{-1} 100 \text{ cc}^{-1}$ tissue for the control group ($P=0.89$). At the follow-up examination, the mean K^{PS} values decreased modestly but not significantly ($P=0.16$) in the drug group to $9 \pm 11 \mu\text{l min}^{-1} 100 \text{ cc}^{-1}$ tissue but increased significantly in the control group, to $33 \pm 12 \mu\text{l min}^{-1} 100 \text{ cc}^{-1}$ ($P<0.05$) when compared with baseline values. In addition, K^{PS} post values were significantly greater in the control group ($33 \pm 12 \mu\text{l min}^{-1} 100 \text{ cc}^{-1}$ tissue) than in the drug-treated group ($9 \pm 11 \mu\text{l min}^{-1} 100 \text{ cc}^{-1}$; $P<0.05$).

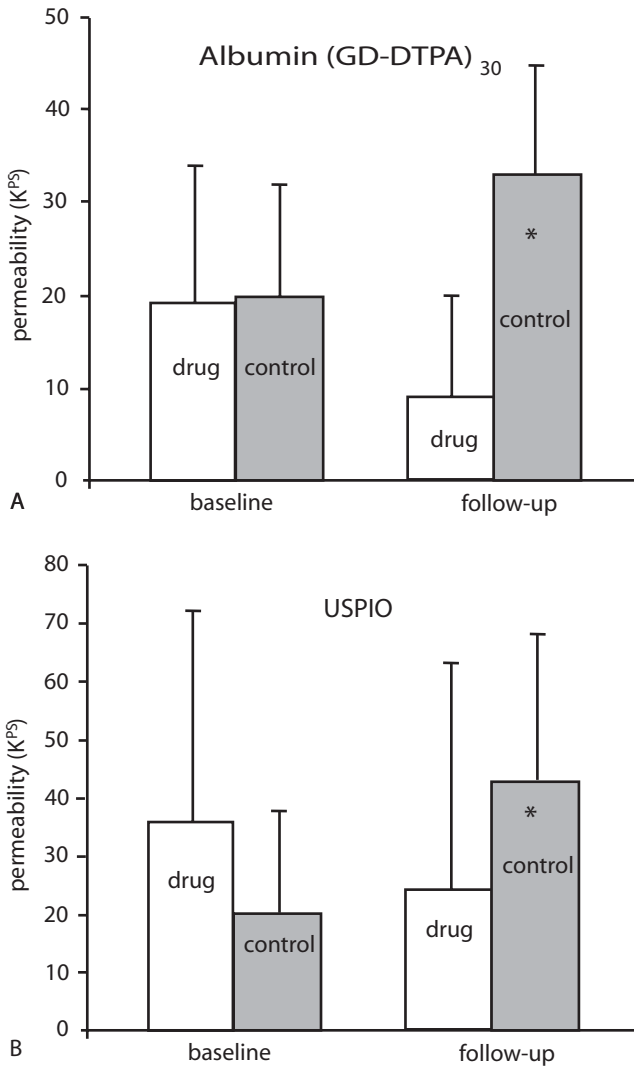


Fig. 1. Transendothelial permeability (K^{PS} in $\mu\text{l min}^{-1} 100 \text{ cc}$ tissue) at baseline and follow-up examinations after saline (= control) or PTK787 treatment based on enhancement with either albumin-(GdDTPA)₃₀ (a) or USPIO (b). *, Statistically significantly different from baseline ($P<0.05$)

Making the same comparisons for USPIO-generated microvascular assays, mean K^{PS} values at baseline were $36 \pm 36 \mu\text{l min}^{-1} 100 \text{ cc}^{-1}$ tissue in the drug group and $20 \pm 18 \mu\text{l min}^{-1} 100 \text{ cc}^{-1}$ tissue in the control group ($P=0.24$). At the follow-up examination, K^{PS} values in the PTK787/ZK 222584 group had decreased modestly ($24 \pm 39 \mu\text{l min}^{-1} 100 \text{ cc}^{-1}$; $P=0.31$) while they had increased significantly in the control group to $43 \pm 25 \mu\text{l min}^{-1} 100 \text{ cc}^{-1}$ tissue ($P<0.05$) (Fig. 1).

Mean fPV values for both contrast agents were not significantly different at baseline, nor was there any evidence of significant change with either drug or placebo treatment.

The mean MVD counts in the drug-treated group (120 ± 37) were statistically significant lower ($P<0.05$) than in the control group (171 ± 57 vessels per high-power field) (Fig. 2). MVD counts correlated fairly strongly with the tumor growth rate ($r=0.64$), moderately with permeability estimates (K^{PS}) ($r=0.46$), and rather poorly with fractional blood volume estimates ($r=-0.07$).

	fPV pre	fPV post	KPS pre	KPS post
Albumin-(GdDTPA) ₃₀				
PTK787/ZK222584	44±18	35±18	19±15	9±11*
Control	42±22	43±19	20±12	33±12**
USPIO				
PTK787/ZK222584	42±21	37±18	36±36	24±39
Control	34±16	36±23	20±18	43±25**

fPV, Fractional plasma volume ($\mu\text{l cc}^{-1}$ tissue); K^{PS}, transendothelial permeability ($\mu\text{l min}^{-1}$ 100 cc^{-1} tissue)

*Statistically significantly different from control group ($P<0.05$);

**statistically significantly different from baseline value ($P<0.05$)

Table 1. MRI estimates of fractional plasma volume (fPV) and transendothelial permeability (K^{PS}) for PTK787/ZK222584-treated and control groups.

there was a decline, albeit nonsignificant, in K^{PS} for the PTK787/ZK 222584-treated tumors over 1 week.

Inter-subject variability in K^{PS} determination reflecting underlying biological differences across times in fact partially shrouds the significance of the individual progression or response data. This is evident in the rather large standard deviations observed in the within-group K^{PS} values. In fact a decline in K^{PS} was observed in eight of ten (80%) drug-treated animals but only one of ten (10%) animals in the contrast group. This response difference was statistically significant (chi test: $P<0.01$) and reflects the general tendency of K^{PS} response in the absence of therapy and reduction in response to drug (Fig. 4). That a small fraction [2/10 (20%)] nonetheless showed elevated K^{PS} post drug treatment may in fact highlight the very clinical scenario that we hope to address, i.e., identification of nonresponders. It may also reflect insufficient amount or duration of drug exposure.

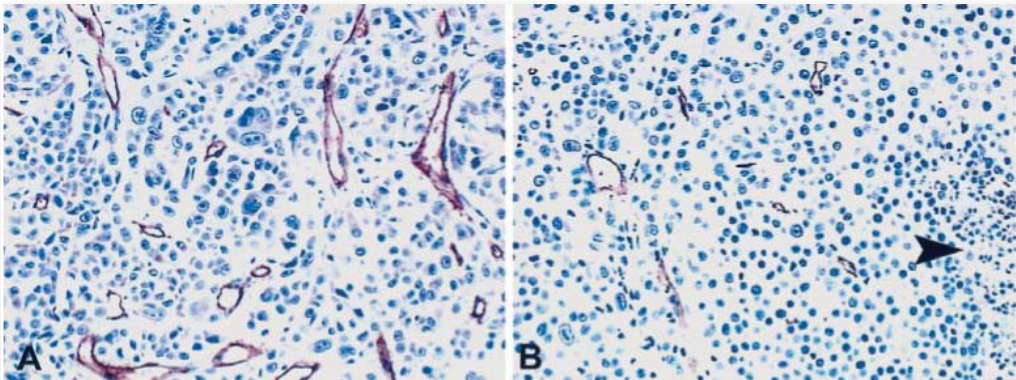


Fig. 2. Human breast carcinoma xenografts showing endothelium immunostained for CD31. The microvascular density of the control tumor (A) is greater than that of the treated tumor (B). The treated tumor also has an area of necrosis (arrowhead)

Discussion

MRI-assayed MDA-MB-435 breast tumor microvascular permeabilities (K^{PS}) and tumor volumes increased significantly ($P<0.05$) in the saline-treated controls. Although PTK787/ZK 222 584-treated tumors also grew over 7 days (Fig. 3), they grew significantly ($P<0.05$) more slowly as measured by the tumor volume growth ratio. Also, while the microvascular permeability in control tumors increased significantly,

These results indicate that MMCM-enhanced MRI as analyzed here can be used to evaluate tumor response to an angiogenesis inhibitor, PTK787/ZK 222584, at least for the circumstances of this study. Not only can MRI be used to measure tumor growth response but data also show its potential to detect a useful differentiated physiologic response in transendothelial permeability. Changes in fractional plasma volume were not useful or sensitive to treatment but perhaps this parameter might become more sensitive after longer periods of drug treatment. The more responsive nature and higher sensitivity of K^{PS} to anti-angiogenic treatment is consistent with the results of Pham et al. [16], who also observed sharp inhibition of K^{PS} and no change in fPV following 1 week of anti-VEGF antibody treatment using the same tumor model enhanced with albumin-(GdDTPA)₃₀ as MR contrast agent.

PTK787/ZK 222584 is representative of a VEGF tyrosine kinase inhibitor which blocks the intracellular molecular cascade at the receptor phosphorylation step of VEGF-mediated angiogenesis. VEGF and its receptors are upregulated especially in the early phases of tumor neovascularization. VEGF stimulates endothelial cell proliferation and cell migration; any inhibition of VEGF, its receptors, or its intracellular molecular cascade mechanism is expected to be associated with morphological and/or functional changes in the tumor microvascularization. Indeed, as shown in this study and in recent literature reports, using various anti-VEGF drugs, tumor growth is slowed significantly [13, 23, 28]. However, tumor growth is not reported to completely halt or to be reversed; cancers treated with VEGF and angiogenesis inhibitors, in general, continue to grow slowly, indicating that other factors are also involved. As well as VEGF, other cytokines such as basic fibroblast growth factor (bFGF), epidermal growth factor (EGF), and platelet-derived growth factor (PDGF) stimulate tumor growth and might even play a compensatory agonist role when VEGF is inhibited [29]. This compensatory mechanism may be the cause for continued tumor growth as observed in the present study. Thus, for more complete tumor growth inhibition, a combination of multiple growth factor inhibitors and/or a combination with cytotoxic drugs (to suppress the stimulatory effect of tumor cells and tumor-associated inflammatory cells for growth factor production) might be necessary.

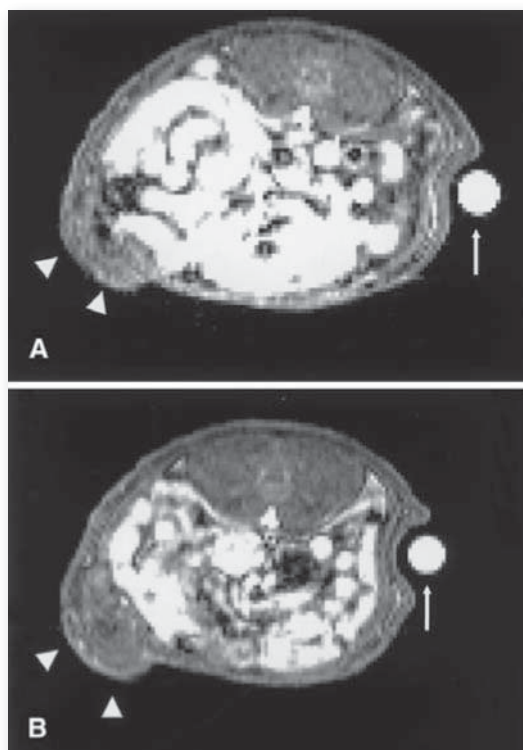


Fig. 3. T1-weighted axial images after i.v. administration of albumin(GdDTPA)₃₀ showing the implanted breast cancer (small arrows) pre (a) and post (b) 7 days of treatment with PTK787/ZK 222584. A phantom was placed in the field of view to correct for temporal spectrometer variation (thick arrow)

VEGF is a multifunctional cytokine. In addition to endothelial cell proliferation, migration, and cell survival, VEGF has a strong effect on vascular permeability, particularly to macromolecular solutes. VEGF is thought to possibly open endothelial pores by loosening intercellular junctions or by induction of endothelial fenestrations [30]. The VEGF-induced macromolecular hyperpermeability of tumors leads to extravasation of plasma proteins and the formation of a gel-like matrix that is considered favorable for new blood vessel growth [12]. Thus, a successful inhibition of VEGF or the VEGF-receptor complex should generate a decreased microvascular permeability to macromolecules. Yano et al. [28] have shown in an experimental lung cancer model that PTK787/ZK 222584 reduces pleural effusions as a function of reducing the tumor-associated vascular hyperpermeability.

In this study transendothelial macromolecular permeability (as estimated by K^{ps} assayed with dynamic contrast-enhanced MRI within the context of a simple mathematical model) decreased slightly in the PTK787/ZK 222584-treated group while a significant increase ($P < 0.05$) in permeability values was observed in the control group using either of two MMCM. Albumin-(GdDTPA)₃₀ has been used successfully as a prototype MMCM to define microvascular characteristics in several experimental studies. These include different physiological and pathological conditions such as tumors [24, 31, 32], inflammation [33, 34], myocardial ischemic states [35], and toxin exposure [36]. Aicher et al. [37] demonstrated in a mouse fibrosarcoma model that the enhancement of tumors with albumin(GdDTPA)₃₀ corresponds to the amount of Evans blue staining with the obvious advantage that the use of this MMCM does not require sacrifice of the animal. However, the incomplete elimination of the gadolinium component of this compound from the body and its potential immunologic response discourage its clinical development. USPIO particles, which have been shown to have the potential to define tumor microvessel characteristics [21], are now being tested in human clinical trials as an angiographic agent [38, 39] and for the assessment of the reticuloendothelial system [40, 41]. Assuming the regulatory approval of USPIO for clinical use, the potential for tumor microvascular characterization might expand their clinical indications and usefulness. USPIO in combination with dynamic MRI and kinetic modeling might prove useful for clinical monitoring of tumor therapy, in particular when anti-angiogenic drugs are used.

As with all contrast-enhanced MRI (and unlike with computed tomography or nuclear medicine methods), accurate quantitation of tracer concentration is potentially limited by the indirect nature of the measured response. In essence we use local water T1 changes to report on the contrast agent concentration. The underlying assumption is that water access to the tracer moiety does not vary in different tissue settings or compartments, i.e., the effective relaxivity of the tracer is contrast. Indeed, given a compartmentalized tracer restricted mostly to the intravascular space, the assumption of fast water exchange (i.e., access of all tissue water to the tracer), seems likely to be inappropriate. Our group and others have previously addressed this issue [26, 27, 42, 43] -the practical conclusion has been to adopt a short TR gradient echo sequence, where fPV overestimates are minimized. Thus we adopted such an image strategy for the purposes of our investigations, for both candidate tracers.

In conclusion, dynamic MRI enhanced with MMCM and analyzed within the context of a simple two-compartment mathematical model of tumor tissue has been applied successfully

to monitor effects of an anti-angiogenic therapy with a VEGF-receptor tyrosine kinase inhibitor. In a clinical setting, transendothelial permeability, estimated here as K^{PS} using MMCM-enhanced MRI and a simple kinetic model, might serve as a functional vascular parameter to follow anti-angiogenesis therapy.

Acknowledgements

This research was supported by NIH grant number RO1 CA82923-01, by the Cancer Research Fund, State of California, under interagency agreement #97-12013 with the Department of Health Services, Cancer Research Program, and by the Erwin Schrödinger Auslandsstipendium, Austria

References

1. Folkman J, Shing Y. Angiogenesis. *J Biol Chem* 1992; 267: 10931-10934.
2. Mendel DB, Laird AD, Smolich BD, et al. Development of SU5416, a selective small molecule inhibitor of VEGF receptor tyrosine kinase activity, as an anti-angiogenesis agent. *Anti-Cancer Drug Design* 2000; 15:29-41.
3. Fontanini G, Lucchi M, Vignati S, et al. Angiogenesis as a prognostic indicator of survival in non-small-cell lung carcinoma: a prospective study. *J Natl Cancer Inst* 1997; 89:881-886.
4. Takahashi Y, Kitadai Y, Bucana CD, Cleary KR, Ellis LM. Expression of vascular endothelial growth factor and its receptor, KDR, correlates with vascularity, metastasis, and proliferation of human colon cancer. *Cancer Res* 1995; 55:3964-3968.
5. Baker CH, Solorzano CC, Fidler IJ. Blockade of vascular endothelial growth factor receptor and epidermal growth factor receptor signaling for therapy of metastatic human pancreatic cancer. *Cancer Res* 2002; 62:1996-2003.
6. Brock CS, Lee SM. Anti-angiogenic strategies and vascular targeting in the treatment of lung cancer. *Eur Respir J* 2002; 19:557-570.
7. Cherrington JM, Strawn LM, Shawver LK. New paradigms for the treatment of cancer: the role of anti-angiogenesis agents. *Adv Cancer Res* 2000; 79:1-38.
8. Fujita M, Hayashi I, Yamashina S, Itoman M, Majima M. Blockade of angiotensin AT1a receptor signaling reduces tumor growth, angiogenesis, and metastasis. *Biochem Biophys Res Commun* 2002; 294:441-447.
9. Gutheil JC, Campbell TN, Pierce PR, et al. Targeted antiangiogenic therapy for cancer using Vitaxin: a humanized monoclonal antibody to the integrin $\alpha v \beta 3$. *Clin Cancer Res* 2000; 6:3056-3061.
10. Hoekman K. SU6668, a multitargeted angiogenesis inhibitor. *Cancer J* 2001; 7 Suppl 3: S134-S138.
11. Naglich JG, Jure-Kunkel M, Gupta E, et al. Inhibition of angiogenesis and metastasis in two murine models by the matrix metalloproteinase inhibitor, BMS-275291. *Cancer Res* 2001; 61:8480-8485.
12. Veikkola T, Karkkainen M, Claesson-Welsh L, Alitalo K. Regulation of angiogenesis via vascular endothelial growth factor receptors. *Cancer Res* 2000; 60:203-212.

13. Strawn LM, McMahon G, App H, et al. Flk-1 as a target for tumor growth inhibition. *Cancer Res* 1996; 56:3540-3545.
14. Gasparini G, Brooks PC, Biganzoli E, et al. Vascular integrin alpha(v)beta3: a new prognostic indicator in breast cancer. *Clin Cancer Res* 1998; 4:2625-2634.
15. Varner JA, Cheresch DA. Integrins and cancer. *Curr Opin Cell Biol* 1996; 8:724-730.
16. Pham CD, Roberts TPL, vanBruggen N, et al. Magnetic resonance imaging detects suppression of tumor vascular permeability after administration of antibody to vascular endothelial growth factor. *Cancer Invest* 1998; 16:225-230.
17. Wikstrom M, Moseley M, White D, et al. Comparison of Gd-DTPA and a macromolecular agent. *Invest Radiol* 1989; 24:609-615.
18. Shames DM, Kuwatsuru R, Vexler V, Muhler A, Brasch RC. Measurement of capillary permeability to macromolecules by dynamic magnetic resonance imaging - a quantitative noninvasive technique. *Magn Reson Med* 1993; 29:616-622.
19. White D, Wang S-C, Aicher K, Dupon J, Engelstad B, Brasch R. Albumin-(DTPA-Gd)₁₅-whole body clearance, and organ distribution of gadolinium. In: *Society of Magnetic Resonance in Medicine, 8th Annual Meeting*. Amsterdam, 1989.
20. Baxter AB, Melnikoff S, Stites DP, Brasch RC. Immunogenicity of gadolinium-based contrast agents for magnetic resonance imaging - induction and characterization of antibodies in animals. *Invest Radiol* 1991; 26:1035-1040.
21. Turetschek K, Huber S, Floyd E, et al. MRI characterization of microvessels in experimental breast tumors using a particulate contrast agent with histopathologic correlation. *Radiology* 2001; 218:562-569.
22. Ogan M, Schmiedl U, Moseley M, Grodd W, Paajenen H, Brasch RC. Albumin labeled with Gd-DTPA: An intravascular contrast enhancing agent for magnetic resonance blood pool imaging: preparation and characterization. *Invest Radiology* 1987; 22:665-671.
23. Wood JM, Bold G, Buchdunger E, et al. PTK787/ZK 222584, a novel and potent inhibitor of vascular endothelial growth factor receptor tyrosine kinases, impairs vascular endothelial growth factor-induced responses and tumor growth after oral administration. *Cancer Res* 2000; 60:2178-2189.
24. Daldrup H, Shames DM, Wendland M, et al. Correlation of dynamic contrast-enhanced MR imaging with histologic tumor grade: comparison of macromolecular and small-molecular contrast media. *AJR Am J Roentgenol* 1998; 171:941-949.
25. Wedeking P, Sotak CH, Telser J, Kumar K, Chang CA, Tweedle MF. Quantitative dependence of MR signal intensity on tissue concentration of Gd(HP-DO3A) in the nephrectomized rat. *Magn Reson Imaging* 1992; 10:97-108.
26. Schwickert HC, Roberts TP, Shames DM, et al. Quantification of liver blood volume: comparison of ultra short TI inversion recovery echo planar imaging (ULSTIR-EPI), with dynamic 3D-gradient recalled echo imaging. *Magn Reson Med* 1995; 34:845-852.
27. Roberts TP. Physiologic measurements by contrast-enhanced MR imaging: expectations and limitations. *J Magn Reson Imag* 1997; 7:82-90.
28. Yano S, Herbst RS, Shinohara H, et al. Treatment for malignant pleural effusion of human lung adenocarcinoma by inhibition of vascular endothelial growth factor receptor tyrosine kinase phosphorylation. *Clin Cancer Res* 2000; 6:957-965.
29. Bruns CJ, Solorzano CC, Harbison MT, et al. Blockade of the epidermal growth factor receptor signaling by a novel tyrosine kinase inhibitor leads to apoptosis of endothelial cells and therapy of human pancreatic carcinoma. *Cancer Res* 2000; 60:2926-2935.

30. Roberts WG, Palade GE. Increased microvascular permeability and endothelial fenestration induced by vascular endothelial growth factor. *J Cell Sci* 1995; 108:2369-2379.
31. Schwickert HC, Stiskal M, Roberts TP, et al. Contrast-enhanced MR imaging assessment of tumor capillary permeability: effect of irradiation on delivery of chemotherapy. *Radiology* 1996; 198:893-898.
32. Gossmann A, Okuhata Y, Shames DM, et al. Prostate cancer tumor grade differentiation with dynamic contrast-enhanced MR Imaging in the rat: comparison of macromolecular and small-molecular contrast media - preliminary experience. *Radiology* 1999; 213:265-272.
33. Helbich T, Roberts TPL, Rollins MD, et al. Non-invasive assessment of wound healing angiogenesis with contrast enhanced MRI. In: *Contrast media research*. Woodstock, Vermont, 1999.
34. Berthezene Y, Vexler V, Kuwatsuru R, et al. Differentiation of alveolitis and pulmonary fibrosis with a macromolecular Mr-imaging contrast agent. *Radiology* 1992; 185:97-103.
35. Saeed M, van Dijke CF, Mann JS, et al. Histologic confirmation of microvascular hyperpermeability to macromolecular MR contrast medium in reperfused myocardial infarction. *J Magn Reson Imaging* 1998; 8:561-567.
36. Berthezene Y, Mühler A, Lang P, et al. Safety aspects and pharmacokinetics of inhaled aerosolized gadolinium. *J Magn Reson Imaging* 1993; 3:125-130.
37. Aicher KP, Dupon JW, White DL, et al. Contrast-enhanced magnetic resonance imaging of tumor-bearing mice treated with human recombinant tumor necrosis factor- α . *Cancer Res* 1990; 50:7376-7381.
38. Engelbrecht MR, Saeed M, Wendland MF, Canet E, Oksendal AN, Higgins CB. Contrast-enhanced 3D-TOF MRA of peripheral vessels: intravascular versus extracellular MR contrast media. *J Magn Reson Imaging* 1998; 8:616-621.
39. Bremerich J, Roberts TPL, Wendland M, et al. Three-dimensional MR imaging of pulmonary vessels and parenchyma with NC100150 (Clariscan). *J Magn Reson Imaging* 2000; 11:622-628.
40. Weissleder R, Elizondo G, Wittenberg J, Rabito CA, Bengel HH, Josephson L. Ultra-small superparamagnetic iron oxide: characterization of a new class of contrast agents for MR imaging. *Radiology* 1990; 175:489-493.
41. Weissleder R, Elizondo G, Wittenberg J, Lee AS, Josephson L, Brady TJ. Ultras-small superparamagnetic iron oxide: an intravenous contrast agent for assessing lymph nodes with MR imaging. *Radiology* 1990; 175:494-498.
42. Donahue KM, Weisskoff RM, Chesler DA, et al. Improving MR quantification of regional blood volume with intravascular T1 contrast agents: accuracy, precision, and water exchange. *Magn Reson Med* 1996; 36:858-867.
43. Donahue KM, Weisskoff RM, Burstein D. Water diffusion and exchange as they influence contrast enhancement. *J Magn Reson Imaging* 1997; 7:102-110.

CHAPTER 8

TUMOR MICROVASCULAR CHANGES IN ANTIANGIOGENIC TREATMENT: ASSESSMENT BY MAGNETIC RESONANCE CONTRAST MEDIA OF DIFFERENT MOLECULAR WEIGHTS

TUMOR MICROVASCULAR CHANGES IN ANTIANGIOGENIC TREATMENT: ASSESSMENT BY MAGNETIC RESONANCE CONTRAST MEDIA OF DIFFERENT MOLECULAR WEIGHTS

8

(JOURNAL OF MAGNETIC RESONANCE IMAGING 2004,
20:138-144)

Karl Turetschek, MD,^{1,2} Anda Preda, MD,^{1,3} Viktor Novikov, MD,¹ Robert C. Brasch, MD,¹
Hanns J. Weinmann, PhD,⁴ Patrick Wunderbaldinger, MD,² and Timothy P.L Roberts, PhD^{1,5}

¹ Center for Pharmaceutical and Molecular Imaging, Department of Radiology,
University of California, San Francisco, California.

² Department of Radiology, University of Vienna, Austria.

³ Department of Radiology, Erasmus MC, University Medical Center Rotterdam,
The Netherlands.

⁴ Schering AG, Berlin, Germany.

⁵ Department of Medical Imaging, University of Toronto, Canada.

Abstract

Purpose

To test magnetic resonance (MR) contrast media of different molecular weights (MWs) for their potential to characterize noninvasively microvascular changes in an experimental tumor treatment model.

Materials and Methods

MD-MBA-435, a poorly differentiated human breast cancer cell line, was implanted into 31 female homozygous athymic rats. Animals were assigned randomly to a control (saline) or drug treatment (monoclonal antibody vascular endothelial growth factor (Mab-VEGF) antibody) group. In both groups, dynamic MR imaging (MRI) was performed in each animal using up to three different contrast media on sequential days at baseline and follow-up examination. The MWs of the contrast media used ranged from 557 Da to 92 kDa. Using a bidirectional kinetic model, tumor microvessel characteristics, including the fractional plasma volume (fPV) and transendothelial permeability (K^{ps}), were estimated for each contrast medium. These microvascular characteristics were compared between drug and control groups and between contrast media of different MWs.

Results

Tumors grew significantly slower ($P < 0.0005$) in the drug treatment group than in the control group. Mean K^{ps} and fPV values decreased significantly ($P < 0.05$) in the Mab-VEGF antibody-treated group compared to baseline values using intermediate or macromolecular contrast media (MMCM), but did not change significantly using small molecular contrast media (SMCM). In the control groups, mean K^{ps} and mean fPV values did not reach statistical significance for any of the contrast media used.

Conclusion

Therapeutic effects of a Mab-VEGF antibody on tumor microvessel characteristics can be monitored by dynamic MRI. Intermediate-size agents, such as Gadomer-17, offer a substantial dynamic range and are less limited by imaging precision and therefore should be considered a practical alternative to monitor antiangiogenesis treatment effects in a clinical setting.

Key Words

magnetic resonance imaging; angiogenesis; vascular endothelial growth factor; contrast media; permeability

Introduction

Tumor neovascularization is crucial for cancer growth and therefore directly influences patient prognosis. The close relationship between tumor angiogenesis, the metastatic

potential of malignant tumors, and, finally, patient survival has already been shown in numerous studies (1-5). Recent advances in the development of angiogenesis inhibitors have led to new forms of tumor treatment. Many drugs are currently under pre-clinical investigation to test their individual potential to stop, reverse, or at least slow down tumor growth (6-10). Although different drugs target tumor angiogenesis at different molecular levels, all of them have in common various morphological changes of the tumor microvasculature: these include apoptosis (11,12), changing the microvascular permeability by loosening endothelial tight junctions (13), increasing the number of transcellular channels or vesiculovacuolar organelles (VVOs) (14), and more.

Dynamic magnetic resonance imaging (MRI), used in combination with macromolecular contrast media (MMCM) and kinetic modeling, has shown the potential to monitor changes in the tumor microvasculature following antiangiogenic therapy by determination of microvessel parameters, such as transendothelial permeability (K^{PS}) or fractional plasma volume (fPV) (15-17). In these studies small molecular contrast media (SMCM), i.e., gadopentetate (GdDTPA), failed to differentiate reliably between pre- and post-drug-induced changes of microvessel characteristics (17). Thus, the widely used contrast medium GdDTPA does not seem to be promising for the purpose of quantitatively monitoring permeability changes in the microvasculature. On the other hand, because the more promising prototype MMCM, albumin-(GdDTPA)₃₀, is not suited for human use, several new MR contrast media are under vigorous development. Despite these research efforts, so far it is not known which size or molecular weight (MW) of a particular contrast medium would be best suited for tumor microvessel characterization. In particular, an ideal agent must show sensitivity to disease progression and responsiveness to interventional therapy, offering a wide dynamic range of target parameters such as permeability, and be amenable to clear-cut demonstrations of both positive and negative effects (change to noise ratio). Furthermore, for clinical applicability, such clear-cut resolution of permeability changes should ideally be derived from only a few minutes of dynamic imaging.

Therefore, the purpose of this study was to investigate different MR contrast media of various sizes/MWs in order to define the cutoff size that would be best suited to enable a reliable, quick, and precise tumor microvessel characterization, sensitive to changes associated with disease progression and therapeutic response. For this purpose, an established model of suppressing tumor angiogenesis was used: tumor neovascularization was blocked by means of an anti-vascular endothelial growth factor (VEGF) antibody in an experimental human breast cancer.

Materials and methods

Animal Model

The study was performed with the approval of the Institutional Committee for Animal Research and in accordance with the guidelines of the National Institutes of Health for the care and use of laboratory animals.

MD-MBA-435, a poorly differentiated human breast cancer cell line with high expression of VEGF, was implanted into 31 four-week-old female homozygous athymic rats (Harlan, Indianapolis, IN). Approximately 5×10^6 human breast cancer cells, MDA-MB-435 (Cell Culture Facility of the University of California, San Francisco), suspended in a total volume of 0.3 mL (1:1 mixed with Matrigel®; Collaborative Biomedical Products, Bedford, MA), were implanted in the mammary fat pad using a 25-Gauge needle (Abbott Laboratories, North Chicago, Ill). All animals were observed daily at the test facility for general appearance, behavior, and tumor growth. Baseline MRI was performed when tumors reached a size of 10-15 mm. Before MRI animals were anesthetized by intraperitoneal injection of 50 mg/kg sodium pentobarbital. A 25-Gauge butterfly catheter (Abbott Laboratories, North Chicago, IL) was inserted into the tail vein for contrast media injection. Rats were placed on a heated water pad to keep the body temperature at physiological levels. Immediately after the MRI examination 2 mL of saline was injected subcutaneously to avoid dehydration effects.

MRI

Contrast agent	MW	Dose
GdDTPA (Magnevist)	547Da	0.1 mmol/kg
ZK159560	8.7kDa	0.1 mmol/kg
Gadomer-17	17kDa	0.1 mmol/kg
ZK181220	25.9kDa	0.1 mmol/kg
Albumin-(GdDTPA) ₃₀	92kDa	0.03 mmol/kg
USPIO (SHU555C)	—	2.5 mgFe/kg

Table 1. Contrast Agents Administered (With Molecular Weights and Doses)

MRI was performed on animals using an Omega CSI-II superconducting system (Bruker Instruments, Fremont, CA) operating at 2 Tesla and equipped with Acustar S-150 self-shielded gradient coils. The rats were placed supine within a birdcage radio frequency coil (inner diameter = 4.5 cm, length = 7.6 cm). A phantom filled with diluted 0.01 mmol/liter gadopentetate dimeglumine was positioned in the field of view (FOV) to correct for potential spectrometer variation in each experiment. A series of precontrast images were acquired using an axial T1-weighted three-dimensional spoiled gradient-recalled (3D-SPGR) sequence with varying repetition times between 30 and 1000 msec; other parameters were TE = 1.4 msec, one excitation, matrix = 128 X 128 X 16, FOV = 50 X 50 X 48 mm, slice thickness = 3 mm, and flip angle (α) = 90°. These sequences were used to calculate baseline relaxation rates ($R_1 = 1/T_1$) for blood and tumor by curve fitting. Dynamic contrast-enhanced MRI was performed using a T1-weighted 3D-SPGR sequence with a keyhole technique consisting of three initial precontrast and dynamic postcontrast images. When small- and medium-size MR contrast media (GdDTPA, ZK159560, ZK181220, Gadomer-17) were used, 37 postcontrast images were acquired with high temporal resolution using a keyhole technique with the following parameters: TR = 50 msec, TE = 1.4 msec, one signal acquired, matrix = 128 X 64 X 8, FOV = 50 X 50 X 48 mm, slice

thickness = 3 mm, and acquisition time = 6 seconds per image. When MMCM (albumin-(GdDTPA)₃₀ or SHU555C) were used precontrast images were immediately followed by 30 dynamic 3D-SPGR postcontrast images with a high spatial resolution (matrix = 128 X 128 X 16, otherwise identical parameters, acquisition time = 1 minute 42 seconds/sequence).

MR Contrast Media

Six different media of different sizes and/or MW have been used in this study (Table 1).

GdDTPA has an MW of 547 and was injected on day 1 at a dose of 0.1 mmol/kg. GdDTPA has a distribution volume approximating the extracellular volume, its plasma disappearance is rapid and multiexponential, and its elimination occurred exclusively via the kidneys (18).

ZK159560 and ZK181220 are prototype MR contrast media developed by Schering AG (Berlin, Germany) and differ only by their MWs (ZK159560, 8.7 kDa; ZK181220, 25.9 kDa). Both ZK159560 and ZK181220 were injected at a dose of 0.1 mmol/kg.

Gadomer-17 is a prototype MR contrast medium from Schering AG (Berlin, Germany) with an MW of 17 kDa (19). Gadomer-17 has 24 Gd complexes bound to each molecule; the distribution volume is 0.11 liter/kg. It is eliminated by the kidneys with only 4% remaining at 24 hours (19). The toxicity is low with an LD₅₀ (lethal dose in 50% of the population) of more than 30 mmol/kg in the rat. Gadomer-17 was injected at a dose of 0.1 mmol/kg.

Albumin-(GdDTPA)₃₀ is a 92-kDa prototype of a water-soluble MMCM with 6 nm diameter, synthesized in our laboratory following the method of Ogan et al (20). Albumin-(GdDTPA)₃₀ has a distribution volume of 0.05 liter/kg (which closely approximates the blood volume) and a plasma half-life of three hours in rats, which produces nearly constant enhancement of normal tissues for 30 minutes or longer after injection. Albumin-(GdDTPA)₃₀ was injected on imaging day 1 at a dose of 0.03 mmol Gd/kg.

SHU555C (Schering AG, Berlin, Germany) consists of ultrasmall superparamagnetic iron oxide (USPIO) particles with a mean core size of 3-4 nm diameter and a total hydrodynamic diameter of ~30 nm. The distribution volume of SHU555C is 0.04 liter/kg and the acute tolerance (in mice, i.v.) is >10 mmol/kg. The R1 (= 1/T1) of the agent in plasma is 22 second⁻¹mM⁻¹ Fe and the R2 (= 1/T2) is 65 second⁻¹mM⁻¹Fe (at 20 MHz, 37°C). The mean plasma half-life in rats is about one hour, and the particles are taken up by the mononuclear phagocyte system. SHU555C was injected 24 hours after the albumin-(GdDTPA)₃₀ injection at a dose of 2.5 mg Fe/kg.

Experimental Protocol

After the baseline MR examinations, animals were randomly assigned to the drug treatment or control group. Each rat was then imaged with one of the two smaller agents, one of the two intermediate agents, and one of the two larger agents (day 0, intermediate; day 1, small, followed after at least two hours by large). Because of the lack of availability of ZK159560 and SHU555C compared to GdDTPA and albumin-GdDTPA, and the prototypical nature of the latter two, more animals were imaged with these better-characterized agents

than their analogs of similar size category. Physiological saline (0.2 mL) was injected i.p. in rats belonging to the control group; the drug group was treated with an i.p. injection of 0.2 mL of monoclonal antibody (Mab)-VEGF antibody (Genentech, South San Francisco, CA). The i.p. injections were done on days 1, 4, and 7. The day following the seventh day of drug/saline treatment all animals were imaged a second time using the identical protocol applied for pretreatment assessment. All animals were killed after the second post-treatment MR examination by an intravenous overdose of 0.3 mL of pentobarbital.

MRI Data and Kinetic Analysis

Images were transferred to, processed, qualitatively examined, and quantitatively analyzed on a Sun Sparc Ultra-10 workstation (Sun Microsystems, Mountain View, CA) using the MR-Vision Software package (The MR-Vision Co., Menlo Park, CA). In each rat and at each time point, regions of interest (ROIs) were defined by a semiautomated threshold-based method in which the strongly contrast-enhancing pixels on a late postcontrast image were selected to represent the tumor periphery. ROIs were also drawn in the phantom and in the inferior vena cava (IVC). The dynamic signal responses were corrected for potential temporal spectrometer variation by dividing by the signal intensity (SI) of the phantom. Postcontrast R1 values were calculated based on the SI and knowledge of precontrast R1 values for each ROI. Differences between the precontrast and postcontrast R1 values at any time ($\Delta R1$) were assumed to be proportional to the concentration of the contrast medium, either in the blood or in the tissue of interest (21-23). This method of $\Delta R1$ determination is limited by the inherent assumption that the fully relaxed SI did not vary significantly on pre- and postcontrast SPGR images (23). The $\Delta R1$ data from blood and tumor were used for kinetic analysis to estimate the coefficient of K^{PS} (mL minute⁻¹ 100 cc⁻¹ of tissue) and the fPV (mL cc⁻¹ of tissue). In brief, while the initial enhancement of relaxation in a voxel of tissue relates to the fractional blood volume, progressive tissue relaxation enhancement relates to contrast agent leak from the intravascular to the extravascular compartment. Constructing the ratio of tissue relaxation enhancement to reference vascular relaxation enhancement (from the IVC) allows approximate graphical visualization of fPV and permeability from the intercept and slope of the plot against time, respectively. Accurate estimations incorporating consideration of plasma tracer disappearance and bidirectional tracer transport between intra- and extravascular compartments are obtained from two-compartment bidirectional kinetic modeling.

All data fitting was performed using a nonlinear least squares numerical approach, implemented in Kaleidagraph 3.5 (Synergy Software, Reading, PA). Fit parameters fPV and K^{PS} are converted to units of mL/cc tissue (equivalent to the fraction given by the intercept of the plot of the ratio of tissue to vascular relaxation enhancement) and mL/100 g/minute (manageable units of volume transport per mass of tissue, derived by scaling fit units of tissue to vascular relaxation enhancement ratio, or fraction, per second, assuming a tissue density of 1 g/cc and rescaling from seconds to minutes).

Tumor volumes were calculated by approximate numerical integration: summation of the measured tumor area on each slice, multiplied by the slice thickness (3 mm).

Statistics

The paired two-tailed Student's t-test was used to compare mean K^{PS} and fPV values in the same tumors pre- and postintervention (drug or control) for each contrast medium. The two-tailed paired Student's t-test was used to calculate differences in the tumor volume over time in each rat. $P < 0.05$ was considered statistically significant.

Results

	Control	Drug group
GdDTPA	9	13
ZK159560	0	7
Gadomer-17	5	7
ZK181220	5	6
SHU555C	6	6
Albumin-(GdDTPA) ₃₀	12	19

Table 2. Study Sample Sizes for Each Contrast Agent and Treatment Arm

Implanted tumors grew to a size of approximately 1.5 cm within 14 days. The final study population consisted of 31 rats, which were randomly assigned to control or drug-treated groups (Table 2).

Taking all animals together, tumor volumes at baseline examination were not significantly different ($P = 0.49$) between the drug-treated ($1076 \pm 763 \text{ mm}^3$) and control ($777 \pm 240 \text{ mm}^3$) groups. Tumors continued growing in both animal groups, from 777 ± 240 to 2594 ± 1121 in the control group, and from 1076 ± 763 to 1830 ± 1408 in the drug-treated group. Hence, tumors grew significantly faster ($P < 0.0005$) in the control group (calculated tumor growth ratio = 3.3 ± 1.0) than in the drug-treated group (tumor growth ratio = 1.79 ± 0.7).

Mean K^{PS} and fPV values at baseline and at the follow-up examination using all contrast media are listed in Table 3 for both groups, drug-treated and control animals. In the Mab-VEGF antibody-treated group, mean K^{PS} and fPV values decreased significantly ($P < 0.05$) from baseline values using any of the four intermediate or larger-size agent: albumin-(GdDTPA)₃₀, SHU555C, Gadomer-17, or ZK181220. Using smaller agents, ZK159560 and GdDTPA, mean K^{PS} and fPV values between pre- and post-treatment exam did not reach statistical significance ($P > 0.05$). In the control groups, mean K^{PS} and fPV values did not reach statistical significance for any of the contrast media used.

Discussion

This study shows that suppression of tumor neoangiogenesis leads to a considerable slowdown in tumor growth within one week of treatment. Although the implanted human breast cancers continued to grow in both groups, no matter if the animals were treated with saline (control group) or a Mab-VEGF antibody (drug group), the tumor growth ratio was statistically significantly ($P < 0.0005$) smaller in the drug-treated group than in the control group.

VEGF is considered to be one of the most important promoters of tumor neoangiogenesis (24-27). VEGF and its receptors are upregulated in early phases of tumor neovascularization, thereby stimulating endothelial cell proliferation and migration. Also, VEGF has crucial effects on the endothelial wall integrity, gaps and channels within endothelial cells are numerically increased, and tight junctions between the cells are loosened. Indeed, VEGF, also known as vascular permeability factor (VPF), induces vessel hyperpermeability, which leads to an extravasation of plasma proteins and the formation of a matrix that is favorable for blood vessel growth (28,29). Thus, inhibition of VEGF is accompanied by a decrease in microvascular permeability to proteins and macromolecules and a suppression of neoangiogenesis, both facts nicely demonstrated in the present study.

It is clear, however, that the property of microvascular permeability must depend upon the physical characteristics (size) of the tracer solutes. Whereas SMCM diffuse through normal and injured vessel walls, MMCM remain strongly intravascular within normal vessels. But as soon as the vessel wall integrity is disrupted—no matter if the underlying cause is neoplastic, inflammatory, or toxic—MMCM diffuse into the interstitial space (30-32). Albumin-(GdDTPA)₃₀ has been used successfully as a prototype MMCM (≈ 92 kDa) to define microvascular characteristics in several experimental studies (15,33). These include different physiological and pathological conditions such as tumors (16,33-35), inflammation (31), myocardial ischemic states (32), wound healing (36), and toxin exposure. The incomplete elimination of the gadolinium part of this compound from the body and its potential immunologic response, however, hinder its clinical use (20). Recently, USPIO particles have been shown in an animal model to have the potential for defining tumor microvessel characteristics (16). K^{PS} and fPV generated with USPIO correlated strongly and statistically significantly ($P < 0.01$) with albumin-(GdDTPA)₃₀-derived K^{PS} and fPV values using dynamic MRI and a bidirectional kinetic model (16). However, both albumin-(GdDTPA)₃₀ and USPIO suffer from very low absolute signal enhancement due to very low rates of contrast media extravasation. Consequently, long scan observation periods are necessitated to observe significant enhancement above the image noise level.

	Control		Drug	
	Pre	Post	Pre	Post
K^{PS}				
GdDTPA	6.75 \pm 7.05	7.35 \pm 8.99	3.27 \pm 18.9	2.56 \pm 3.16
ZK159560	Not studied	Not studied	1.34 \pm 1.47	2.81 \pm 1.65
Gadomer-17	1.121 \pm 0.358	1.205 \pm 0.307	1.064 \pm 0.420	0.445 \pm 0.234*
ZK181220	0.418 \pm 0.307	0.430 \pm 0.199	0.469 \pm 0.348	0.196 \pm 0.160*
SHU555C	0.010 \pm 0.009	0.021 \pm 0.025	0.018 \pm 0.016	0.002 \pm 0.003*
Albumin-(GdDTPA) ₃₀	0.016 \pm 0.011	0.012 \pm 0.020	0.019 \pm 0.020	0.007 \pm 0.010*
fPV				
GdDTPA	34.4 \pm 18.4	42.2 \pm 17.0	38.8 \pm 13.2	33.8 \pm 14.1
ZK159560	Not studied	Not studied	9.1 \pm 10.0	9.5 \pm 4.4
Gadomer-17	11.4 \pm 6.1	14.7 \pm 4.0	12.3 \pm 6.3	6.1 \pm 4.4*
ZK181220	13.5 \pm 5.8	10.5 \pm 4.7	10.4 \pm 3.2	6.3 \pm 3.3*
SHU555C	4.4 \pm 1.4	5.1 \pm 3.0	5.4 \pm 2.1	3.0 \pm 1.0*
Albumin-(GdDTPA) ₃₀	6.1 \pm 2.8	6.1 \pm 1.5	7.25 \pm 2.43	4.33 \pm 1.46*

* = Statistically significant from baseline ($P < .05$).

K^{PS} = coefficient of permeability surface area product (ml/min/100cc tissue); fPV = fractional plasma volume (%); Drug = Mab-VEGF antibody.

Table 3. Mean Permeability Values (K^{PS}) and Fractional Plasma Volume (fPV) Using Different Contrast Media for the Control (Saline) Drug-Treated (Mab-VEGF antibody) Groups

Using SMCM, like GdDTPA (MW = 547) and ZK159560 (MW = 8.7 kDa), for determining K^{PS} and fPV, no statistically significant correlation between pre- and post-Mab-VEGF antibody-treated subjects was found, largely due to the very rapid and very pronounced signal enhancement observed, which precluded simple kinetic modeling, yielding estimates of fPV and K^{PS} with high uncertainties and large within group standard deviations. In some sense, kinetic modeling of dynamic enhancement with such agents can be considered to be limited by ceiling effects, in contrast to the floor limits associated with albumin-Gd-DTPA and USPIO.

Hence, the development of intermediate-size agents might facilitate considerably the monitoring and calculation of effects of changes in K^{PS} following anti-angiogenic therapy.

Indeed, using Gadomer-17, in comparison to GdDTPA and albumin-GdDTPA, Su et al (37) have demonstrated MR determination of microvascular permeability in an N-ethyl-N-nitrosourea (ENU) model of breast cancer in the rat. In their study, they show that the intermediate permeability of Gadomer-17 was able to distinguish low-grade from high-grade cancers, but unable to resolve benign from low-grade, because of permeability range overlap. GdDTPA failed to differentiate between low- and high-grade malignant tumors. Albumin could differentiate both, high- from low-grade malignant tumors and benign from malignant tumors, but its low contrast-to-noise ratio raised major concerns.

This study in fact shows that intermediate-size contrast media with an MW in the

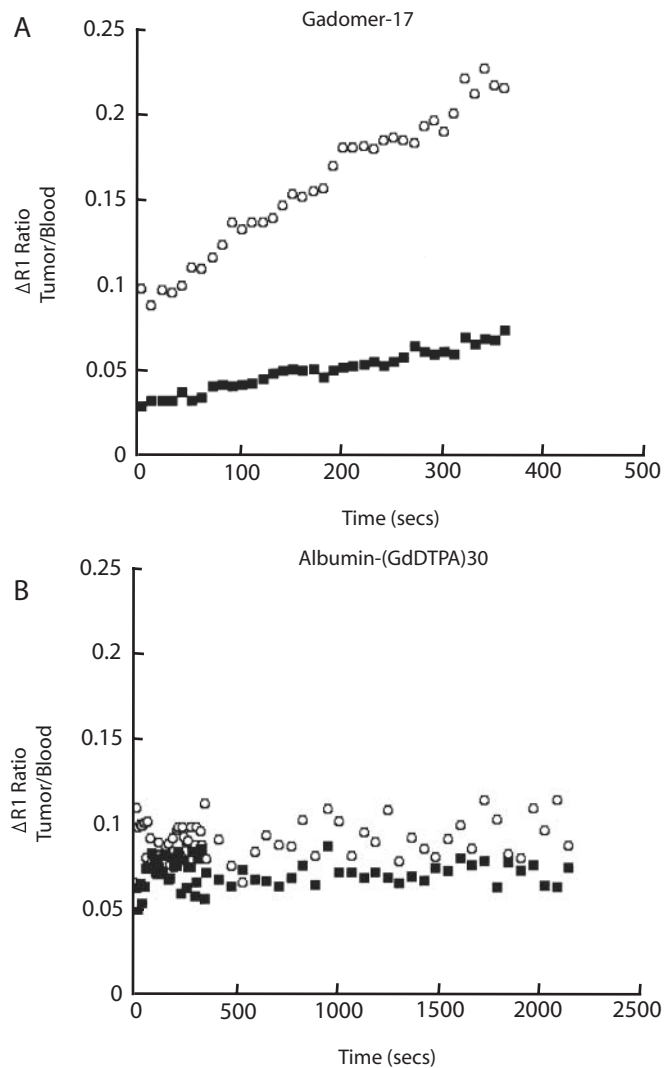


Figure 1. a: $\Delta R1$ ratios in tumors pre- (○) and post- (■) Mab-VEGF antibody treatment over one week demonstrate substantial signal enhancement within five minutes using an intermediate agent, represented here by Gadomer-17. b: In contrast, using MMCM (i.e., albumin-(GdDTPA)₃₀) imaging precision is limited because of very small signal enhancement, comparable to image noise levels.

range of 20-30 kDa also allow tumor microvessel characterization, in a therapy model, in a fashion similar to that in larger macromolecules. Both medium-size contrast media, Gadomer-17 (MW = 17 kDa) and ZK181 (MW = 25.9 kDa), revealed a statistically significant difference ($P < 0.05$) in permeability and fPV values between pre- and post-treatment examinations.

Additionally, resolution of such treatment effects was in fact facilitated using Gadomer-17 and ZK181220 by the greater degree of enhancement, or rate of contrast media extravasation, compared to the prototype MMCM. In such a way, imaging precision did not appear to limit permeability estimation to the same extent as seen with the low leak rates and very small signal enhancement of MMCM, comparable to image noise levels. Consequently, for MMCM contrast media leakage over a period of up to one hour is generally required for unambiguous observation of progressive signal enhancement (as opposed to mere image noise). Intermediate agents demonstrated substantial ($\sim 100\%$) signal enhancement within five minutes. This observation alone is of considerable practical utility when translating to a clinical setting (Fig. 1).

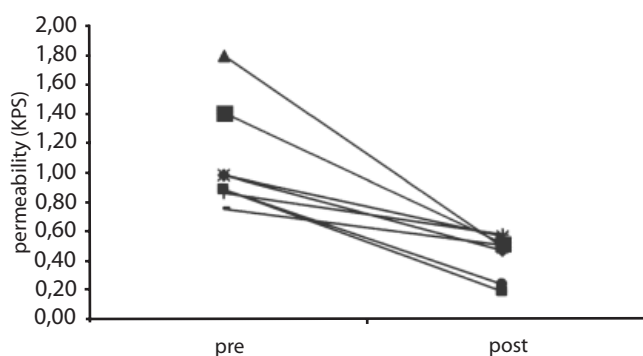


Figure 2. Individual permeability values, $K^{PS} \mu\text{L minute}^{-1} 100 \text{ cc}^{-1}$ of tissue) before and after one week of drug treatment in the group imaged with Gadomer-17.

Clarity of resolution of treatment effects with Gadomer-17 and ZK181220 can be further documented by considering individual instead of group effects. In all seven rats treated with Mab-VEGF antibody, Gadomer-17- K^{PS} estimates decrease over the treatment period (Fig. 2). While group comparison showed a significant decrease in mean K^{PS} for albumin-(GdDTPA)₃₀, there was not a similar 100% concordance observed in the individual data, in which

only 76% of cases showed a decrease in K^{PS} . In general, as can be seen from Fig. 3, there is an approximately exponential decrease in K^{PS} values with increasing MW. In fact, the correlation coefficient of $\ln(K)$ vs. MW is $r = -0.98$, indicating a strong negative correlation when considering the pooled pre-treatment values from both control and treated groups. This can be rationalized intuitively if one considers the impediments to larger molecule transport, including slower diffusion (to the extent that diffusion is a mechanism), greater sensitivity to elevated tumor interstitial pressure (to the extent that convection is the transport mechanism), and reduced access to fenestrae in the vascular wall.

The intermediate agents were not, however, so leaky (compared to GdDTPA, for example) that documentation of progressive enhancement was rendered impractical because of high first-pass extraction fraction ($\sim 50\%$ for GdDTPA). However, both intermediate contrast media did overestimate fPV (as did the SMCM) when compared to the bigger reference MMCM, albumin-(GdDTPA)₃₀ and SHU555C. It is possible that this overestimation can in part be attributed to partial first-pass extravasation.

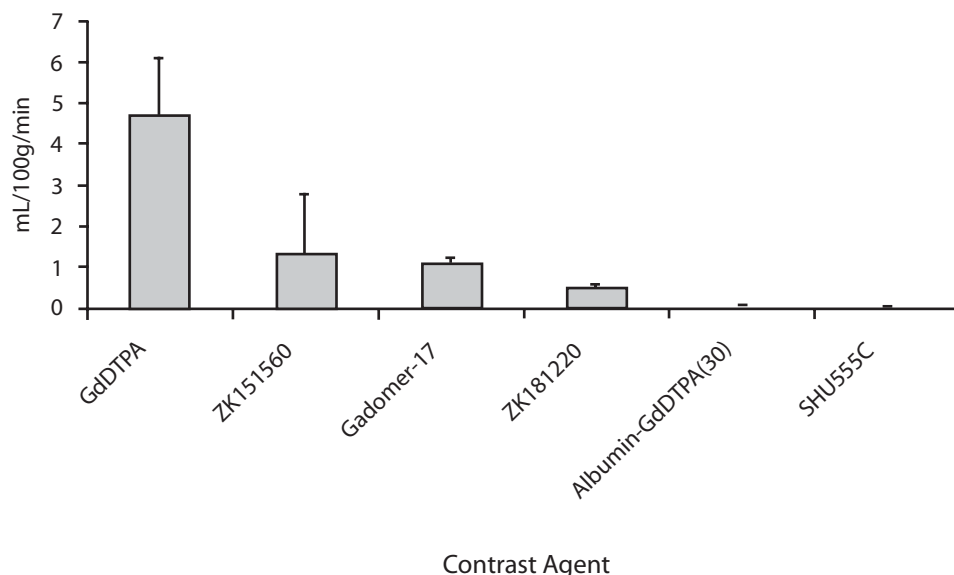


Figure 3. Pooled pretreatment (precontrol) K^{PS} values as a function of MW indicate an approximately exponential decrease in K^{PS} with MW. The correlation coefficient between $\ln(K)$ and MW is $r = -0.98$.

There are three possible explanations for the apparent lack of utility of permeability assessment using SMCM to document treatment success in this study: 1) insufficient image acquisition rates to capture the more rapid dynamics; 2) inappropriate modeling, violating extraction fraction assumptions; and 3) biological irrelevance, i.e., K^{PS} to SMCM may not in fact be affected by Mab-VEGF antibody action. Although there have been a number of reports of the successful use of dynamic contrast-enhanced MRI for characterizing tumor microvasculature phenomena in clinical patients, most of these methodologies do not rely on the elucidation of a parameter with physiologically specific interpretation (such as microvascular permeability). Rather, they rely on observed or derived descriptors of signal change, typically sensitive to a combination of perfusion, vascular volume, and microvascular permeability. Examples include the use of first-pass $T2^*$ -based imaging (measuring the peak change in $1/T2^*$ observed) (38) or constructions such as the initial area under the curve (IAUC) (39). Both can be demonstrated to be robustly determined and of some clinical utility, but lack the above physiologically specific interpretation and, as such, are subject to a number of potential confounds (e.g., systemic changes in cardiac output or blood pressure as well as local perfusion alterations that may be incidental to the mechanism of action of the drug).

In conclusion, the quantitative use of microvascular permeability estimation as an index of antiangiogenic therapeutic efficacy is constrained by two limits. If the MW of the tracer is too small, estimates of f_{PV} and K^{PS} have high uncertainties and true values are usually overestimated considerably. If, on the other hand, the MW is too big, contrast media enhancement of tumors is confounded by image noise and difficult or even impossible to determine.

A successful compromise appears delivered by intermediate-size agents, such as Gadomer-17, whereby a substantial dynamic range of permeability offers clear delineation of treatment effects, much less limited by imaging precision, and thus practically requiring shorter observation times to observe significant enhancement.

In summary, therapeutic effects of a Mab-VEGF antibody on tumor microvessel characteristics can be monitored by dynamic MRI. Intermediate-size agents, such as Gadomer-17, offer a substantial dynamic range and are less limited by imaging precision and therefore should be considered a practical alternative to monitor antiangiogenesis treatment effects in a clinical setting.

Acknowledgments

We thank Schering AG for the generous donation of contrast media, and Genentech Inc. (South San Francisco, CA) for the Mab-VEGF antibody. This research was supported by a grant from the Whitaker Foundation (to T.P.L.R.). K.T. was supported by the Erwin Schrödinger Auslandsstipendium, Austria.

References

1. Fontanini G, Lucchi M, Vignati S, et al. Angiogenesis as a prognostic indicator of survival in non-small-cell lung carcinoma: a prospective study. *J Natl Cancer Inst* 1997;89:881-886.
2. Takahashi Y, Kitadai Y, Bucana CD, Cleary KR, Ellis LM. Expression of vascular endothelial growth factor and its receptor, KDR, correlates with vascularity, metastasis, and proliferation of human colon cancer. *Cancer Res* 1995;55:3964-3968.
3. Brock CS, Lee SM. Anti-angiogenic strategies and vascular targeting in the treatment of lung cancer. *Eur Respir J* 2002; 19:557-570.
4. Cherrington JM, Strawn LM, Shawver LK. New paradigms for the treatment of cancer: the role of anti-angiogenesis agents. *Adv Cancer Res* 2000;79:1-38.
5. Folkman J. Angiogenesis and breast cancer [Editorial; Comment]. *J Clin Oncol* 1994;12:441-443.
6. Hoekman K. SU6668, a multitargeted angiogenesis inhibitor. *Cancer J* 2001;7 (Suppl 3): S134-S138.
7. Strawn LM, McMahon G, App H, et al. Flk-1 as a target for tumor growth inhibition. *Cancer Res* 1996;56:3540-3545.
8. Varner JA, Cheresh DA. Integrins and cancer. *Curr Opin Cell Biol* 1996;8:724-730.
9. GutheilJC, Campbell TN, Pierce PR, et al. Targeted antiangiogenic therapy for cancer using Vitaxin: a humanized monoclonal anti-body to the integrin alphavbeta3. *Clin Cancer Res* 2000;6:3056-3061.
10. Fujita M, Hayashi I, Yamashina S, Itoman M, Majima M. Blockade of angiotensin AT1a receptor signaling reduces tumor growth, angiogenesis, and metastasis. *Biochem Biophys Res Commun* 2002; 294:441-447.

11. Brooks PC, Montgomery AMP, Rosenfeld M, et al. Integrin α -(v) β (3) antagonists promote tumor-regression by inducing apoptosis of angiogenic blood vessels. *Cell* 1994;92:391–400.
12. Bruns CJ, Solorzano CC, Harbison MT, et al. Blockade of the epidermal growth factor receptor signaling by a novel tyrosine kinase inhibitor leads to apoptosis of endothelial cells and therapy of human pancreatic carcinoma. *Cancer Res* 2000;60:2926–2935.
13. Roberts WG, Palade GE. Neovasculature induced by vascular endothelial growth factor is fenestrated. *Cancer Res* 1997;57:765–772.
14. Qu H, Nagy JA, Senger DR, Dvorak HF, Dvorak AM. Ultrastructural localization of vascular permeability factor/vascular endothelial growth factor (VPF/VEGF) to the albuminal plasma membrane and vesiculovacuolar organelles of tumor microvascular endothelium. *J Histochem Cytochem* 1995;43:381–389.
15. Shames DM, Kuwatsuru R, Vexler V, Muhler A, Brasch RC. Measurement of capillary permeability to macromolecules by dynamic magnetic resonance imaging—a quantitative noninvasive technique. *Magn Reson Med* 1993;29:616–622.
16. Turetschek K, Huber S, Floyd E, et al. MRI characterization of microvessels in experimental breast tumors using a particulate contrast agent with histopathologic correlation. *Radiology* 2001; 218:562–569.
17. Turetschek K, Preda A, Floyd E, et al. MRI monitoring of tumor response following angiogenesis inhibition in an experimental human breast cancer model. *Eur J Nucl Med Mol Imaging* 2003;30: 448–455.
18. Weinmann H, Laniado M, Mützel W. Pharmacokinetics of Gd-DTPA/dimeglumine after intravenous injection into healthy volunteers. *Physiol Chem Phys Med NMR* 1984;16:167–172
19. Adam G, Neuerburg J, Spuentrup E, Muehler A, Schere K, Guenther R. Dynamic contrast enhanced MR-imaging properties of gadobutol, gadolinium-DTPA-polylysine, and Gd-DTPA-cascadeopolymer. *Magn Reson Med* 1994;32:622–628.
20. Ogan M, Schmiedl U, Moseley M, Grodd W, Paaenen H, Brasch RC. Albumin labeled with Gd-DTPA: an intravascular contrast enhancing agent for magnetic resonance blood pool imaging: preparation and characterization. *Inv Radiol* 1987;22:665–671.
21. Wedeking P, Sotak CH, Telser J, Kumar K, Chang CA, Tweedle MF. Quantitative dependence of MR signal intensity on tissue concentration of Gd(HP-DO3A) in the nephrectomized rat. *Magn Reson Imaging* 1992;10:97–108.
22. Schwickert HC, Roberts TP, Shames DM, et al. Quantification of liver blood volume: comparison of ultra short TI inversion recovery echo planar imaging (ULSTIR-EPI), with dynamic 3D-gradient recalled echo imaging. *Magn Reson Med* 1995;34:845–852.
23. Roberts TP. Physiologic measurements by contrast-enhanced MR imaging: expectations and limitations. *J Magn Reson Imaging* 1997;7:82–90.
24. Martiny-Baron G, Marmé D. VEGF-mediated tumour angiogenesis: a new target for cancer therapy. *Curr Opin Biotechnol* 1995;6:675–680.
25. Arai S, Mori A, Uchida S, Fujimoto K, Shimada Y, Imamura M. Implication of vascular endothelial growth factor in the development and metastasis of human cancers. *Hum Cell* 1999;12:25–30.

26. Dreves J, Hofmann I, Hugenschmidt H, et al. Effects of PTK787/ZK 222584, a specific inhibitor of vascular endothelial growth factor receptor tyrosine kinases, on primary tumor, metastasis, vessel density, and blood flow in a murine renal cell carcinoma model. *Cancer Res* 2000;60:4819–4824.
27. Karkkainen MJ, Petrova TV. Vascular endothelial growth factor receptors in the regulation of angiogenesis and lymphangiogenesis. *Oncogene* 2000;19:5598–5605.
28. Claffey KP, Robinson GS. Regulation of VEGF/VPF expression in tumor cells: consequences for tumor growth and metastasis. *Cancer Metastasis Rev* 1996;15:165–176.
29. Veikkola T, Karkkainen M, Claesson-Welsh L, Alitalo K. Regulation of angiogenesis via vascular endothelial growth factor receptors. *Cancer Res* 2000;60:203–212.
30. Brasch R, Pham C, Shames D, et al. Assessing tumor angiogenesis using macromolecular MR imaging contrast media. *J Magn Reson Imaging* 1997;7:68–74.
31. Berthezene Y, Vexler V, Kuwatsuru R, et al. Differentiation of alveolitis and pulmonary fibrosis with a macromolecular MR imaging contrast agent. *Radiology* 1992;185:97–103.
32. Saeed M, van Dijke CF, Mann JS, et al. Histologic confirmation of microvascular hyperpermeability to macromolecular MR contrast medium in reperfused myocardial infarction. *J Magn Reson Imaging* 1998;8:561–567.
33. Daldrup H, Shames DM, Wendland M, et al. Correlation of dynamic contrast-enhanced MR imaging with histologic tumor grade: comparison of macromolecular and small-molecular contrast media. *AJR Am J Roentgenol* 1998;171:941–949.
34. Schwickert HC, Stiskal M, Roberts TP, et al. Contrast-enhanced MR imaging assessment of tumor capillary permeability: effect of irradiation on delivery of chemotherapy. *Radiology* 1996;198:893–898.
35. Gossman A, Okuhata Y, Shames DM, et al. Prostate cancer tumor grade differentiation with dynamic contrast-enhanced MR imaging in the rat: comparison of macromolecular and small-molecular contrast media—preliminary experience. *Radiology* 1999;213:265–272.
36. Helbich T, Roberts TPL, Rollins MD, et al. Non-invasive assessment of wound healing angiogenesis with contrast enhanced MRI. *Acad Radiol* 2002;9(Suppl 1):145–147.
37. Su M-Y, Wang Z, Carpernter PM, Lao X, Muhler A, Nalcioğlu O. Characterization of N-ethyl-N-nitrosourea-induced malignant and benign breast tumors in rats by using three MR contrast agents. *J Magn Reson Imaging* 1999;9:177–186.
38. Kuhl C, Bieling H, Gieseke J, et al. Breast neoplasms: T2* susceptibility-contrast, first-pass perfusion MR imaging. *Radiology* 1997;202:87–95.
39. Evelhoch J. Key factors in the acquisition of contrast kinetic data for oncology. *J Magn Reson Imaging* 1999;10:254–259.

CHAPTER 9

MRI MONITORING OF AVASTIN™ ANTIANGIOGENESIS THERAPY
USING B22956/1, A NEW BLOOD POOL CONTRAST AGENT,
IN AN EXPERIMENTAL MODEL OF HUMAN CANCER

MRI MONITORING OF AVASTIN™ ANTIANGIOGENESIS THERAPY USING B22956/1, A NEW BLOOD POOL CONTRAST AGENT, IN AN EXPERIMENTAL MODEL OF HUMAN CANCER

9

(JOURNAL OF MAGNETIC RESONANCE IMAGING
2004, 20:865-873)

Anda Preda, MD,^{1,2} Viktor Novikov, MD,¹ Martina Möglich, MD,¹ Karl Turetschek, MD,¹ David M. Shames, MD,¹ Robert C. Brasch, MD,¹ Friedrich M. Cavagna, PhD,³ and Timothy P.L. Roberts, PhD^{1,4}

¹ Center for Pharmaceutical and Molecular Imaging, Department of Radiology, University of California-San Francisco, San Francisco, California.

² Department of Radiology, Erasmus University Medical Center, Rotterdam, The Netherlands.

³ Bracco S.p.A., Milan, Italy.

⁴ Department of Medical Imaging, University of Toronto, Toronto, Canada.

Abstract

Purpose

To evaluate the diagnostic and prognostic potential of a new protein-binding contrast medium, B22956/1, for quantitatively characterizing tumor microvessels by MRI and monitoring response to antiangiogenic therapy.

Materials and Methods

Dynamic contrast-enhanced MRI (DCE-MRI) was performed in an experimental cancer model with the use of the novel protein-binding agent B22956/1, a low molecular contrast agent (ProHanceTM), and a macromolecular contrast medium, albumin-(Gd-DTPA). MDA-MB-435, a human cancer cell line, was implanted in 22 athymic rats. Animals were assigned randomly to a control (saline) or drug-treated (AvastinTM) group. MRI was performed at baseline and after nine days of treatment. The transendothelial permeability (K^{ps}) and the fractional blood volume (fBV) were estimated from the kinetic analysis of dynamic MR data using a two-compartment model. Tumor growth was also measured from volumetric MRI.

Results

Tumors grew more slowly, although not significantly ($P = 0.07$), in the drug-treated group. The K^{ps} determined for B22956/1 decreased significantly in the drug-treated group compared to baseline ($P < 0.05$), and progressed significantly in the control group. However, no significant changes were resolved with the use of ProHance or albumin-(Gd-DTPA).

Conclusion

With the use of appropriate contrast media, the therapeutic effects of an anti-VEGF antibody on tumor microvessels can be monitored by dynamic MRI. The dynamic range of permeability to B22956/1, and the sensitivity to change of this parameter suggest a potential application in the clinical setting.

Key Words

magnetic resonance imaging; tumor angiogenesis; microvascular permeability; contrast agent; therapy

Introduction

Angiogenesis, the process whereby new blood vessels are formed from preexisting vasculature, plays a pivotal role in the development, growth, and metastasis of malignant tumors (1,2). Several growth factors have been identified as possible regulators of angiogenesis (3). One of these growth factors, vascular endothelial growth factor (VEGF), a cytokine that is present in various human tumors and a potent inducer of vascular permeability, is considered to play an important role in tumor angiogenesis (4-7). The expression of VEGF and its receptors has been demonstrated to correlate with the degree of tumor vascularization, and has been proposed as a prognostic factor in patient survival (8). The suppression of tumor angiogenesis has become a promising strategy in cancer

treatment. Several experimental studies have indicated that the inhibition of VEGF decreases tumor neovascularization and inhibits primary tumor growth and metastasis (5,8-17). In the current study, an intraperitoneally administered, humanized anti-VEGF antibody (Avastin™, rhu-MAb-VEGF; Genentech Inc., South San Francisco, CA) was used to directly inhibit VEGF.

Magnetic resonance imaging (MRI) offers investigators a possible means of noninvasively characterizing tumors. The ability of dynamic MRI enhanced with macromolecular contrast agents to quantitatively define the permeability of tumor microvessels has been shown in several experimental models (18-20). The potential of MRI to monitor the effects of antiangiogenesis therapy with this humanized anti-VEGF antibody (Avastin) has also been demonstrated (21,22). However, the reference contrast medium used in these studies, albumin-(gadolinium (Gd)-DTPA), is considered unsuitable for clinical use due to its potential immunogenic properties and prolonged retention in the body (23,24). Additionally, long scan times have been necessary to resolve progressive extravasation of the albumin-(Gd-DTPA) molecule, and large population sizes have been necessary to demonstrate statistically significant effects.

Recently, several MR contrast media were studied with respect to their diagnostic potential for quantitatively describing tissue microvessels. These contrast agents include ultrasmall superparamagnetic iron oxide particles (USPIO) such as NC100150 (Clariscan; Nycomed Amersham, Oslo, Norway) (25) and SHU 555C (Resovist; Schering AG, Berlin, Germany) (26), and blood pool agents such as MS-325 (Angiomark; Schering AG, Berlin, Germany) (27) and P792 (Vistarem; Guerbet, Aulnay-sous-Bois, France) (28). However, many of these agents fail to resolve treatment effects, require extended imaging periods to achieve adequate "leak," or offer characterization only at the expense of conspicuity.

The purpose of the current study was to evaluate the use of a novel protein-binding contrast agent, B22956/1 (gadocoletic acid trisodium salt), for MRI assessments of tumor microvascular characteristics in an experimental human breast cancer model. Microvascular characteristics, transendothelial permeability, and fractional blood volume derived from the kinetic analysis of data acquired with dynamic MRI enhanced with B22956/1, ProHance (a prototypical small molecular agent that has been found in many studies to be less amenable to physiologically-specific kinetic modeling and resolution of treatment effects), and albumin-(Gd-DTPA) (a prototypical macromolecule that has been demonstrated to resolve treatment effects, but only with extended (approximately one hour) scan times, and is unlikely to proceed clinically due to incomplete or slow elimination and potential immunogenicity) were compared and correlated with tumor growth. In particular, the microvascular permeability of the contrast agents was studied as a marker of disease progression and response to antiangiogenesis therapy with the recombinant humanized monoclonal antibody to VEGF (Avastin; Genentech Inc., South San Francisco). The hypothesis of this study was that permeability to B22956/1 may be a more sensitive measure of disease progression and/or response to antiangiogenesis therapy than permeability to either low-molecular-weight agents, such as ProHance, or covalently bound albumin-(Gd-DTPA), a prototype macromolecular contrast medium.

Materials and methods

Animals and Tumor Models

The study was conducted with the approval of the committee for animal research at our institution, and conformed with the guidelines of the National Institutes of Health for the care and use of laboratory animals. The human cancer cell line MDA-MB-435 (Cell Culture Facility, University of California-San Francisco) was used for tumor induction. This cell line is representative of human breast cancer, and although current debate is challenging its origin as a melanocyte, recent studies have continued to consider its origin as breast cancer (29). Of importance for the purposes of this study, this cell line is known to express VEGF. We implanted approximately 5×10^6 tumor cells, suspended in a total volume of 0.3 mL (one part sterile saline: one part Matrigel[®] (Collaborative Biomedical Products, Bedford, MA)) in the mammary fat pad of 22 4-week-old female homozygous athymic rats (Harlan, Indianapolis, IN), using a 25-gauge needle. The animals were inspected daily for tumor growth and general appearance.

MRI

MRI was performed with the use of a Bruker Omega CSI-II magnet (Bruker Instruments, Fremont, CA) operating at 2 Tesla. This system is equipped with Acustar S-150 (Bruker Instruments, Fremont, CA) self-shielded gradient coils (± 20 G/cm, 15-cm inner diameter). The animals were placed supine in a birdcage radiofrequency coil with a length of 7.6 cm and an inner diameter of 4.5 cm. A phantom filled with diluted 0.01 mmol/liter gadopentate dimeglumine was included in the field of view (FOV), close to each animal, to allow correction for potential spectrometer variation.

Precontrast T1 mapping was performed by means of a single-slice inversion recovery (IR) snapshot fast low-angle shot (FLASH) sequence (29) with the following parameters: TR = 3 msec, TE = 1.5 msec, one acquisition, FOV = 55×55 mm, matrix = 64×64 , slice thickness = 3 mm, and flip angle = 5° . Per slice, nine images at nine different IR times (TI = 100, 400, 700, 1000, 1300, 1600, 1900, 2200, and 2500 msec) were acquired. A total of eight slices were obtained. After the TI, the data were acquired with a snapshot FLASH read-out scheme with centric reordering to maintain the appropriate T1 contrast for the center of the k-space. This sequence was used to calculate baseline longitudinal relaxation rates ($R_1 = 1/T_1$) for the tumors by curve-fitting (31).

We performed dynamic contrast-enhanced MRI (DCE-MRI) using an axial T1-weighted, three-dimensional, spoiled gradient-recalled (SPGR) sequence with a keyhole technique consisting of three initial precontrast and 37 dynamic postcontrast images with the following parameters: TR = 30 msec, TE = 4.83 msec, one acquisition, FOV = $55 \times 55 \times 48$ mm, keyhole acquisition matrix = $128 \times 16 \times 8$ (the keyhole technique achieves high temporal resolution by only partially updating imaging data with high spatial frequencies, or substituting detailed structures from a slower full-matrix scan), effective slice thickness = 3 mm, and flip angle = 90° . The temporal resolution was six seconds per three-dimensional dataset. The 40 high-temporal-resolution keyhole images were followed by 30 full-matrix, dynamic, three-dimensional SPGR postcontrast images (matrix = $128 \times 128 \times 16$) with an acquisition time of one minute per volume of 16 slices. The total examination time was 35 minutes.

Experimental Protocol

MR examinations were performed over a two-day period at baseline (when the tumor diameter was approximately 15 mm) and again over a two-day period after nine days of treatment (or placebo).

Before the MRI sessions, the animals were anesthetized by intraperitoneal administration of pentobarbital sodium (50 mg/kg body weight). Analgesia was achieved by intraperitoneal injection of 0.03 mg/kg buprenorphine hydrochloride (Buprenex[®]; Reckitt & Colman Products, Hull, UK), which is an opiate. A 25-gauge butterfly cannula (Abbott Laboratories, North Chicago, IL) was inserted into a tail vein for contrast medium injection. The animals were placed on a heated water pad to maintain the body temperature at physiological levels, and 2 mL of saline were injected intravenously to avoid dehydration effects that may occur after anesthesia. After the baseline MR examinations, the animals were randomly assigned to either the drug treatment group or the control group. The drug-treatment group was treated with a recombinant humanized monoclonal anti-VEGF antibody (Avastin, rhuMAb-VEGF; Genentech Inc., South San Francisco, CA), injected intraperitoneally at a dose of 1 mg every third day, for a total of three doses. The control group received saline, also injected intraperitoneally (0.1 mL) every third day, for a total of three doses. On the day following the last injection of Avastin or saline, all of the animals were imaged a second time by the same protocol applied for the baseline assessment. After a second MR examination was completed on the following day, all of the animals were killed by an intravenous overdose of 0.3 mL pentobarbital.

MR Contrast Media

B22956/1, a novel protein-binding contrast medium (Bracco, S.p.A., Milan, Italy) (32), is a Gd chelate with a low molecular weight (molecular mass = 1059 Dalton). B22956/1 is the trisodium salt of a polyaminocarboxylate Gd complex linked to deoxycholic acid through a flexible spacer (33), and it has a high affinity for serum proteins (94% for a 0.5 mM solution in Seronorm[®] for human serum albumin, and 84% for rat serum albumin). The relaxivity of this contrast agent is 27 mM⁻¹second⁻¹ at 20 MHz in human serum.

B22956/1 was injected on imaging day 1 at a dose of 0.1 mmol/kg. Gadoteridol (ProHance) was injected on day 2, 24 hours after the B22956/1 injection, at a dose of 0.1 mmol/kg. Albumin-(Gd-DTPA) is a prototype of a water-soluble macromolecular contrast medium with a molecular weight of 92,000 Dalton. It has a distribution volume of 0.05 liter/kg and a plasma half-life of three hours in rats, which produces nearly constant enhancement of normal tissues for 30 minutes or longer after injection (34). Albumin-(Gd-DTPA) was also injected on day 2, four hours after the injection of ProHance, at a dose of 0.1 mmol Gd/kg. At the time albumin-(Gd-DTPA) was injected, the tumor signal potentially influenced by the previous administration of ProHance had returned to baseline values. On days 9 and 10, similar imaging was performed (B22956/1 on day 9, and Prohance and Albumin-GdDTPA on day 10, four hours apart).

Kinetic Analysis of Dynamic MRI Data

The MR images were transferred, processed, and analyzed with the use of a Sun SPARC 10 workstation (Sun Microsystems, Mountain View, CA) and an image analysis program

(MRVision Co., Menlo Park, CA). Signal intensity (SI) values for each time point were obtained from multiple (three to six) regions of interest (ROIs) defined by a threshold-based semiautomated selection of strongly enhancing pixels on a late postcontrast image. SIs for the blood within the inferior vena cava (IVC), the phantom, and the tumor periphery were measured in the central section of the imaging volume. The tumor periphery was defined as the peripheral zone of strong contrast enhancement (usually 1-2 mm thick). Corresponding ROI measurements were made in each of three adjacent slice images, each of which contained a minimum of 30 pixels, and were averaged. We corrected the mean SIs from the tumors and the blood in the vena cava for potential spectrometer variation over time by dividing the SI of each ROI by the SI from the phantom. Precontrast longitudinal relaxation rates $R1$ ($1/T1$) estimates for tumors were obtained by curve-fitting based on nine sets of IR snapshot FLASH images. The precontrast $R1$ value for IVC blood was assumed to be 0.724 ($1/1.38$) based on numerous previous measurements in rat blood (31). Postcontrast $R1$ values were calculated based on the observed SIs and knowledge of precontrast $R1$ according to:

$$R1_{\text{post contrast}} = -1/TR \ln\{1 - SI_{\text{post contrast}}/SI_{\text{pre contrast}} \times [1 - \exp(-TR \cdot R1_{\text{pre contrast}})]\} \quad (1)$$

The difference between the postcontrast $R1$ value at any time point and the precontrast $R1$, $\Delta R1$ (t) is assumed to be directly proportional to the concentration of the contrast medium, in either the blood or the tissue (31,35). Although this assumption is limited in the presence of intermediate or slow water exchange, previous studies (31,35) suggested that this level of approximation is nonetheless acceptable, provided that a short TR (30 msec in this case) is used.

We used the $\Delta R1$ data from blood and tumor for kinetic analysis to estimate the transendothelial permeability (K^{PS} , $\text{mL} \cdot \text{minute}^{-1} 100 \text{ g}^{-1} \text{ tissue}$) and the fractional blood volume of the tumor tissue (fBV,%) using a two-compartment, kinetic model (35-39). In this model, a biexponential function fitted to the $\Delta R1$ data from blood was used as an input function for the blood response in the tumor tissue. The ratio of $\Delta R1$ tumor/ $\Delta R1$ blood, plotted against a “pseudo time,” was used to fit a straight line to the MR data. Pseudo-time can be calculated (39) from the integral of the contrast agent volume that has passed from time zero to the current time, divided by the instantaneous contrast agent concentration. The slope of the curve approximated the transendothelial permeability K^{PS} , and the intercept represented the fractional blood volume. The pseudo-time related to the time required for a constant unit of intravascular contrast medium to pass. The linearity of this plot (determined from linear regression) implied the validity of neglecting the reflux of contrast medium to the intravascular space over this time period, and justified the use of the simpler unidirectional model. We calculated tumor volumes by summing the measured tumor area on each slice, multiplied by the slice thickness (3 mm).

Table 1.MRI Estimates of Fractional Blood Volume (fBV) and Transendothelial Permeability (K^{PS}) for Avastin™-Treated and Control Groups

	fBV pre	fBV post	K^{PS} pre	K^{PS} post
B22956/1				
Avastin™	24.3 ± 1.7	21.1 ± 1.9	0.131 ± 0.026	0.076 ± 0.025 ^a
Control	21.7 ± 2.4	17.1 ± 1.8	0.148 ± 0.020	0.236 ± 0.040 ^a
Prohance™				
Avastin™	32.5 ± 4.5	35.6 ± 5.3	2.434 ± 1.214	2.749 ± 1.081
Control	35.9 ± 5.0	32.9 ± 5.2	1.211 ± 0.408	1.987 ± 0.736
Albumin-(Gd-DTPA)				
Avastin™	9.2 ± 0.8	7.9 ± 0.7	0.007 ± 0.004	0.008 ± 0.003
Control	7.7 ± 0.8	8.4 ± 1.1	0.008 ± 0.003	0.014 ± 0.004

^aIndicates significant difference from pre- to post-Avastin (or control) treatment, $P < 0.05$.fBV=fractional blood volume (%), K^{PS} =transendothelial permeability ($\text{mL} \cdot \text{min}^{-1} 100 \text{ g}^{-1} \text{ tissue}$).

Statistics

A paired two-tailed Student's t-test was used to compare mean values of K^{PS} and fBV values in the same tumor before and after therapy (drug or control) for each contrast agent. The same statistical test was used to compare changes in tumor volume over time in each rat. An unpaired two-tailed Student's t-test was used to compare mean values for K^{PS} and fBV between the control and the treated groups. A P-value of < 0.05 was considered statistically significant.

Results

The tumors grew in all implanted animals within 14 days. MRI was completed successfully in all 22 animals (11 controls and 11 drug-treated).

There was no significant difference ($P = 0.11$) between groups with respect to tumor volume at baseline: $3.24 \pm 0.55 \text{ cm}^3$ (mean \pm SD) in the drug treatment group, and $4.52 \pm 0.64 \text{ cm}^3$ in the control group. At the second MRI examination following nine days of treatment, mean tumor volume had increased significantly in both groups ($P < 0.05$), to $5.86 \pm 1.20 \text{ cm}^3$ in the Avastin-treated group, and $9.84 \pm 1.28 \text{ cm}^3$ in the control group. The tumors grew significantly more slowly ($P > 0.05$) in the drug-treated group, as measured by the difference between mean tumor volume at follow-up examination and mean tumor volume at baseline ($2.62 \pm 0.79 \text{ cm}^3$) compared to the control group ($5.32 \pm 0.77 \text{ cm}^3$). However, the tumor volume ratio between baseline and follow-up examinations in the drug-treated group (1.76 ± 0.17) did not reach a statistically significant difference ($P = 0.07$) from the control group (2.27 ± 0.24). This minor disparity is probably attributable to the extra uncertainty introduced in the "ratio" construction, in combination with a relatively small sample size. The mean values for K^{PS} and fBV obtained in the pre-and post-therapy studies for each contrast agent are shown in Table 1. Using B22956/1, the mean K^{PS} values at baseline were for the drug group $0.131 \pm 0.026 \text{ mL} \cdot \text{minute}^{-1} 100 \text{ g}^{-1}$, and $0.148 \pm 0.020 \text{ mL} \cdot \text{minute}^{-1} 100 \text{ g}^{-1}$ for the control group ($P = 0.59$). At the follow-up examination, the mean K^{PS} values decreased significantly ($P < 0.05$) in the anti-VEGF-treated group ($0.076 \pm 0.025 \text{ mL} \cdot \text{minute}^{-1} 100 \text{ g}^{-1}$) compared to baseline, and increased significantly in the control group to $0.236 \pm 0.040 \text{ mL} \cdot \text{minute}^{-1} 100 \text{ g}^{-1}$ ($P < 0.05$). In addition, K^{PS} post values were significantly greater in the control group ($0.236 \pm 0.040 \text{ mL} \cdot \text{minute}^{-1} 100 \text{ g}^{-1}$) than in the drug-treated group ($0.076 \pm 0.025 \text{ mL} \cdot \text{minute}^{-1} 100 \text{ g}^{-1}$, $P < 0.05$) (Figs. 1 and 2).

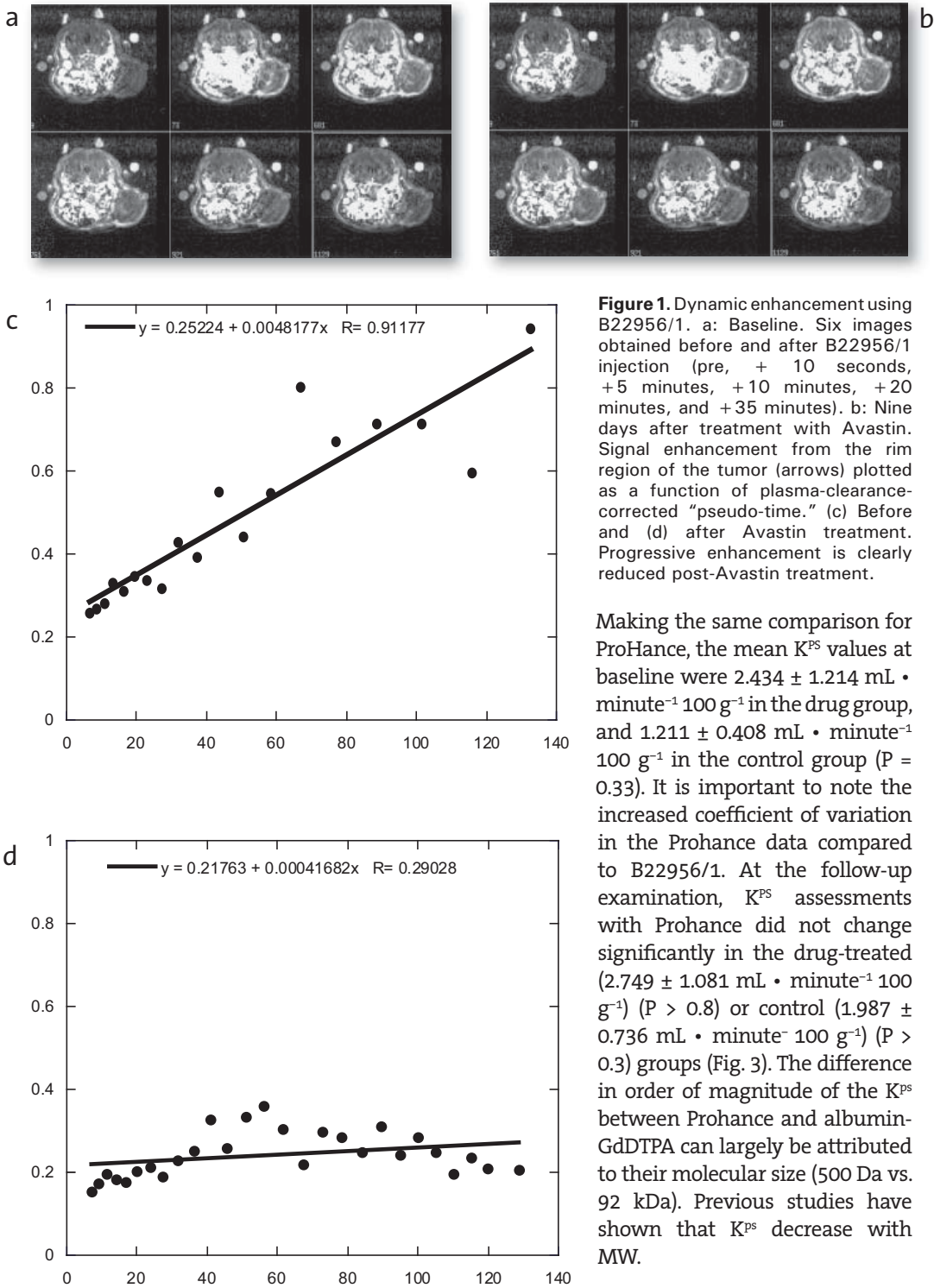


Figure 1. Dynamic enhancement using B22956/1. a: Baseline. Six images obtained before and after B22956/1 injection (pre, + 10 seconds, +5 minutes, +10 minutes, +20 minutes, and +35 minutes). b: Nine days after treatment with Avastin. Signal enhancement from the rim region of the tumor (arrows) plotted as a function of plasma-clearance-corrected "pseudo-time." (c) Before and (d) after Avastin treatment. Progressive enhancement is clearly reduced post-Avastin treatment.

Making the same comparison for ProHance, the mean K^{PS} values at baseline were $2.434 \pm 1.214 \text{ mL} \cdot \text{minute}^{-1} 100 \text{ g}^{-1}$ in the drug group, and $1.211 \pm 0.408 \text{ mL} \cdot \text{minute}^{-1} 100 \text{ g}^{-1}$ in the control group ($P = 0.33$). It is important to note the increased coefficient of variation in the Prohance data compared to B22956/1. At the follow-up examination, K^{PS} assessments with Prohance did not change significantly in the drug-treated ($2.749 \pm 1.081 \text{ mL} \cdot \text{minute}^{-1} 100 \text{ g}^{-1}$) ($P > 0.8$) or control ($1.987 \pm 0.736 \text{ mL} \cdot \text{minute}^{-1} 100 \text{ g}^{-1}$) ($P > 0.3$) groups (Fig. 3). The difference in order of magnitude of the K^{PS} between Prohance and albumin-GdDTPA can largely be attributed to their molecular size (500 Da vs. 92 kDa). Previous studies have shown that K^{PS} decrease with MW.

With albumin-(Gd-DTPA), the mean K^{PS} values at baseline were $0.007 \pm 0.004 \text{ mL} \cdot \text{minute}^{-1} 100 \text{ g}^{-1}$ in the drug group, and $0.008 \pm 0.003 \text{ mL} \cdot \text{minute}^{-1} 100 \text{ g}^{-1}$ in the control group ($P = 0.88$). Albumin-(Gd-DTPA) also failed to demonstrate a significant reduction in K^{PS} as a consequence of Avastin therapy (0.008 ± 0.003 vs. $0.007 \pm 0.004 \text{ mL} \cdot \text{minute}^{-1} 100 \text{ g}^{-1}$, $P > 0.8$), although K^{PS} tended ($P = 0.18$) to be lower than in the control group ($0.014 \pm 0.004 \text{ mL} \cdot \text{minute}^{-1} 100 \text{ g}^{-1}$) (Fig. 4). Again, the limitation of effect resolution with albumin might be expected from the large coefficients of variation.

The mean fBV values (between groups) for all three contrast agents were not significantly different at baseline, nor was there any evidence of significant change with either drug or placebo treatment. However, consistent with previous studies using a similar methodology, we found that small molecules such as Prohance lead to overestimation of fBV and can better be interpreted in terms of a distribution volume that includes extravascular space. It appears that the unbound form of B22956/1 also undergoes a certain rapid extravasation leading to overestimation of fBV compared to albumin-GdDTPA, which more faithfully represents the vascular fraction.

Discussion

With DCE-MRI, one can quantitatively assess certain properties of tumor tissue, such as capillary permeability and blood volume, and analyze the kinetics of the distribution of the contrast medium in the tissue. These microvascular characteristics are estimated

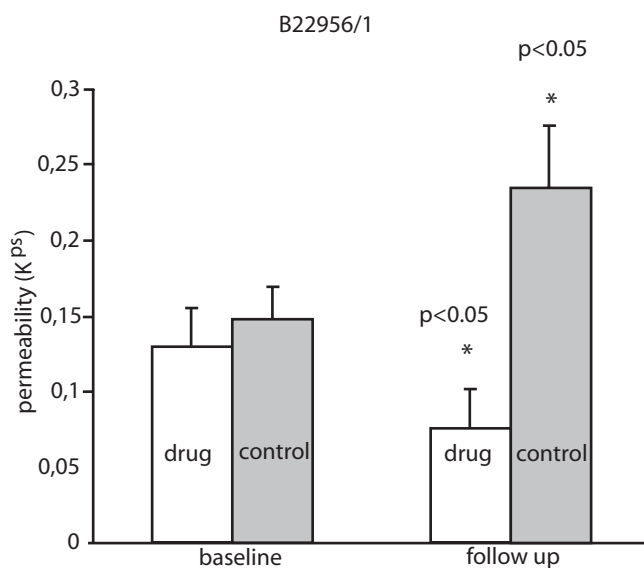


Figure 2. Transendothelial permeability (K^{PS} in $\text{ml} \cdot \text{minute}^{-1} 100 \text{ g}^{-1}$ tissue) at baseline and follow-up examination after saline (control) or Avastin treatment, based on enhancement with B22956/1.

from kinetic analyses of dynamic enhancement data, with simple models of the tissue represented as a compartmentalized system (36-39). Usually, two compartment tissue models (representing the blood plasma and the extravascular extracellular space) are used. The contrast agent concentration, modeled as a function of time, can be derived from MR SI data, assuming that changes in longitudinal relaxation rates R_1 ($1/T_1$) after administration of the contrast medium are proportional to the contrast agent concentration, according to:

$$\frac{1}{T_1}_{\text{post contrast}} = \frac{1}{T_1}_{\text{pre contrast}} + r_1 C_t \quad (2)$$

where C_t is the tissue concentration of the contrast agent, and r_1 is a constant of proportionality, known as the relaxivity ($\text{mM}^{-1} \text{second}^{-1}$). Based on the observed MR SIs, these changes in R_1 are calculated accordingly to Eq. [1]. Thus, the increased enhancement can be translated to contrast agent concentration and quantified by kinetic modeling to yield estimates of microvascular characteristics. By measuring these functional parameters, one can obtain an accurate, noninvasive, quantitative description of the microcirculation of individual tumors. Following up the MRI-derived estimates of the microvascular characteristics provides a tool for in vivo monitoring of tumor response to therapy.

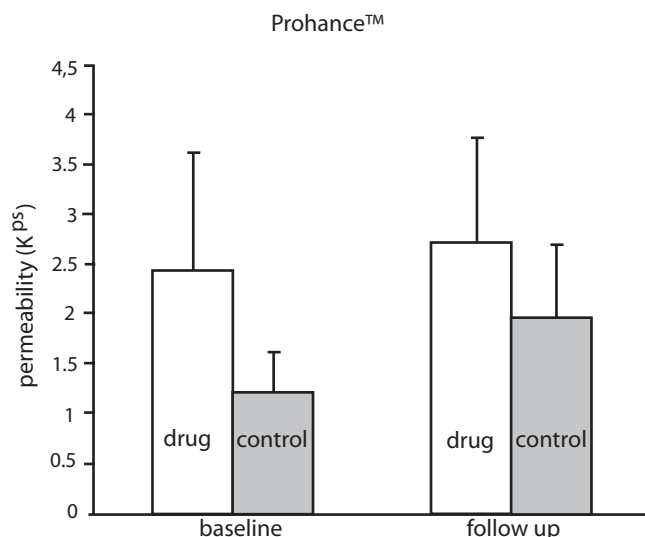


Figure 3. Transendothelial permeability (KPS in $\text{ml} \cdot \text{minute}^{-1} 100 \text{ g}^{-1} \text{ tissue}$) at baseline and follow-up examination after saline (control) or Avastin treatment, based on enhancement with Prohance.

Although the tumors treated with anti-VEGF antibody also grew over nine days of treatment, they grew more slowly ($P = 0.07$), as indicated by the tumor growth rates. The difference between mean tumor volume at follow-up examination and mean tumor volume at baseline was significantly ($P < 0.05$) higher in the control group compared to the drug-treated group, but it lost its significance after it was normalized to the mean tumor volume at baseline. The relatively small ($N=11$) number of experiments (as well as the extra uncertainty introduced by the mathematical process of normalization, or division) probably explains the lack of significance of

the difference in tumor growth rates. This result is in agreement with several other studies that indicated that treatment with various anti-VEGF drugs is associated with a significant reduction in tumor growth rate (5,9-12,14-17,21). However, tumor growth has not been reported to be completely stopped or reversed. Malignant tumors treated with angiogenesis inhibitors continue to grow slowly, indicating that other factors are probably involved. Cytokines such as basic fibroblastic growth factor (bFGF), epidermal growth factor (EGF), and platelet-derived growth factor (PDGF) also play a role in stimulating tumor growth, and may be responsible for the observed continued tumor progression by a compensatory agonist mechanism when VEGF is inhibited (40).

Data from this study indicate that the effects of antiangiogenesis treatment can be successfully monitored by MRI. Dynamic MRI enhanced with B22956/1 defined significant declines in the microvascular permeability of experimental human breast cancer as a result of a nine-day therapy with an anti-VEGF antibody. The tumor microvascular permeability to B22956/1 decreased significantly ($P < 0.05$) compared to baseline in the animal group

treated with anti-VEGF antibody. A decline of K^{PS} was observed in eight of 11 (73%) drug-treated animals, but in only two of 11 (18%) animals in the placebo group. This difference in response was statistically significant (chi test: $P < 0.05$). Conversely, only three of 11 of the drug-treated animals demonstrated an increase in K^{PS} , compared to nine of 11 control animals. The fact that a small fraction (27%) (three of 11 animals) showed an increase in K^{PS} values after drug therapy may play a role in a clinical setting, allowing the identification and assessment of nonresponders to therapy (and thus candidates for alternative treatment). It may also reflect a sampling error in comparing ROIs nine days apart, or an insufficient

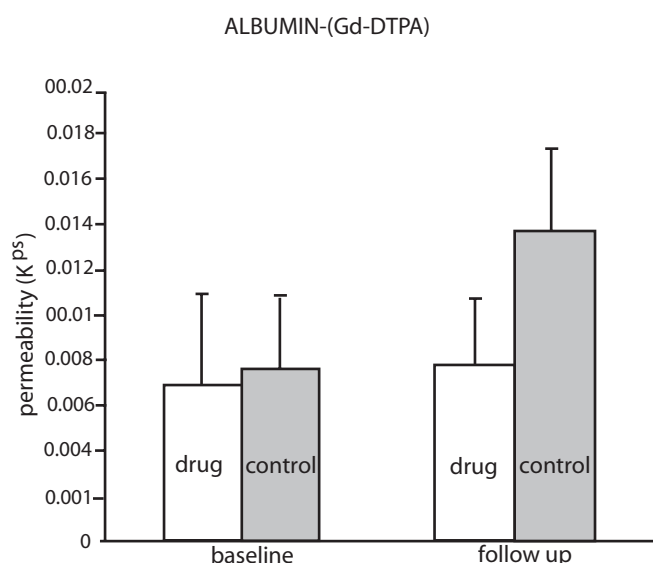


Figure 4. Transendothelial permeability (K^{PS} in $\text{ml} \cdot \text{minute}^{-1} 100 \text{ g}^{-1} \text{ tissue}$) at baseline and follow-up examination after saline (control) or Avastin treatment, based on enhancement with albumin-(Gd-DTPA).

vessel permeability outside the central nervous system, because such contrast agents diffuse unrestrictedly from the blood to the extravascular space through the endothelium of both normal vessels and tumor vessels (42-44). However, unlike previous experiments by our group, using the same tumor model as in the current study (21) or an intraperitoneally-growing ovarian tumor (22), no significant reduction of microvascular permeability to albumin-(Gd-DTPA) was resolved as a result of rhuMab-VEGF treatment. This may be attributed to the smaller sample size, or, more likely, the shorter scan times (35 minutes) used in the current study, which did not permit adequate contrast agent extravasation for robust permeability determination. This discrepancy highlights a potential difficulty of using a large (92,000 Dalton) tracer in such a model—namely, the demands on imaging precision and examination duration (to achieve an adequate “effect-to-noise ratio”)—when trying to distinguish between low permeability values (this can be considered a “floor” effect of near-zero permeability values). In any case, it is clear that individualized decision-making will require more sensitive determinations of physiologic parameters than can be achieved with conventional or prototypical macromolecular contrast media. B22956/1 offers one potentially clinically viable alternative.

amount or duration of drug therapy. Dynamic imaging with Prohance, a low molecular weight contrast medium, did not resolve any significant changes in the microvascular characteristics in either the drug-treated or the control group. Furthermore, with albumin-(Gd-DTPA), prototype macromolecular contrast medium, no significant declines in microvascular permeability were demonstrated following the antiangiogenesis therapy.

Our results are in general agreement with previous studies (18,41). This suggests that small molecular contrast media are not appropriate for detecting abnormal micro-

B22956/1, a research product of Bracco S.p.A., is a new Gd-based blood-pool contrast medium with a high affinity for serum proteins. Its potential for angiographic imaging and three-dimensional MR pulmonary perfusion was recently demonstrated in an experimental model of pulmonary embolism (33). To our knowledge, B22956/1 has not been previously tested for its ability to characterize tumor microvessels. The behavior of the relatively low-molecular-weight agent B22956/1 as a blood-pool contrast medium can be explained by its binding with serum proteins. B22956/1 bound to serum albumin, similar to macromolecular contrast media (as used as prototypical references in this study), will selectively leak through the endothelium of malignant tumors into the extravascular extracellular fluid. In this study, B22956/1 demonstrated a number of favorable imaging characteristics. In a short examination time, substantial (but, importantly, not overwhelming) progressive enhancement was observed, allowing clear visualization of the effects of vascular permeability and changes thereof. Furthermore, over a 5-10-minute period, bidirectional kinetic modeling was reduced to the simpler special case of unidirectional transport (revealed by the linearity of the ΔR_1 ratio vs. pseudo-time plots). This is of considerable advantage in pixel-wise mapping, where computation essentially reduces to the analytic linear regression (in contradistinction to typical nonlinear least squares approaches). Finally, the dynamic range of permeability changes observed spanned a wide range, rendering observation of progressive disease and the permeability-reducing effects of successful antiangiogenic therapy readily resolved.

The relative roles of free and bound B22956/1 in the observed signal and relaxation rate enhancement dynamics cannot be finally assessed at this point. In rat plasma, in contrast to human plasma, a sizable proportion of B22956/1 is in the free state. One might expect this free fraction to diffuse readily across the endothelium and to bind again to serum albumin in the interstitial space of the tumor, gaining again high relaxivity in the process. On the vascular side, equilibrium levels of the free ion would quickly be reestablished by dissociation of the chelate-albumin complex. The net effect of this would have to be an observed signal enhancement in tumor tissue, as well as an enhanced relaxation rate ratio, both peaking soon after administration of B22956/1, reflecting concentration of extravasated contrast agent and interstitial albumin in tumor tissue. However, our results show that this is clearly not the case. Thus, to explain the results, we have to hypothesize that transendothelial diffusion and/or mixing in the interstitium of the free gadocoletic acid ion is restricted by some specific interaction of the free ion with interstitial moieties. This is not unlikely given the binding affinity of the free B22956/1 moiety. As a consequence, the concentration gradient driving the flux across the microvessel wall would be only slowly restored, limiting the clearance and thus release of the unbound B22956/1 moiety from its intravascular bound form. Evidence in support of this hypothesis comes from the overestimation of fBV, which may be accounted for by a rapid early-phase distribution of agent just beyond the vessel wall (on the interstitial side). This hypothesis must be explored in further studies.

Changes in fractional blood volume did not show any evidence of significant change as a result of therapy. The higher sensitivity of K^{ps} (permeability) to antiangiogenic therapy is consistent with results from other studies, which demonstrated no changes in fractional plasma volume of the tumor tissue following one week of anti-VEGF antibody treatment

(21) or a VEGF receptor tyrosine kinase inhibitor treatment (45) using the same tumor model enhanced with albumin-(Gd-DTPA) (21,45) and SHU555C (45) as contrast agents. It is both possible and likely that different treatment durations will lead to different relative impacts of fBV and K^{PS} .

The search for a contrast agent suitable for characterizing the vessels of tumors in a clinical setting has been extensive. Since the prototype macromolecular contrast medium albumin-(Gd-DTPA) is not appropriate for human use, the feasibility of several other contrast media for quantitatively assessing the properties of tumor microvessels has been recently evaluated. USPIO such as NC100150 (Clariscan; Nycomed Amersham, Oslo, Norway) and SHU 555C (Schering AG, Berlin, Germany) could be used successfully to define the tumor microvasculature in a chemically induced rodent breast cancer model (25,26). However, one limitation of using USPIO for characterizing tumor microvessels is the fact that the positive signal enhancement associated with T1 shortening is associated with negative enhancement induced by the T2* shortening (35,46). Especially when higher doses of USPIO are used, the positive enhancement caused by the T1 shortening can be overwhelmed by the T2* effects. A second factor that can negatively influence the use of USPIO for quantitatively estimating microvessel properties is the dependence of the T2* effects on the compartmentalization of the iron particles in the tissue (26). These limiting factors associated with USPIO can be avoided with the use of B22956/1. Because of the low r2/r1 ratio (~1) of B22956/1, the T2* shortening effect is less pronounced (33).

VEGF has been demonstrated to both stimulate endothelial cell proliferation and increase the vascular permeability. The observed reduction in tumor microvascular permeability in the current study as a result of therapy with anti-VEGF antibody reflects the successful suppression of VEGF-induced hyperpermeability, and is in agreement with previous reports (47).

One limitation of the current study was that the tumors were implanted in athymic rats, which exhibit a pattern of immune response different from that in humans. Nevertheless, this is the regime in which antiangiogenic agents are first to be evaluated. Indeed, clinical imaging protocols may not differ from the experimental imaging approaches discussed above, since experimental imaging is performed at the clinically-relevant field strength of 2T.

The data in this study support the hypothesis that estimates of transendothelial permeability to B22956/1 are an appropriate measure of tumor response to therapy, and are superior in resolution and responsiveness (dynamic range) to either low-molecular-weight or macromolecular contrast agents.

In conclusion, dynamic MRI enhanced with the new contrast medium B22956/1 has shown potential for measuring the effects of antiangiogenesis therapy with an anti-VEGF antibody in an experimental rat model. Quantitative microvascular characterization of tumors with dynamic MRI using such a contrast agent could prove to be clinically useful in monitoring the results of antiangiogenesis treatment, and serve to provide an early and physiologically-specific indicator of the biological activity of such therapeutics. It may also

provide a useful selection criterion for inclusion of patients into clinical trials to evaluate putative antiangiogenic agents. Importantly, with the use of an agent such as B22956/1, it appears that a straightforward resolution of the effects of antiangiogenic treatments can be revealed within very reasonable scan times of 5-10 minutes (i.e., without the need for the 30 full-matrix images acquired after the initial 40 keyhole images (approximately six minutes), since inclusion of these data added no precision. This offers a straightforward translation from an experimental to a clinical implementation.

Acknowledgments

Mab-VEGF was generously provided, through a material transfer agreement (T.R.), by Genentech Inc., South San Francisco, CA. Contrast media were generously provided by Bracco S.p.A., Milan, Italy (T.R.). This study was supported in part by a grant from the Whitaker Foundation (T.R.) and a research grant from Bracco S.p.A. (T.R.). Anda Preda was supported in part by the Drie Lichten Foundation and the Johan Vermeij Foundation, the Netherlands. Tim Roberts thanks the Canada Research Chair Program/Canadian Institutes of Health Research for awarding him the Canada Research Chair in Imaging Research.

References

1. Plate KH, Breier G, Risau W. Molecular mechanisms of developmental and tumor angiogenesis. *Brain Pathol* 1994;4:207-218.
2. Hanahan D, Folkman J. Patterns and emerging mechanisms of the angiogenic switch during tumorigenesis. *Cell* 1996;86:353-364.
3. Klagsbrun M, D'Amore PA. Regulators of angiogenesis. *Annu Rev Physiol* 1991;53:217-239.
4. Brown L, Berse B, Jackman RW, et al. Expression of vascular permeability factor (vascular endothelial growth factor) and its receptors in breast cancer. *Hum Pathol* 1995;26:86-91.
5. Warren RS, Yuan H, Matli MR, Gilett NA, Ferrara N. Regulation by vascular endothelial growth factor of human colon cancer tumorigenesis in a mouse model of experimental liver metastasis. *J Clin Invest* 1995;95:1789-1797.
6. Boock CA, Charnock-Jones DS, Sharkey AM, et al. Expression of vascular endothelial growth factor and its receptors flt and KDR in ovarian carcinoma. *J Natl Cancer Inst* 1995;87:506-516.
7. Berkman RA, Merrill MJ, Reinhold WC, et al. Expression of the vascular permeability factor/vascular endothelial growth factor gene in central nervous system neoplasms. *J Clin Invest* 1993;91:153-159.
8. Veikkola T, Karkkainen M, Claesson-Welsh L, Alitalo K. Regulation of angiogenesis via vascular endothelial growth factor receptors. *Cancer Res* 2000;60:203-212.
9. Kim JK, Li B, Winer J, et al. Inhibition of vascular endothelial growth factor-induced angiogenesis suppresses tumor growth in vivo. *Nature* 1993;362:841-844.
10. Melnyk O, Shuman MA, Kim KJ. Vascular endothelial growth factor promotes tumor dissemination by a mechanism distinct from its effect on primary tumor growth. *Cancer Res* 1996;56:921-924.

11. Melnyk O, Zimmerman M, Kim KJ, Shuman M. Neutralizing antivascular endothelial growth factor antibody inhibits further growth of established prostate cancer and metastases in a pre-clinical model. *J Urol* 1999;161:960-963.
12. Prewett M, Huber J, Li Y, et al. Antivascular endothelial growth factor receptor (fetal liver kinase 1) monoclonal antibody inhibits tumor angiogenesis and growth of several mouse and human tumors. *Cancer Res* 1999;59:5209-5218.
13. Okamoto K, Oshika Y, Fukushima Y, et al. Inhibition of liver metastasis of colon cancer by in vivo administration of anti-vascular endothelial growth factor antibody. *Oncol Rep* 1999;6:553-556.
14. Rowe DH, Huang J, Kayton ML, et al. Anti-VEGF antibody suppresses primary tumor growth and metastasis in an experimental model of Wilms tumor. *J Pediatr Surg* 2000;35:30-32.
15. Huang J, Moore J, Soffer S, et al. Highly specific antiangiogenic therapy is effective in suppressing growth of experimental Wilms tumors. *J Pediatr Surg* 2001;36:357-361.
16. Shaheen RM, Tseng WW, Vellagas R, et al. Effects of an antibody to vascular endothelial growth factor receptor-2 on survival, tumor vascularity, and apoptosis in a murine model of colon carcinomatosis. *Int J Oncol* 2001;18:221-226.
17. Shaheen RM, Ahmad SA, Liu W, et al. Inhibited growth of colon cancer carcinomatosis by antibodies to vascular endothelial and epidermal growth factor receptors. *Br J Cancer* 2001;85:584-589.
18. Daldrup H, Shames DM, Wendland M, et al. Correlation of dynamic contrast-enhanced MR imaging with histologic tumor grade: comparison of macromolecular and small-molecular contrast media. *AJR Am J Roentgenol* 1998;171:941-949.
19. Schwickert HC, Stiskal M, Roberts TP, et al. Contrast-enhanced MR imaging assessment of tumor capillary permeability: effect of irradiation on delivery of chemotherapy. *Radiology* 1996;198:893-898.
20. Gossman A, Okuhata Y, Shames DM, et al. Prostate cancer tumor grade differentiation with dynamic contrast-enhanced MR imaging in the rat: comparison of macromolecular and small-molecular contrast media—preliminary experience. *Radiology* 1999;213:265-272.
21. Pham C, Roberts T, van Bruggen N, et al. Magnetic resonance imaging detects suppression of tumor vascular permeability after administration of antibody to vascular endothelial growth factor. *Cancer Invest* 1998;6:224-230.
22. Gossman A, Helbich TH, Mesiano S, et al. Magnetic resonance imaging in an experimental model of human ovarian cancer demonstrating altered microvascular permeability after inhibition of vascular endothelial growth factor. *Am J Obstet Gynecol* 2000;183:956-963.
23. White D, Wang S-C, Aicher K, Dupon J, Engelstad B, Brasch R. Albumin-(Gd-DTPA)₁₅₋₂₀: whole body clearance, and organ distribution of gadolinium. In: *Proceedings of the 8th Annual Meeting of SMRM, Amsterdam, The Netherlands, 1989*. p 807.
24. Baxter AB, Melnikoff S, Stites DP, Brasch RC. Immunogenicity of gadolinium-based contrast agents for MRI. *Invest Radiol* 1991;26:1035-1040.
25. Turetschek K, Huber S, Floyd E, et al. MR imaging characterization of microvessels in experimental breast tumors by using a particulate contrast agent with histopathologic correlation. *Radiology* 2001;218:562-569.
26. Turetschek K, Roberts TPL, Floyd E, et al. Tumor microvascular characterization using ultrasmall superparamagnetic iron oxide particles (USPIO) in an experimental breast cancer model. *J Magn Reson Imaging* 2001;13:882-888.

27. Turetschek K, Floyd E, Helbich T, et al. MRI assessment of microvascular characteristics in experimental breast tumors using a new blood pool contrast agent (MS-325) with correlation to histopathology. *J Magn Reson Imaging* 2001;14:237–242.
28. Turetschek K, Floyd E, Shames DM, et al. Assessment of a rapid clearance blood pool MR contrast medium (P792) for assays of microvascular characteristics in experimental breast tumors with correlation to histopathology. *Magn Reson Med* 2001;45:880–886.
29. Sellappan S, Grijalva R, Zhou X, et al. Lineage infidelity of MDAMB-435 cells: expression of melanocyte proteins in a breast cancer cell line. *Cancer Res* 2004;64:3479–3485.
30. Haase A. Snapshot FLASH MRI. Applications to T1, T2, and chemical shift imaging. *Magn Reson Med* 1990;13:77–89.
31. Schwickert HC, Roberts TP, Shames DM, et al. Quantification of liver blood volume: comparison of ultra short TI inversion recovery echo planar imaging (ULSTIR-EPI), with dynamic 3D-gradient recalled echo imaging. *Magn Reson Med* 1995;34:845–852.
32. Cavagna FM, Zheng J, Lorusso V, Magionni F, Li D, Finn PJ. New protein binding Gd chelate with high vascular containment for MR coronary angiography. *J Cardio Magn Reson* 1999;1:387–388.
33. Zheng J, Carr J, Harris K, et al. Three-dimensional MR pulmonary perfusion imaging and angiography with an injection of a new blood pool contrast agent B-22956/1. *J Magn Reson Imaging* 2001;14:425–432.
34. Schmiedl U, Ogan M, Moseley M, et al. Comparison of the contrastenhancing properties of albumin-(Gd-DTPA) and Gd-DTPA at 2.0 T: an experimental study in rats. *AJR Am J Roentgenol* 1986;147:1263–1270.
35. Roberts TP. Physiologic measurements by contrast-enhanced MR imaging: expectations and limitations. *J Magn Reson Imaging* 1997;7:82–90.
36. Tofts PS, Kernmode AG. Measurement of the blood-brain barrier permeability and leakage space using dynamic MR imaging. I. Fundamental concepts. *Magn Reson Med* 1991;17:357–367.
37. Larsson HBW, Stubgaard M, Frederiksen JL, Jenssen M, Henriksen O, Paulson OB. Quantitation of blood-brain-barrier defect by magnetic resonance imaging and gadolinium-DTPA in patients with multiple sclerosis and brain tumors. *Magn Reson Med* 1990;16:117–131.
38. Brix G, Semmler W, Port R, Schad LR, Layer G, Lorenz WJ. Pharmacokinetic parameters in CNS Gd-DTPA enhanced MR imaging. *J Comput Assist Tomogr* 1991;15:621–628.
39. Shames D, Kuwatsuru R, Vexler V, Muhler A, Brasch RC. Measurement of capillary permeability to macromolecules by dynamic magnetic resonance imaging: a quantitative non-invasive technique. *Magn Reson Med* 1993;29:616–622.
40. Bruns CJ, Solorzano CC, Harbison MT, et al. Blockade of the epidermal growth factor receptor signaling by a novel tyrosine kinase inhibitor leads to apoptosis of endothelial cells and therapy of human pancreatic carcinoma. *Cancer Res* 2000;60:2926–2935.
41. Van Dijke C, Brasch R, Roberts T, et al. Mammary carcinoma model: correlation of macromolecular contrast-enhanced MR imaging characterizations of tumor microvasculature and histologic capillary density. *Radiology* 1996;198:813–818.
42. Dvorak H, Nagy J, Dvorak J, Dvorak A. Identification and characterization of the blood vessels of solid tumors that are leaky to circulating macromolecules. *Am J Pathol* 1988;133:95–109.
43. Prato F, Wisenberg G, Marshall T, Uksik P, Zabel P. Comparison of the biodistribution of gadolinium-153 DTPA and technetium-99m DTPA in rats. *J Nucl Med* 1988;29:1683–1687.

44. Tong C, Prato S, Wisenberg G, et al. Measurement of the extraction efficiency and distribution volume for Gd-DTPA in normal and diseased canine myocardium. *Magn Reson Med* 1993;30:337–346.
45. Turetschek K, Preda A, Floyd E, et al. MRI monitoring of tumor response following angiogenesis inhibition in an experimental human breast cancer model. *Eur J Nucl Med* 2003;30:448–455.
46. Bremerich J, Roberts TPL, Wendland M, et al. Three-dimensional MR imaging of pulmonary vessels and parenchyma with NC100150 (Clariscan). *J Magn Reson Imaging* 2000;11:622–628.
47. Yuan F, Chen Y, Dellian M, Safabakhsh N, Ferrara N, Jain RK. Time-dependent vascular regression and permeability changes in established human tumor xenografts induced by an anti-vascular endothelial growth factor/vascular permeability factor antibody. *Proc Natl Acad Sci U S A* 1996;93:14765–14770.

CHAPTER 10

DYNAMIC CONTRAST-ENHANCED MRI USING
MACROMOLECULAR CONTRAST MEDIA FOR MONITORING
THE RESPONSE TO ISOLATED LIMB PERFUSION IN
EXPERIMENTAL SOFT-TISSUE SARCOMAS

DYNAMIC CONTRAST- ENHANCED MRI USING MACROMOLECULAR CONTRAST MEDIA FOR MONITORING THE RESPONSE TO ISOLATED LIMB PERFUSION IN EXPERIMENTAL SOFT-TISSUE SARCOMAS

10

(MAGMA 2004, 17:296-302)

A. Preda¹, P. A. Wielopolski¹, T. L. M. ten Hagen², M. van Vliet¹, J. F. Veenland¹,
G. Ambagtsheer², S. T. van Tiel², M. W. Vogel¹, A. M. M. Eggermont², G. P. Krestin¹,
C. F. van Dijke¹

¹ Department of Radiology, Erasmus MC-University Medical Center Rotterdam,
The Netherlands.

² Department of Surgical Oncology, Erasmus MC-University Medical Center Rotterdam,
Rotterdam, The Netherlands.

Abstract

The objective of this study was to evaluate the potential of dynamic contrast-enhanced MRI for quantitative characterization of tumor microvessels and to assess the microvascular changes in response to isolated limb perfusion with TNF- α and melphalan. Dynamic contrast-enhanced MRI was performed in an experimental cancer model, using a macromolecular contrast medium, albumin-(Gd-DTPA)₄₅. Small fragments of BN 175, a soft-tissue sarcoma, were implanted in 11 brown Norway (BN) rats. Animals were assigned randomly to a control (Haemaccel) or drug-treated group (TNF- α /melphalan). MRI was performed at baseline and 24 h after ILP. The transendothelial permeability (K^{PS}) and the fractional plasma volume (fPV) were estimated from the kinetic analysis of MR data using a two-compartment bi-directional model. K^{PS} and fPV decreased significantly in the drug-treated group compared to baseline ($p < 0.05$). In addition, K^{PS} post therapy was significantly lower ($p < 0.05$) in the drug-treated group than in the control group. There was no significant difference in fPV between the drug-treated and the control group after therapy. Tumor microvascular changes in response to isolated limb perfusion can be determined after 24 h by dynamic contrast-enhanced MRI. The data obtained in this experimental model suggest possible applications in the clinical setting, using the appropriate MR contrast agents.

Keywords

Magnetic resonance imaging · Isolated limb perfusion · Tumor angiogenesis · Microvascular permeability · Soft-tissue sarcoma

Introduction

Low concentration of anti-tumor agents can be the cause of failure of tumor treatment. In isolated limb perfusion (ILP) local drug concentrations are increased while systemic exposure to the drug is minimal. Tumor necrosis factor alpha (TNF- α), a cytokine with known anti-tumor activity, cannot be used systemically in dosages high enough to obtain tumor response. However, in ILP with TNF- α , tumors are exposed to concentrations up to 15-20 times higher than those reached after systemic administration of the maximum tolerated dose without major side effects [1]. TNF- α is directly cytotoxic for tumor cells [2] and has indirect toxicity by affecting endothelial cells and tumor vascularization [3-5]. By combining TNF- α and a cytostatic drug like melphalan, a synergistic effect on the tumor activity can be obtained, because of an immediate TNF- α mediated tumor-selective enhanced drug uptake of the cytostatic agent [6, 7], dependent on the vascularity of the tumor [8], followed by a tumor-selective eradication of the tumor-associated vasculature [9]. In the clinical setting the combination of TNF- α , interferon- γ and melphalan in isolated limb perfusion has lead to a limb salvage rate of 90% in isolated limb perfusion for irresectable melanomas and sarcomas [9-11].

Magnetic resonance imaging (MRI) offers the possibility to noninvasively characterize tumors. The ability of dynamic MRI enhanced with macromolecular contrast agents to quantitatively define the permeability of tumor microvessels has been shown in several experimental models [12-14].

The purpose of the current study was to evaluate whether blood-pool enhanced MRI could identify and monitor the effect of a combined treatment with TNF- α and melphalan. Microvascular characteristics, such as transendothelial permeability and fractional plasma volume, derived from the kinetic analysis of data acquired with dynamic MRI enhanced with albumin-(Gd-DTPA)₄₅, were studied as a marker of disease progression and response to anti-tumor therapy by isolated limb perfusion with TNF- α and melphalan. Although hemorrhagic necrosis and destruction of the endothelial cells will develop in time after TNF- α administration, the hypothesis of this study was that the synergistic anti-tumor effects could be demonstrated 24 h after initiation of ILP.

Material and methods

Animal and tumor model

The study was conducted with the approval of the Committee for Animal Research at our institution. Male inbred BN strain rats weighing 250-300 g were used (Harlan-CPB, Austerlitz, The Netherlands). Small fragments (3-5 mm) of the syngenic BN 175 soft-tissue sarcoma were implanted subcutaneously in the right hind limb just above the ankle. BN 175 sarcoma is a rapidly growing and metastasizing tumor. The animals were inspected daily for tumor growth and general appearance. The tumors were imaged when they reached 15 mm in diameter. Before the MR imaging, the animals were anesthetized by administration of Hypnorm (Janssen Pharmaceutica, Beerse, Belgium). Analgesia was achieved by intraperitoneal injection of ketamine (Alfasan, Woerden, The Netherlands). A 25-gauge butterfly canula was inserted into a tail vein for contrast medium injection.

Magnetic resonance imaging

Magnetic resonance imaging was performed using a MR Signa CV/i scanner (General Electric Medical Systems, Milwaukee, WI, USA) operating at 1.5 T. A single-loop (custom-made) surface coil with an internal diameter of 1.7 cm was constructed specifically to create a high signal-to-noise ratio. A phantom filled with corn oil was positioned in the field of view as a T1 reference. Pre-contrast T1 mapping was performed using a three-dimensional spoiled gradient-recalled sequence (3D-SPGR) with the following parameters: TR 17 ms, TE 4 ms, slice thickness 3 mm, matrix 256 × 224 × 80, FOV 4.0 × 4.0 × 3.2 cm, and varying flip angles of 5°, 15°, 30°, 45° and 60°. Data from this sequence was used to calculate baseline longitudinal relaxation rates ($R_1 = 1/T_1$) for tumor by curve fitting [15]. Subsequently dynamic images (pre-contrast $n = 2$, post-contrast $n = 10$) were acquired serially at three-minute intervals with the parameters described above, except the flip angle was fixed at 60°.

Magnetic resonance contrast media

Albumin-(Gd-DTPA)₄₅ is a prototype of a water-soluble macromolecular contrast medium with a molecular weight of 92,000 Da, synthesized following the method of Ogan [16] (Center of

Pharmaceutical and Molecular Imaging, Department of Radiology, University of California San Francisco, CA, USA). It has a distribution volume of 0.05 l/kg and a plasma half-life of 3 h in rats, which produces nearly constant enhancement for 30 min or longer after injection. Albumin-(Gd-DTPA)₄₅ was injected at a dose of 0.03 mmol Gd/kg.

Experimental protocol

Magnetic resonance examination was performed at baseline (when tumor size was approximately 15 mm) and 24 h after treatment (or placebo). After the baseline MR examinations, animals were randomly assigned to either the drug treatment or the control group. One day after the baseline MR imaging, each rat was perfused according to the ILP technique as reported by Manusama [17]. Briefly, the animals were anesthetized with Hypnorm and ketamine and 50 units heparin were injected intravenously. The femoral artery and vein of anesthetized rats were cannulated with silastic tubing. Collaterals were occluded by groin tourniquet and perfusion was started after the tourniquet was tightened. An oxygenation reservoir and a roller pump were included in the circuit. The perfusion was performed with 5 ml Haemaccel (Behring Pharma, Amsterdam, The Netherlands) and the hemoglobin content of the perfusate was 0.9 mmol/l. 50 µg TNF- α (Boehringer, Ingelheim, Germany) in combination with 40 µg melphalan (Alkeran, Wellcome, Beckenham, UK) were added as boluses to the oxygenation reservoir (drug treatment group). In the control group no drugs were added to the perfusate. During the perfusion, the hind leg of the rat was kept at a temperature of 38–39°C with a warm water mattress. Perfusion was maintained for 30 min at a flow rate of 1.8 ml min⁻¹. A washout with 5 ml oxygenated Haemaccel was performed at the end of the ILP. In order to restore physiological limb perfusion, the femoral artery was decannulated and sutured. A second MRI examination using the same parameters and contrast medium as for the baseline examination was performed 24 h after ILP. After completing the MR examination, all animals were sacrificed by intravenous injection of ketamine.

Kinetic analysis of dynamic MRI data

The MR images were transferred, processed and analyzed using a GE AW2 workstation (General Electric Medical Systems, Milwaukee, WI, USA). Signal intensity values (SI) for each time point were obtained from multiple (3–6) regions of interest (ROIs) placed in the femoral vein, the phantom and the tumor periphery. The tumor periphery was defined as the peripheral zone of the tumor, 8–10 pixels thick. The size of the ROI was dependent on the size of the tumor. Corresponding ROI measurements were made in each of three adjacent images and were averaged. The mean signal intensities from the tumors and the blood in the femoral vein were corrected for potential variation over time by dividing the SI of each ROI by the SI of the phantom. Pre contrast longitudinal relaxation rates R1 (1/T1) estimates for tumors were obtained by curve fitting based on five sets of SPGR images. The pre-contrast R1 value for femoral vein blood was assumed to be 0.724 s⁻¹ (1/1.38) based upon numerous previous measurements in rat blood [15]. Due to incomplete clearance of the contrast agent, the post-treatment pre-contrast R1 value for femoral vein blood had to be determined separately. Using five additional rats, not included in the final analysis, an average post-treatment pre-contrast R1 for femoral vein blood of 1.026 s⁻¹ was found. Post-contrast R1 values were calculated based on the observed signal intensities and knowledge of pre-contrast R1 values for each ROI as previously described [12]. The difference between the post-contrast R1 value at any time point and the pre-contrast R1, $\Delta R1(t)$, was assumed

to be directly proportional to the concentration of the contrast medium, either in the blood or in the tissue [15,18]. Although this assumption is limited in the presence of intermediate or slow water exchange, previous studies [15,18] suggest that this level of approximation is nonetheless acceptable, provided that a short TR is used (17 ms in this case). The $\Delta R1$ data from blood and tumor were used for kinetic analysis to estimate the transendothelial permeability (K^{PS} , $\text{ml} \times \text{min}^{-1} 100 \text{ cc}^{-1} \text{ tissue}$) and the fractional plasma volume of the tumor tissue (fPV, $\text{ml cc}^{-1} \text{ tissue}$) using a two-compartment, bi-directional kinetic model as previously described in detail [12,19]. In this model, a mono-exponential function fitted to the $\Delta R1$ data from blood was used as an input function for the plasma response in the tumor tissue, after scaling for fractional plasma volume. The K^{PS} values determined from the model were multiplied by 100, thereby scaling our permeability measure for 100 cc of tissue. All data fitting was performed with the commercially available SAAM II computer program (SAAM Institute, Seattle, WA, USA), which employs standard variance-weighted nonlinear regression. The uncertainty of the estimates of the model parameters was determined from the covariance matrix at the least squares fit.

Statistics

The paired two-tailed Student's t-test was used to compare mean values of K^{PS} and fPV in the same tumor before and after therapy (drug or sham). The unpaired two-tailed Student's t-test was used to compare mean values for K^{PS} and fPV between the control and the treated groups. A p-value of <0.05 was considered statistically significant.

Results

The tumors grew in all implanted animals. The MR imaging was completed successfully in 11 animals (four sham and seven drug-treated). *Figure 1* shows an example of a tumor before and after ILP with TNF- α and melphalan and a tumor before and after sham-ILP.

The mean values for K^{PS} and fPV obtained in the pre-and post-therapy studies are shown in *Table 1*. The mean K^{PS} values at baseline were $0.115 \pm 0.044 \text{ ml} \times 100 \text{ cc}^{-1} \text{ min}^{-1}$ for the drug group and $0.086 \pm 0.038 \text{ ml} \times 100 \text{ cc}^{-1} \text{ min}^{-1}$ for the control group ($p = 0.28$). At the follow-up examination, the mean K^{PS} values decreased significantly ($p < 0.05$) in the drug treated group ($0.045 \pm 0.019 \text{ ml} \times \text{min}^{-1} 100 \text{ cc}^{-1}$) compared to baseline. In the control group, the mean K^{PS} values did not significantly differ from the baseline ($0.096 \pm 0.021 \text{ ml} \times 100 \text{ cc}^{-1} \text{ min}^{-1}$ vs. $0.086 \pm 0.038 \text{ ml} \times 100 \text{ cc}^{-1} \text{ min}^{-1}$, $p = 0.52$). In addition, K^{PS} post values were significantly lower in the drug-treated group ($0.045 \pm 0.019 \text{ ml} \times 100 \text{ cc}^{-1} \text{ min}^{-1}$) than in the control group ($0.096 \pm 0.021 \text{ ml} \times 100 \text{ cc}^{-1} \text{ min}^{-1}$, $p < 0.05$) as illustrated in *Fig. 2*.

Mean fPV values were not significantly different at baseline ($0.088 \pm 0.033 \text{ ml cc}^{-1}$ for the drug group versus $0.082 \pm 0.027 \text{ ml cc}^{-1}$ in the control group, $p = 0.78$). At the follow-up examination, the mean fPV values decreased significantly ($p < 0.05$) in the drug treated group ($0.024 \pm 0.018 \text{ ml cc}^{-1}$) compared to baseline. In the control group, the mean fPV values did not significantly differ ($p = 0.08$) from the baseline ($0.043 \pm 0.034 \text{ ml cc}^{-1}$). Post-therapy fPV values did not differ in the control group ($0.043 \pm 0.034 \text{ ml cc}^{-1}$) from the drug-treated group ($0.024 \pm 0.018 \text{ ml cc}^{-1}$, $p = 0.36$), as illustrated in *Fig. 3*.

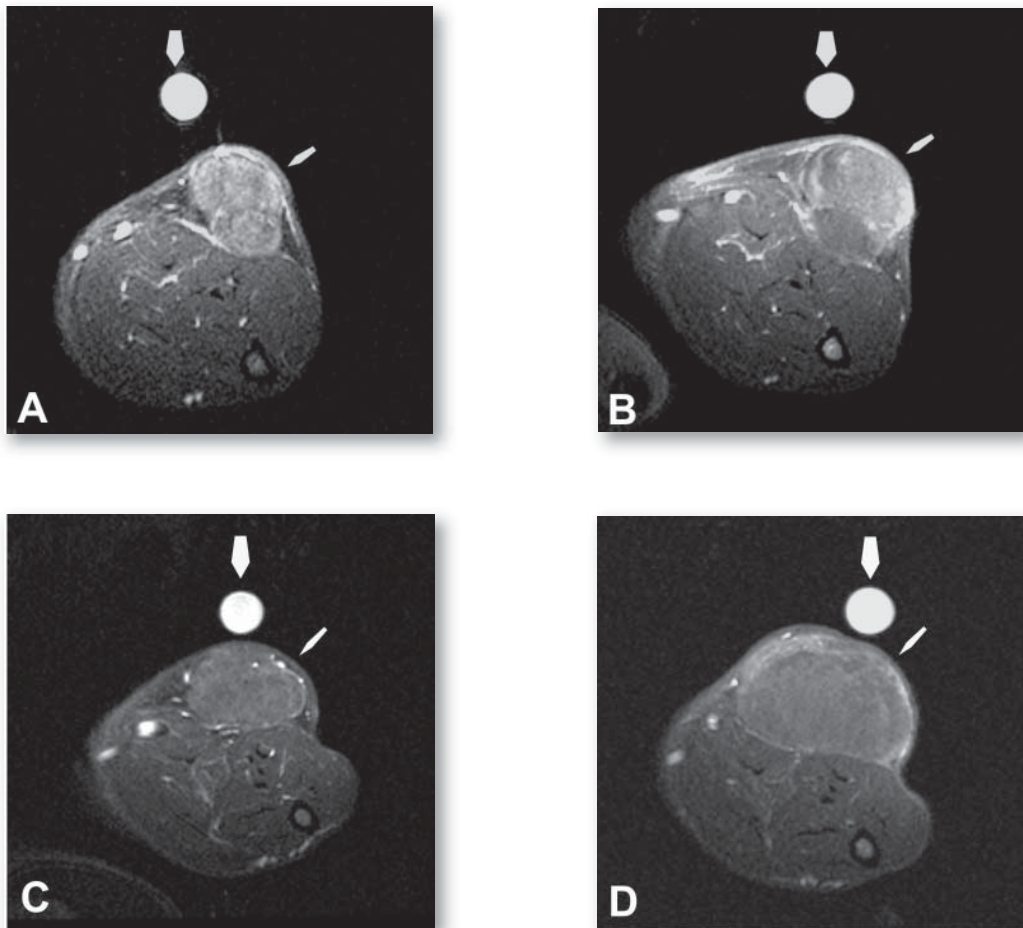


Fig. 1a-d T1-weighted axial images after i.v. administration of albumin-(Gd-DTPA)₄₅ showing an implanted sarcoma (small arrow). A phantom was placed in the field of view (thick arrow). **a, b** Pre (a) and post (b) ILP with TNF- α and melphalan. **c, d** Pre (c) and post (d) ILP with haemaccel (sham perfusion).

	fPV pre	fPV post	K ^{PS} pre	K ^{PS} post
Drug-treated	0.088 \pm 0.033	0.024 \pm 0.018*	0.115 \pm 0.044	0.045 \pm 0.019*, **
Control	0.082 \pm 0.027	0.043 \pm 0.034	0.086 \pm 0.038	0.096 \pm 0.021

fPV fractional plasma volume (ml cc⁻¹ tissue)

K^{PS} transendothelial permeability (ml \times min⁻¹ 100 cc⁻¹ tissue)

*Statistically significantly different from baseline value ($p < 0.05$)

**Statistically significantly different from control group ($p < 0.05$)

Table 1 MRI estimates of fractional plasma volume (fPV) and transendothelial permeability (K^{PS}) for the drug-treated and control group.

Discussion

Microvascular characteristics of tumors such as capillary permeability and plasma volume can be quantitatively assessed by contrast-enhanced MRI by analyzing the kinetics of the distribution of the contrast medium in tumor tissue. These parameters can be estimated from kinetic analysis of dynamic enhancement data using simple models of the tissue as a compartmentalized system [19-22]. Usually two-compartment tissue models are used, representing the blood plasma and the extra-

vascular extracellular space. The contrast agent concentration, modeled as a function of time, can be derived from MR signal intensity data, assuming that changes in longitudinal relaxation rates R_1 ($1/T_1$) after administration of contrast medium are proportional to contrast agent concentration. Based on the observed MR signal intensities, these changes in R_1 can be calculated. Thus the increase of the enhancement can be translated to contrast agent concentration and quantified using kinetic modeling, providing estimates

of microvascular characteristics.

The measurement of these functional parameters enables an accurate noninvasive quantitative description of the microcirculation of individual tumors. The follow-up of the MRI-derived estimates of microvascular characteristics provides a tool for in vivo monitoring of the tumor response to therapy. Data from this pilot study indicate that the effects of anti-tumor treatment by isolated limb perfusion can be successfully monitored by MRI after 24 h. We found that dynamic MRI, enhanced with albumin-(Gd-DTPA)₄₅, was able to detect significant declines in

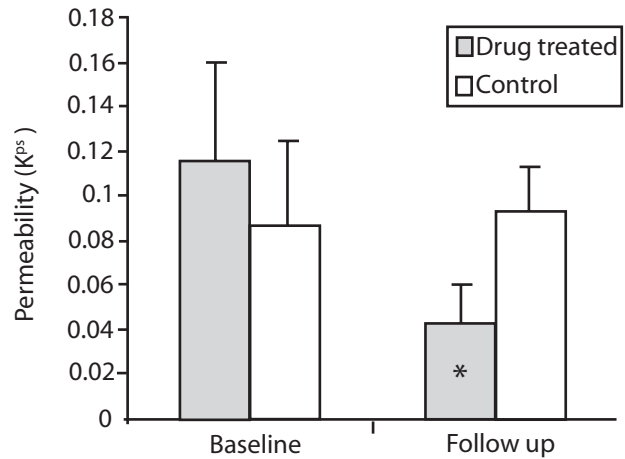


Fig. 2 Transendothelial permeability (K^{ps}) in $\text{ml} \times 100 \text{ cc}^{-1} \text{ min}^{-1}$ tissue at baseline and follow-up examinations for the drug-treated and the control group. *statistically significantly different from baseline value and from control group ($p < 0.05$).

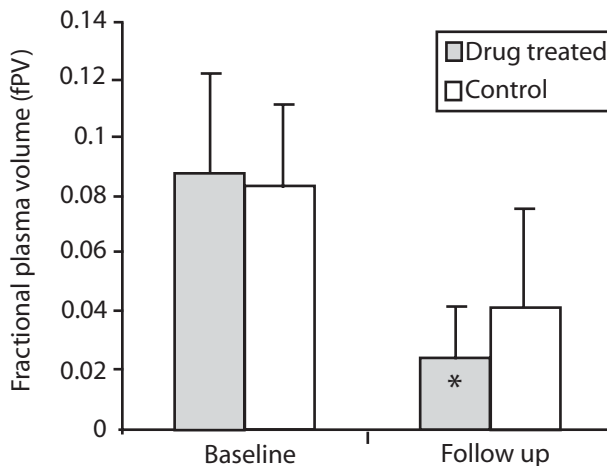


Fig. 3 Fractional plasma volume (fPV) in ml cc^{-1} tissue at baseline and follow-up examinations for the drug-treated and the control group. *statistically significantly different from baseline value ($p < 0.05$)

the microvascular permeability of experimental soft-tissue sarcoma as a result of anti-tumor therapy by isolated limb perfusion with a combination of TNF- α and melphalan. The estimated tumor microvascular permeability, K^{PS} , to albumin-(Gd-DTPA)₄₅ decreased significantly ($p < 0.05$) compared to baseline in the animal group treated with TNF- α and melphalan. Moreover, K^{PS} post values were significantly lower in the drug-treated group than in the control group ($p < 0.05$).

Fractional plasma volume showed no evidence of significant change as a result of therapy. Although there was a decrease in the fPV after ILP in the drug group, the post-therapy fPV values were not significantly different in the drug and the control group. The higher sensitivity of K^{PS} to anti-tumor therapy is consistent with results from other studies, which demonstrated no changes in fractional plasma volume of the tumor tissue following one week of anti-VEGF antibody treatment [23] or a VEGF receptor tyrosine kinase inhibitor treatment [24] using an experimental model of human breast cancer enhanced with albumin-(Gd-DTPA)₃₀ [23,24] and SHU555C [24] as contrast agents.

The kinetic analysis was limited to the tumor periphery, which is typically the most vascularized and the least necrotic region of the tumor [25,26]. Results of previous studies have shown that the tumor periphery is the most representative region for oncologic activity [27], and the most responsive to angiogenesis inhibition [28], radiation therapy [29] and chemotherapy [13]. The ROIs in the tumor periphery were selected on a late post-contrast image and in the same position on the baseline and follow-up studies. We did not analyze the whole tumor, since we expected tumor necrosis in the center after isolated limb perfusion, which could distort the tumor contrast-enhanced characterization.

In the present study, we were primarily interested in quantifying the short-term effects of ILP on the microvascular characteristics of the tumor; we did not take into account the long-term effects of ILP. In a future study, we plan to evaluate the effect of ILP in an even shorter time frame: within 0.5-1 h after treatment DCE-MRI will be performed. This way, the almost immediate effects of ILP on the microvasculature of the tumor can be studied.

The search for a contrast agent suitable for characterizing the vessels of tumors in a clinical setting has been extensive. Since the prototype macromolecular contrast medium albumin-(Gd-DTPA) is not appropriate for human use [30,31], due to its potential immunologic response and the incomplete and prolonged elimination of gadolinium, the feasibility of several other contrast media to quantitatively assess the properties of tumor microvessels has been evaluated. Recently, several MR contrast media were studied with respect to their diagnostic potential for quantitative description of tissue microvessels. These contrast agents include ultra-small superparamagnetic iron oxide particles (USPIO) such as NC100150 (Clariscan, Nycomed Amersham, Oslo, Norway) [32] and SHU 555C (Resovist, Schering AG, Berlin, Germany) [33] and blood-pool agents such as MS-325 (Angiomark, Schering AG, Berlin, Germany) [34] and P792 (Vistarem, Guerbet, Aulnay-sous-Bois, France) [35]. However, one limitation of the use of USPIO for characterization of tumor microvessels is the fact that the positive signal enhancement associated with T1 shortening is associated with negative enhancement induced by the T2* shortening [18,36]. Especially when higher doses of USPIO are used, the positive enhancement caused by the T1 shortening can be

overwhelmed by the $T2^*$ effects. A second factor that can negatively influence the use of USPIO in the quantitative estimation of the microvessel properties is the dependence of the $T2^*$ effects on the compartmentalization of the iron particles in the tissue [33].

To obtain further insight into the mechanisms underlying the positive results obtained with ILP in humans, extremity perfusion models were developed in rats using BN 175 sarcoma in brown Norway rats and ROS-1 osteosarcoma in WAG rats [17,37]. In both models, a strong synergistic anti-tumor effect was observed after ILP with $TNF-\alpha$ and melphalan. The observations from these studies confirmed that $TNF-\alpha$ has its major effect on larger tumors with well-developed vasculature, in contrast with small tumors (diameters less than 3 mm) lacking a developed capillary bed [38,39]. $TNF-\alpha$ may exert its effect through the vasculature of the tumor, which is more abundant in larger tumors. Early endothelial damage and platelet aggregation were observed after ILP with $TNF-\alpha$ and melphalan and this is believed to lead to ischemic necrosis, which is in line with observations in patients [40]. The observed decrease in tumor vascular permeability in the present study in the group that underwent ILP with $TNF-\alpha$ and melphalan might be explained by the destruction of the tumor blood vessels. Previous studies have demonstrated the selective destructive effect of the ILP with TNF on tumor-associated vessels using pre-perfusion and post-perfusion angiography [41].

The data in this study support the hypothesis that estimates of transendothelial permeability are an appropriate measure of tumor microvascular changes in response to isolated limb perfusion, although a limited number of animals have been examined. Although albumin-(Gd-DTPA)₄₅ is a useful prototype for animal studies, this macromolecular contrast agent is considered unlikely for ultimate clinical use because of incomplete elimination. However, since several blood-pool contrast agents are at this moment under clinical investigation, examination of the feasibility of blood-pool enhanced MR in this ILP model seems to be of interest.

In conclusion, dynamic MRI enhanced with the macromolecular contrast agent albumin-(Gd-DTPA)₄₅ has shown a potential to measure, after 24 h, the effects of isolated limb perfusion on tumor microvasculature in an experimental model of soft-tissue sarcoma. Quantitative microvascular characterization of tumors with dynamic MRI using a blood-pool contrast agent could prove to be clinically useful in monitoring the changes induced by anti-tumor treatment and serve to provide an early and physiologically-specific indicator of biological activity of such a therapeutic approach.

Acknowledgements

Albumin-(Gd-DTPA)₄₅ was generously provided by RC Brasch, Center of Pharmaceutical and Molecular Imaging, Department of Radiology, University of California San Francisco, CA, USA.

References

1. Benckhuijsen C, Kroon BB, van Geel AN et al. (1998) Regional perfusion treatment with melphalan for melanoma in a limb: an evaluation of drug kinetics. *Eur J Surg Oncol* 14:157–163
2. Goeddel DV, Aggarwal BB, Gray PW et al. (1986) Tumor necrosis factors: gene structure and biological activities. In: *Cold Spring Harb Symp Quant Biol*. 51 Pt 1: 597–609
3. Camussi G, Bussolino F, Salvidio G, Baglioni C (1987) TNF/cachectin stimulates peritoneal macrophages, polymorphonuclear neutrophils and vascular endothelial cells to synthesis and release of platelet activating factor. *J Exp Med* 166:1390–1404
4. Gamble JR, Harlan JM, Klebanoff SJ, Vadas MA (1985) Stimulation of the adherence of neutrophils to umbilical vein endothelium by human TNF. *Proc Natl Acad Sci USA* 82:8667–8671
5. Watanabe N, Niitsu Y, Umeno H, Kiriyaama H, Neda H, Yamauchi N (1988) Toxic effect of TNF on tumor vasculature in mice. *Cancer Res* 49:2179–2183
6. De Wilt JH, ten Hagen TL, de Boeck G, van Tiel ST, de Bruijn EA, Eggermont AM (2000) Tumour necrosis factor alpha increases melphalan concentration in tumour tissue after isolated limb perfusion. *Br J Cancer* 82:1000–1003
7. Van der Veen AH, de Wilt JH, Eggermont AM, van Tiel ST, ten Hagen TL (2000) TNF- α augments intratumoural concentration of doxorubicin in TNF- α -based isolated limb perfusion in rat sarcoma models and enhances antitumour effects. *Br J Cancer* 82:973–980
8. Van Etten B, de Vries M, van Ijken M et al. (2003) Degree of tumour vascularity correlates with drug accumulation and tumour response upon TNF-based isolated hepatic perfusion. *Br J Cancer* 87:314–319
9. Eggermont AM, Schraffordt Koops H, Klausner JM et al. (1996) Isolated limb perfusion with tumor necrosis factor alpha and melphalan in 186 patients with locally advanced extremity soft tissue sarcomas. The cumulative multicenter European experience. *Ann Surg* 224(6):754–764; discussion 764–765
10. Eggermont AM, Schraffordt Koops H, Lienard D et al. (1996) Isolated limb perfusion with high dose tumor necrosis factor alpha (TNF-alpha), interferon-gamma (IFN-gamma) and melphalan for non-resectable extremity soft tissue sarcomas: a multi-center trial. *J Clin Oncol* 14(10):2653–2665
11. Lienard D, Eggermont AM, Schraffordt Koops H et al. (1994) Isolated perfusion of the limb with high-dose tumor necrosis factor alpha (TNF-alpha), interferon-gamma (IFN-gamma) and melphalan for melanoma stage III: results of a multi-centre pilot study. *Melanoma Res* 4(suppl 1):21–27
12. Daldrup H, Shames DM, Wendland M et al. (1998) Correlation of dynamic contrast-enhanced MR imaging with histologic tumor grade: comparison of macromolecular and small-molecular contrast media. *Am J Roentgenol* 171:941–949
13. Schwickert HC, Stiskal M, Roberts TP et al. (1996) Contrast-enhanced MR imaging assessment of tumor capillary permeability: effect of irradiation on delivery of chemotherapy. *Radiology* 198:893–898
14. Gossman A, Okuhata Y, Shames DM et al. (1999) Prostate cancer tumor grade differentiation with dynamic contrast-enhanced MR imaging in the rat: comparison of macromolecular and small-molecular contrast media-preliminary experience. *Radiology* 213:265–272

15. Schwickert HC, Roberts TP, Shames DM et al. (1995) Quantification of liver blood volume: comparison of ultrashort TI inversion recovery echo planar imaging (ULSTIR-EPI), with dynamic 3D-gradient recalled echo imaging. *Magn Reson Med* 34:845–852
16. Ogan M, Schmiedl U, Moseley ME, Grodd W, Paaenen H, Brasch RC (1987) Albumin labeled with Gd-DTPA. An intravascular contrast-enhancing agent for magnetic resonance blood pool imaging: preparation and characterization. *Invest Radiol* 22:665–671
17. Manusama ER, Nooijen PT, Stavast J, Durante NM, Marquet RL, Eggermont AM (1996) Synergistic antitumour effect of recombinant human tumor necrosis factor alpha with melphalan in isolated limb perfusion in the rat. *Br J Surg* 83:551–555
18. Roberts TP (1997) Physiologic measurements by contrast-enhanced MR imaging: expectations and limitations. *J Magn Reson Imaging* 7:82–90
19. Shames D, Kuwatsuru R, Vexler V, Muhler A, Brasch RC (1993) Measurement of capillary permeability to macromolecules by dynamic magnetic resonance imaging: a quantitative non-invasive technique. *Magn Reson Med* 29:616–622
20. Tofts PS, Kermode AG (1991) Measurement of the blood-brain barrier permeability and leakage space using dynamic MR imaging. 1. Fundamental concepts. *Magn Reson Med* 17:357–367
21. Larsson HBW, Stubgaard M, Frederiksen JL, Jenssen M, Henriksen O, Paulson OB (1990) Quantitation of blood-brain-barrier defect by magnetic resonance imaging and gadolinium-DTPA in patients with multiple sclerosis and brain tumors. *Magn Reson Med* 16:117–131
22. Brix G, Semmler W, Port R, Schad LR, Layer G, Lorenz WJ (1991) Pharmacokinetic parameters in CNS Gd-DTPA enhanced MR imaging. *J Comput Assist Tomogr* 15:621–628
23. Pham C, Roberts T, van Bruggen N et al. (1998) Magnetic resonance imaging detects suppression of tumor vascular permeability after administration of antibody to vascular endothelial growth factor. *Cancer Invest* 6:224–230
24. Turetschek K, Preda A, Floyd E et al. (2003) MRI monitoring of tumor response following angiogenesis inhibition in an experimental human breast cancer model. *Eur J Nucl Med* 30:448–455
25. Jain R (1987) Transport of molecules across tumor vasculature. *Cancer Metastasis Rev* 6:559–593
26. Jain R, Baxter LT (1998) Mechanisms of heterogenous distribution of monoclonal antibodies and other molecules in tumors : significance of elevated interstitial pressure. *Cancer Res* 48(24pt 1):7022–7032
27. Van Dijke CF, Brasch RC, Roberts TP et al. (1996) Mammary carcinoma model: correlation of macromolecular contrast-enhanced MR imaging characterizations of tumor microvasculature and histologic capillary density. *Radiology* 198:813–818
28. Brasch R, Pham C, Shames D et al. (1997) Assessing tumor angiogenesis using macromolecular MR imaging contrast media. *J Magn Reson Imaging* 7:68–74
29. Cohen FM, Kuwatsuru R, Shames DM et al. (1994) Contrast-enhanced magnetic resonance imaging estimation of altered capillary permeability in experimental mammary carcinomas after X-irradiation. *Invest Radiol* 29:970–977
30. White D, Wang S-C, Aicher K, Dupon J, Engelstad B, Brasch R (1989) Albumin-(Gd-DTPA)15–20: whole body clearance, and organ distribution of gadolinium. In: proceedings of the society of magnetic resonance in medicine, 8th annual meeting, Amsterdam, p. 807

31. Baxter AB, Melnikoff S, Stites DP, Brasch RC (1991) Immunogenicity of gadolinium-based contrast agents for MRI. *Invest Radiol* 26:1035–1040
32. Turetschek K, Huber S, Floyd E et al. (2001) MR imaging characterization of microvessels in experimental breast tumors by using a particulate contrast agent with histopathologic correlation. *Radiology* 218:562–569
33. Turetschek K, Roberts TPL, Floyd E et al. (2001) Tumor microvascular characterization using ultrasmall superparamagnetic iron oxide particles (USPIO) in an experimental breast cancer model. *J Magn Reson Imaging* 13:882–888
34. Turetschek K, Floyd E, Helbich T et al. (2001) MRI assessment of microvascular characteristics in experimental breast tumors using a new blood pool contrast agent (MS-325) with correlation to histopathology. *J Magn Reson Imaging* 14:237–242
35. Turetschek K, Floyd E, Shames DM et al. (2001) Assessment of a rapid clearance blood pool MR contrast medium (P792) for assays of microvascular characteristics in experimental breast tumors with correlation to histopathology. *Magn Reson Med* 45:880–886
36. Bremerich J, Roberts TP, Wendland M et al. (2000) Three-dimensional MR imaging of pulmonary vessels and parenchyma with NC100150 (Clariscan). *J Magn Reson Imaging* 11:622–628
37. Manusama ER, Stavast J, Durante NM et al. (1996) Isolated limb perfusion in a rat osteosarcoma model: a new anti-tumour approach. *Eur J Surg Oncol* 22:152–157
38. Manda T, Nishigaki F, Mukumoto S et al. (1990) The efficacy of combined treatment with recombinant tumor necrosis factor- α and fluorouracil is dependent on the development of capillaries in tumor. *Eur J Cancer* 26:93–99
39. Mulle JJ, Asher A, McIntosh J et al. (1988) Antitumor effect of recombinant tumor necrosis factor- α against murine sarcomas at visceral sites: tumor size influences the response to therapy. *Cancer Immunol Immunother* 26:202–208
40. Eggermont AM, ten Hagen TM (2001) Isolated limb perfusion for extremity soft-tissue sarcomas, in-transit metastases, and other unresectable tumors: credits, debits and future perspectives. *Curr Oncol Rep* 3:359–367
41. Eggermont AM, Schraffordt Koops H, Lienard D et al. (1994) Angiographic observations before and after high dose TNF isolated limb perfusion in patients with extremity soft tissue sarcomas. *Eur J Surg Oncol* 20:323–324

CHAPTER 11

SUMMARY AND CONCLUSION

Dynamic contrast-enhanced magnetic resonance imaging (DCE-MRI) offers the opportunity to quantitatively assess physiologic properties of tumor tissue. MRI enables the noninvasive investigation of the anatomy and function of the tumor microvessels and can help in distinction of malignant tumor blood vessels from normal vessels. The subject of this dissertation is the evaluation of the role of dynamic MRI enhanced with macromolecular contrast media in noninvasive characterization of the pathophysiology of tumor microvessels and in the monitoring of antiangiogenesis therapy.

Chapter 1 provides a general introduction to this thesis.

Chapter 2 presents an overview of the current applications and limitations of macromolecular contrast media for quantitative MR characterization of tumor microvessels, investigated either in experimental animal studies or in clinical trials, with or without drug interventions.

In **chapter 3**, a meta-analysis of quantitative MRI breast tumor characterizations acquired in three separate experimental studies of rodent breast cancers demonstrated that transendothelial permeability values based on MR data obtained from a region of interest limited to the periphery of tumors correlated significantly better ($r=0.784$, $P<0.001$) with the tumor histologic grade than did K^{ps} estimated from data analysis from regions of interest covering the whole tumor cross section ($r=0.604$). Based on these results, future efforts to characterize tumor grade based on MRI analysis should focus on regions of interest confined to the tumor periphery, at least as a major component in a more complete analysis.

In **chapter 4**, the utility of a new rapid clearance blood pool MR contrast medium (P792) for the assessment of microvessels characteristics was evaluated in a chemically induced rodent breast tumor model and compared to the prototype contrast agent albumin-(Gd-DTPA)₃₀. Using P792-enhanced data, neither the transendothelial permeability K^{ps} nor the fractional plasma volume of the tumor tissue showed a significant correlation with the tumor histologic grade or with the microvascular density counts ($P>0.05$). Conversely, using albumin-(Gd-DTPA)₃₀, K^{ps} values correlated significantly ($r=0.55$, $P<0.001$) with the tumor grade and the microvessel density count ($r=0.34$, $P<0.05$). The analysis suggests that contrast media of relatively large (on the order of 90 kDa) molecular weight, such as albumin-(Gd-DTPA)₃₀, are more accurate for the characterization of tumor microvessels.

In **chapter 5**, the potential of carboxymethyldextran-A2-Gd-DOTA, a slow clearance blood pool contrast medium, for characterization of tumor microvessels was evaluated in a chemically induced rodent breast tumor model of various malignancy grades. No significant correlations were found between the MR-estimated transendothelial permeability ($r=0.09$, $P>0.05$) or plasma volumes ($r=0.19$, $P>0.05$) of the tumor tissue and the tumor histologic grade. Analysis of carboxymethyldextran-A2-Gd-DOTA-enhanced MR kinetic data failed to demonstrate feasibility for the differentiation of benign from malignant tumors or for image-based tumor grading.

In **chapter 6**, the diagnostic potential of USPIO for defining the properties of tumor microvessels was investigated. Transendothelial permeability K^{PS} correlated significantly ($P < 0.05$) with the histologic grade of the experimental breast tumors of varying malignancy for both the USPIO ($r = 0.36$) and the reference macromolecule albumin-(Gd-DTPA)₃₀ ($r = 0.54$). The study concluded that USPIO, a macromolecular particulate MR imaging contrast agent, could be applied successfully to characterize tumor vessels.

In **chapter 7**, the ability of dynamic MRI enhanced with two macromolecular contrast media, USPIO and albumin-(Gd-DTPA)₃₀, to monitor the effects of an antiangiogenic therapy with a VEGF tyrosine kinase inhibitor was investigated in a human breast cancer xenograft. Control tumors increased significantly ($P < 0.05$) in size and in microvascular permeability K^{PS} based on MRI assays using both macromolecular contrast media. In contrast, tumor growth was significantly reduced ($P < 0.05$) in animals treated with the VEGF receptor tyrosine kinase inhibitor and the K^{PS} values declined slightly ($P > 0.05$ for both contrast agents). Microvascular density counts correlated fairly ($r = 0.64$) with the tumor growth and were statistically significant higher ($P < 0.05$) in the control than in the drug-treated group. MRI measurements of tumor microvascular permeability, using either of two macromolecular contrast media, were able to detect effects of an antiangiogenic therapy.

In **chapter 8**, the utility of six contrast media of different molecular weights for monitoring the microvascular changes caused by an antiangiogenic treatment was investigated. The experimental breast tumors grew significantly ($P < 0.05$) slower in the drug group treated with an anti-VEGF antibody. Mean values for the transendothelial permeability and tumor fractional plasma volume decreased significantly ($P < 0.05$) in the drug-treated group compared to baseline values using intermediate (ZK181220 and Gadomer-17) or macromolecular contrast media (SHU555C and albumin-(Gd-DTPA)₃₀), but did not change significantly using small molecular contrast media (Gd-DTPA and ZK159560). The study showed the potential of dynamic contrast-enhanced MRI to monitor the effects of an antiangiogenic treatment on tumor microvessels. Intermediate-sized contrast agents with a molecular weight of 20-30 kDa also allowed tumor microvessel characterization in a fashion similar to that in larger macromolecules.

In **chapter 9**, a novel protein-binding contrast agent (B22956/1) was compared to a low molecular, clinically available contrast medium (ProHance) and a prototype macromolecular contrast agent, albumin-(Gd-DTPA) for monitoring the tumor response to antiangiogenic therapy with an anti-VEGF antibody. The transendothelial permeability of tumor microvessels K^{PS} determined for B22956/1 decreased significantly ($P < 0.05$) in the animal group treated with the angiogenesis inhibitor compared to baseline, and progressed significantly ($P < 0.05$) in the control group. However, no significant changes were distinguished using either the low- or macromolecular contrast agent. Data from this study indicate that dynamic MRI enhanced with B22956/1 can successfully monitor the effects of antiangiogenesis treatment with anti-VEGF antibody.

In **chapter 10**, the role of DCE-MRI enhanced with the prototype macromolecular contrast agent albumin-(Gd-DTPA)₄₅ in monitoring the microvascular changes associated with isolated limb perfusion was investigated in an experimental soft-tissue sarcoma. Transendo-

thelial permeability K^{PS} and fractional plasma volume of the tumors decreased significantly ($P < 0.05$) in the drug-treated (TNF- α /melphalan) group compared to baseline. In addition, K^{PS} post therapy was significantly lower ($P < 0.05$) in the drug-treated group than in the control group. The study demonstrated that tumor microvascular changes in response to isolated limb perfusion could be determined after 24 hours by DCE-MRI.

Conclusion

The use of dynamic MRI enhanced with macromolecular media has the potential to improve the differentiation between benign and malignant tumors and to allow the non-invasive grading of tumors.

The studies included in the first part of this thesis suggest that the specificity of MR contrast agents for the definition and measurement of abnormal vascular permeability of tumor tissue increases with the molecular weight of the contrast agent. The permeability of tumor microvessels to contrast agents is influenced by the morphology of the vessel wall and the size of the applied contrast medium. Thus when evaluating the microvascular permeability to a specific contrast agent, the size of the MR contrast agent must be taken into account. If a contrast agent is too small (< 1 kDa), like the widely used and well-tolerated extracellular contrast agents represented by gadopentetate dimeglumine, differentiation based on contrast-enhancement properties between benign and malignant tissue is difficult. Contrast agents with a higher molecular weight that remain in the blood vessels for a longer time can improve the assessment of permeability, but they are still in preclinical evaluation or in clinical trials and are not currently approved for human use.

The immediate challenge is to identify a macromolecular contrast agent that might be suitable for clinical development and that shows promise in animal studies for tumor characterization. Some of the requirements that need to be met in the design of the contrast medium include:

1. The molecular weight of the contrast agent should be sufficiently high that the contrast agent does not extravasate across the normal microvascular endothelial barriers, but it should diffuse across the distorted endothelium of tumor micro vessels.
2. The size of the contrast agent should be tolerated in humans.
3. The interaction of the contrast agent with the tissue should be minimal.
4. The contrast agent should be stable *in vivo*.
5. The contrast agent should be completely cleared from the body.

Dynamic MRI enhanced with macromolecular contrast media MRI is a promising technique for evaluating the therapeutic response to antiangiogenic drugs. The studies included in the second part of this thesis indicate that the effects of antiangiogenesis treatment could be monitored by MRI enhanced with: (1) contrast agents with high molecular weight like USPIO and albumin-(Gd-DTPA)₃₀; (2) contrast media with intermediate molecular weight (ZK181220 and Gadomer-17); and (3) contrast agents with low molecular weight that bind reversibly to plasma proteins (B22956/1). In the future, DCE-MRI-based imaging assessments of angiogenesis could have widespread clinical applications. DCE-MRI might

objectify the effects of an antiangiogenic treatment, possibly even before morphological changes, such as reduction in tumor size, become apparent.

The anticipated availability of clinically approved macromolecular contrast agents and the technological advances in the area of MRI systems, imaging techniques and pharmacokinetic modeling are expected to improve the characterization of tumors and the non-invasive evaluation of therapy effects in clinical practice.

Dynamische magnetische resonantie (MR) tomografie met intraveneus contrast biedt de mogelijkheid voor kwantitatieve evaluatie van de fysiologische eigenschappen van tumorweefsel. MR tomografie maakt de niet-invasieve beoordeling van de anatomie en de functie van microbloedvaten in tumoren mogelijk. Ook kan de techniek bijdragen aan het onderscheiden van maligne en normale bloedvaten. Dit proefschrift evalueert de rol van de dynamische MR tomografie met macromoleculaire contrastmiddelen, in de karakterisering van tumor microbloedvaten en in het monitoren van de anti-angiogenese behandeling.

Hoofdstuk 1 is de algemene inleiding op het proefschrift.

Hoofdstuk 2 geeft een overzicht van de gangbare toepassingen en beperkingen van macromoleculaire contrastmiddelen voor kwantitatieve karakterisering van microbloedvaten in tumoren middels MR tomografie. Dit overzicht is gebaseerd op dierproeven en klinische studies, zowel met als zonder medicamenteuze behandeling.

Hoofdstuk 3 presenteert een meta-analyse van kwantitatieve karakterisering van mammatumor studies door middel van MR tomografie. Hieruit blijkt dat berekening van de permeabiliteitwaarden van de vaatwand op basis van MR data van een *region of interest* (ROI) in de periferie van de tumor, beter correleert met de histologische gradering ($r=0.784, P<0.001$), dan de permeabiliteitwaarden gebaseerd op een ROI in de gehele tumor ($r=0.604$). Deze resultaten suggereren dat toekomstige pogingen om tumoren te graderen op basis van MR beelden zich zouden moeten richten op ROI's in de periferie van de tumor, tenminste als een belangrijke component van een meer complete analyse.

In **hoofdstuk 4** worden de toepassingen onderzocht van een nieuw *bloodpool* contrastmiddel met een snelle eliminatie (P792) voor de beoordeling van de eigenschappen van microbloedvaten. Dit contrastmiddel werd gebruikt in een knaagdier mammatumor en werd vergeleken met het prototype macromoleculaire contrastmiddel albumine-(Gd-DTPA)₃₀. Uit analyse van MR beelden na toediening van P792 bleek geen significante correlatie te bestaan tussen enerzijds de histologische graad van de tumor en de permeabiliteit van de vaatwanden en anderzijds het fractionele plasmavolume van het tumorweefsel, of de microvasculaire dichtheid ($P>0.05$).

Een significante correlatie ($r=0.55, P<0.001$) tussen vaatwand permeabiliteit en de histologische graad van de tumor en de microvasculaire dichtheid ($r=0.34, P<0.05$) werd wel gevonden na toediening van albumine-(Gd-DTPA)₃₀. Deze resultaten suggereren dat contrastmiddelen met een relatief hoog moleculair gewicht (circa 90 kDa), zoals albumine-(Gd-DTPA)₃₀, accurater zijn voor de typering van microbloedvaten in een tumor.

Hoofdstuk 5 beschrijft een onderzoek naar de bruikbaarheid voor tumorkarakterisering van carboxymethyldextran-A2-Gd-DOTA, een *blood pool* contrastmiddel met een trage uitscheiding. Dit middel werd toegepast in een knaagdier mammatumormodel met verschillende maligniteitsgraden. Er werd geen significante correlatie gevonden tussen de MR-gebaseerde permeabiliteit van de vaatwand ($r=0.09$, $P>0.05$), of het plasmavolume van het tumorweefsel en de histologische graad van de tumor ($r=0.19$, $P>0.05$). Het differentiëren tussen maligne en benigne tumoren blijkt daarom niet goed mogelijk op basis van MR data, verkregen na toediening van carboxymethyldextran-A2-Gd-DOTA.

De potentiële toepasbaarheid van ultrasimale superparamagnetische ijzeroxide partikels (USPIO), een macromoleculair contrastmiddel, wordt onderzocht in **hoofdstuk 6**. De permeabiliteit van de vaatwanden berekend op basis van MR beelden na toediening van zowel USPIO ($r=0.36$) als albumine-(Gd-DTPA)₃₀ ($r=0.54$), correleerde significant ($P<0.05$) met de histologische graad van experimentele mammatumoren. De conclusie van deze studie is dat USPIO met succes gebruikt kan worden voor de karakterisering van tumorbloedvaten.

Hoofdstuk 7 beschrijft hoe met behulp van MR beelden de effecten van een anti-angiogenese behandeling met een VEGF tyrosine kinase inhibitor kunnen worden gevolgd. Deze MR beelden werden verkregen van in knaagdieren geplaatste mammacarcinoom xenografts, na toediening van twee macromoleculaire contrastmiddelen (USPIO en albumine-(Gd-DTPA)₃₀). De tumoren behandeld met VEGF tyrosine kinase inhibitor groeiden significant minder ($P<0.05$) dan de onbehandelde tumoren. De vaatwand permeabiliteitswaarden op basis van MR beelden na toediening van zowel USPIO als albumine-(Gd-DTPA)₃₀, steeg significant in de controlegroep ($P<0.05$). In tegenstelling tot de controletumoren, was de tumorgroei significant lager ($P<0.05$) na behandeling met VEGF tyrosine kinase inhibitor. De permeabiliteitswaarden daalden minder uitgesproken ($P>0.05$) bij beide contrastmiddelen. De microvasculaire dichtheid, die vrij goed correleerde met de tumorgroei ($r=0.64$), was statistisch significant ($P<0.05$) hoger in de controlegroep dan in de behandelde groep. De effecten van een anti-angiogenese behandeling kunnen worden vastgesteld met behulp van microvasculaire permeabiliteitsmetingen, na de toediening van twee macromoleculaire contrastmiddelen.

In **hoofdstuk 8** wordt de toepasbaarheid onderzocht van zes contrastmiddelen van laag, intermediair en hoog moleculair gewicht, voor het vervolgen van microvasculaire veranderingen tijdens anti-angiogenese behandeling. De experimentele mammatumoren groeiden significant ($P<0.05$) langzamer in de proefdieren behandeld met een anti-VEGF antilichaam. Na toediening van contrastmiddelen met een hoog (SHU555C and albumine-(Gd-DTPA)₃₀) of intermediair (ZK181220 en Gadomer-17) moleculair gewicht daalden de gemiddelde waarden van de permeabiliteit van de vaatwanden en het fractionele plasmavolume van de tumoren significant ($P<0.05$) in de behandelde groep. De waarden daalden niet significant na toediening van contrastmiddelen met een laag moleculair gewicht (Gd-DTPA en ZK159560). Deze studie toont aan dat de effecten van een anti-angiogenese behandeling van de tumor microbloedvaten kunnen worden gevolgd met dynamische MR tomografie. Contrastmiddelen met een intermediair moleculair gewicht van 20-30 kDa kunnen op een vergelijkbare manier worden toegepast bij de typering van tumor microbloedvaten als contrastmiddelen met een hoger moleculair gewicht.

In **hoofdstuk 9** worden verschillende contrastmiddelen vergeleken voor het vervolgen van het effect van anti-VEGF antilichaam behandeling op tumoren. Het gaat hier om een nieuw contrastmiddel met eiwitbinding (B22956/1), een laagmoleculair, klinisch verkrijgbaar contrastmiddel (ProHance) en een prototype macromoleculair contrastmiddel, albumine-(Gd-DTPA). De permeabiliteit van microbloedvaten bepaald voor B22956/1 daalde significant ($P < 0.05$) in de groep behandeld met de anti-VEGF en steeg significant ($P < 0.05$) in de controlegroep. Er konden echter geen significante veranderingen vastgesteld worden op basis van MR beelden na toediening van een laagmoleculair of hoogmoleculair contrastmiddel. Dit onderzoek suggereert dat de effecten van de anti-angiogenese behandeling met succes kunnen worden gevolgd met MR tomografie na toediening van B22956/1.

Hoofdstuk 10 beschrijft hoe dynamische MR tomografie met toediening van het prototype macromoleculair contrastmiddel albumine-(Gd-DTPA)₄₅ kan worden ingezet in het volgen van microvasculaire veranderingen, geassocieerd met geïsoleerde extremiteitperfusie. Hierbij wordt gebruik gemaakt van een experimenteel model van het weke delen sarcoom.

De permeabiliteit van de vaatwand en het fractionele plasmavolume van deze tumoren daalde significant ($P < 0.05$) in de groep proefdieren behandeld met TNF- α /melphalan. De permeabiliteitwaarden waren na de behandeling significant lager in de behandelde groep ($P < 0.05$) dan in de controlegroep. Dit onderzoek toont aan dat de microvasculaire veranderingen als gevolg van geïsoleerde extremiteitperfusie binnen 24 uur na het starten van de behandeling kunnen worden vastgesteld door middel van dynamisch MR tomografie met albumine-(Gd-DTPA)₄₅.

Conclusie

Met behulp van dynamische magnetische resonantie tomografie met macromoleculaire contrastmiddelen is het mogelijk een beter onderscheid te maken tussen maligne en benigne tumoren, door microbloedvaten van tumoren te typeren. Het gebruik van deze methode biedt tevens mogelijkheden voor niet-invasieve gradering van de tumoren.

De onderzoeken die beschreven zijn in het eerste gedeelte van dit proefschrift geven aan dat contrastmiddelen specifiek zijn voor het definiëren en meten van de abnormale vasculaire permeabiliteit van het tumorweefsel, naarmate het moleculair gewicht van het contrastmiddel stijgt. De permeabiliteit van tumor microbloedvaten voor contrastmiddelen wordt onder meer bepaald door de morfologie van de vaatwand en het moleculaire gewicht van het toegepaste contrastmiddel. Concluderend moet bij de evaluatie van tumor microbloedvaten middels MR tomografie rekening gehouden worden met het moleculaire gewicht van het contrastmiddel. Als het contrastmiddel een laag moleculair gewicht heeft (< 1 kDa), zoals de breed toegepaste extracellulaire contrastmiddelen, waaronder gadopentetate dimeglumine, kan het onderscheid tussen benigne en maligne weefsel problematisch zijn. Contrastmiddelen met een hoger moleculair gewicht blijven langer endovasculair en kunnen de evaluatie van de permeabiliteit van de vaatwand verbeteren. Deze middelen bevinden zich echter nog in het stadium van preklinische, of klinische studies en hun gebruik is op dit moment niet toegestaan voor reguliere patiëntenzorg.

De uitdaging is het identificeren van een contrastmiddel dat geschikt is voor verdere klinische ontwikkeling en dat goede resultaten laat zien bij het typeren van tumoren in dierproeven. Het contrastmiddel zou moeten voldoen aan de volgende voorwaarden:

1. Het contrast middel moet een moleculair gewicht hebben dat zodanig hoog is dat het contrastmiddel niet door het endotheel van normale bloedvaten kan passeren, maar lekt door het beschadigde endotheel van tumorbloedvaten;
2. Het moet goed verdragen worden door het menselijk lichaam;
3. Het middel heeft een minimale interactie met het weefsel;
4. Het is stabiel in vivo;
5. Het wordt volledig uitgescheiden.

Dynamische MR tomografie met macromoleculaire contrastmiddelen is eveneens een veelbelovende techniek voor het volgen van de respons op behandeling met anti-angiogenese medicatie. De onderzoeken die in het tweede gedeelte van dit proefschrift aan de orde komen laten zien dat de volgende contrastmiddelen daartoe geschikt zijn: (1) hoogmoleculaire contrastmiddelen zoals USPIO and albumine-(Gd-DTPA)₃₀; (2) contrastmiddelen met een intermediair moleculair gewicht zoals ZK181220 and Gadomer-17; en (3) laagmoleculaire contrastmiddelen met reversibele eiwitbinding zoals B22956/1. In de toekomst zou de evaluatie van angiogenese met behulp van dynamische MR tomografie met gebruik van contrastmiddel uitgebreide klinische toepassingen kunnen hebben. Dynamisch MR onderzoek zou de effecten van anti-angiogenese behandeling kunnen objectiveren, zelfs voordat een afname in de tumorafmetingen vastgesteld kan worden.

De verwachting is dat de typering van tumoren en de niet-invasieve evaluatie van de behandeling verder zal verbeteren door het beschikbaar komen van macromoleculaire contrastmiddelen voor gebruik in patiënten en door de technische vooruitgang op het gebied van MR tomografiesystemen, afbeeldingstechnieken en farmacologische modellen.

CURRICULUM

VITAE

Anda Huurman-Preda was born on September 30th, 1967, in Bucharest, Romania. She attended high school at the Nicolae Balcescu Lyceum in Bucharest and studied medicine at the Carol Davila Medical University in Bucharest (1986-1992). She obtained the Dutch medical board certification at the medical faculty of the University of Utrecht (1993-1995). Between 1995 and 1998 she worked as a resident at the department of Gynecology of St. Elizabeth Hospital in Amersfoort, St. Elizabeth Hospital in Tilburg, Bronovo Hospital in the Hague and Vrije Universiteit Hospital in Amsterdam. In October 1998 she started her residency in radiology at the Erasmus MC-University Medical Center Rotterdam. Between September 1999 and March 2001 she was a visiting research fellow at the Center for Pharmaceutical and Molecular Imaging (director Prof. R.C. Brasch) at the University of California in San Francisco (UCSF). After the fellowship at the UCSF she continued her Ph.D. research and residency at the Erasmus MC-University Medical Center Rotterdam.

PUBLICATIONS

Preda A, Novikov V, Möglich M, Turetschek K, Shames DM, Brasch RC, Cavagna FM, Roberts TPL. MRI monitoring of Avastin™ antiangiogenesis therapy using B22956/1, a new blood pool contrast agent, in an experimental model of human cancer. *J Magn Reson Imaging* 2004;20:865-873.

Preda A, Wielopolski PA, ten Hagen TLM, van Vliet M, Veenland JF, Ambagtsheer G, van Tiel ST, Vogel MW, Eggermont AMM, Krestin GP, van Dijke CF. Dynamic contrast-enhanced MRI using macromolecular contrast media for monitoring the response to isolated limb perfusion in experimental soft-tissue sarcomas. *MAGMA* 2004; 17:296-302.

Preda A, Turetschek K, Daldrup H, Floyd E, Novikov V, Shames DM, Roberts TPL, Carter WO, Brasch RC. The choice of region of interest measures in contrast-enhanced MRI characterization of experimental breast tumors. *Invest Radiol* 2005; 40:349-354.

Preda A, Novikov V, Möglich M, Floyd E, Turetschek K, Shames DM, Roberts TPL, Corot C, Carter WO, Brasch RC. MR characterization of tumor microvessels in experimental breast tumors using a slow clearance blood pool agent (carboxymethyldextran-A2-Gd-DOTA) with histopathologic correlation (*European Radiology*, in press).

Turetschek K, **Preda A**, Novikov V, Brasch RC, Weinmann HJ, Wunderbaldinger P, Roberts TPL. Tumor microvascular changes in antiangiogenic treatment: assessment by magnetic resonance contrast media of different molecular weights. *J Magn Reson Imaging* 2004; 20:138-144.

Turetschek K, **Preda A**, Floyd E, Shames DM, Novikov V, Roberts TPL, Wood JW, Fu Y, Carter WO, Brasch RC. MRI monitoring of tumor response following angiogenesis inhibition in an experimental human breast cancer model. *Eur J Nucl Med* 2003;30:448-455.

Turetschek K, **Preda A**, Floyd E, Shames DM, Novikov V, Roberts TPL, Wood JW, Fu Y, Carter WO, Brasch RC. MRI monitoring of tumor response to a novel VEGF tyrosine kinase inhibitor in an experimental breast cancer model. *Acad Radiol* 2002;9 (Suppl 2):S519-520.

Roberts TPL, Turetschek K, **Preda A**, Novikov V, Moeglich M, Shames DM, Brasch RC, Weinmann HJ. Tumor microvascular changes to anti-angiogenic treatment assessed by MR contrast media of different molecular weights. *Acad Radiol* 2002;9 (Suppl 2):S511-S513.

Turetschek K, Roberts TPL, Floyd E, **Preda A**, Novikov V, Shames DM, Carter WO, Brasch RC. Tumor microvascular characterization using ultrasmall superparamagnetic iron oxide particles (USPIO) in an experimental breast cancer model. *J Magn Reson Imaging* 2001;13:882-888.

Turetschek K, Floyd E, Shames DM, Roberts TPL, **Preda A**, Novikov V, Corot C, Carter WO, Brasch RC. Assessment of a rapid clearance blood pool MR contrast medium (P792) for assays of microvascular characteristics in experimental breast tumors with correlations to histopathology. *Magn Reson Med* 2001;45:880-886.

Preda A, Van Dijk LC, van Oostaijen JA, Pattynama PMT. Complication rate and diagnostic yield of 515 consecutive ultrasound-guided biopsies of renal allografts and native kidneys using a 14-gauge Biopsy gun. *Eur Radiol* 2003;13:527-530.

Presentations

Preda A, Roberts TP, Turetschek K, Novikov V, Möglich, Shames DM, Brasch RC, Cavagna FM. Permeability of B22956/1, a novel protein-binding contrast agent, resolves antiangiogenic therapy in human breast cancer. *ESMRMB, 19th Annual Scientific Meeting, Cannes, France, August 22-25, 2002.*

Preda A, Wielopolski PA, Ten Hagen TM, Van Dijke CF, Krestin GP, Eggermont AMM. High-resolution contrast-enhanced MRI for monitoring anti-tumor therapy by isolated limb perfusion in human and experimental sarcomas. *88th Scientific Assembly and Annual Meeting of the Radiological Society of North America (RSNA), December 1-6, 2002, Chicago, USA. (Certificate of Excellence in Design for Education Exhibit).*

Preda A, Wielopolski PA, Van Dijke CF, Ten Hagen TM, Krestin GP, Eggermont AMM. Pre- and post therapeutic MR angiography of tumor blood vessels in an experimental sarcoma model. *88th Scientific Assembly and Annual Meeting of the Radiological Society of North America (RSNA), December 1-6, 2002, Chicago, USA.*

ACKNOWLEDGEMENTS

Prof. Dr. R.C. Brasch: Dear Bob, in your letter from April 1999 you wrote me: “I hope that your time in San Francisco will be among the most pleasant, useful and memorable periods of your life.” You were so right; I really had the time of my life! Working in your worldwide renowned research laboratory was wonderful and inspiring. Thank you and your wife Mimi for your kindness, hospitality and support during my fellowship and for all the memorable days I have spent in this most beautiful city.

Prof. Dr. G.P. Krestin: Thank you for giving me the opportunity to work on this research project in San Francisco and for creating the scientific environment to continue it in Rotterdam. Thank you for your confidence.

Dr. C.F. Van Dijke: Beste Kees, bedankt voor al je steun, adviezen en begeleiding van het Rotterdamse gedeelte van dit promotieonderzoek.

Dr. K. Turetschek: Dear Karli, from teaching me how to catch and anaesthetise a rat to letting me and Ruud live in your beautiful apartment during the Christmas holiday, you were such a great friend for me. Thank you for all the nice moments we spent in Bob’s laboratory and, not to be forgotten, in Napa Valley and Lake Tahoe!

Dr. V. Novikov: Dear Viktor, it was great working with you! Your humor, kindness, patience, dedication and computer skills were so important for this research. Thank you for everything.

Dr. D.M. Shames: Dear David, thank you for all your high quality work in the kinetic analysis of the MR data. Thank you also for the great moments spent on your yacht on the San Francisco Bay. We have enjoyed it so much!

Dr. T.P.L. Roberts: Dear Tim, your profound understanding of the MR physics, your ability in designing new pulse sequences and rapidly solving all our imaging problems do not cease to amaze me. Thank you for entrusting me with the research project of B22956/1 and for all your help in completing it.

Cherie Pinsky: Dear Cherie, thank you for all your help with the organization of these research projects, but above all, for all your kindness and the enthusiasm in guiding me in the fascinating world of San Francisco.

Dr. M. Möglich: Dear Martina, your enthusiasm, dedication and humor made working with you a real pleasure. Thank you for your scientific input in several projects.

Dr. M. Wendland: Dear Mike, thank you for many enlightening discussions on MR physics.

Marion van Vliet: Beste Marion, ik ben je veel dank verschuldigd voor je tomeloze inzet voor dit onderzoek, van het imagen van de ratten tot het insturen van artikelen. Je harde werk, behulpzaamheid, optimisme en altijd goede stemming waardeert ik zeer.

Dr. J.F. Veenland: Beste Jifke, heel veel dank voor je waardevolle en onmisbare bijdrage in de kinetische analyse van het ILP project.

Dr. P. Wielopolski: Dear Piotr, thank you for all the hours you spent designing the pulse sequence for the isolated limb perfusion project and imaging the animals.

Gisela Ambagtsheer en Sandra van Tiel, bedankt voor jullie minutieuze werk voor het ILP project en voor alle hulp bij de MRI experimenten.

Dr. T.M.L. ten Hagen: Beste Timo, veel dank voor de prettige samenwerking met je onderzoeksteam van de afdeling Experimentele Chirurgische Oncologie.

Dirk Verver, met veel geduld en professionaliteit heb jij vorm gegeven aan dit proefschrift. Dank je!

Karin ten Wolde, bedankt voor je hulp met het fotografische werk en met het vormgeven van de omslag van dit proefschrift.

Adriaan Moelker, wat een verlies voor de IT dat je radioloog wordt! Bedankt voor je geduld en steun, iedere keer dat ik je om hulp kwam vragen met mijn computerperikelen. En wees gerust, dit zal ik in de toekomst nog blijven doen!

Collega's van de Experimentele Radiologie, **Mika Vogel, Marc Kock, Thomas de Weert en Mohamed Ouhlous,** bedankt voor de gezelligheid en voor jullie hulp met computerzaken!

Andries Zwamborn en Teun Rijdsdijk, bedankt voor de leuke tijd op de afdeling Experimentele Radiologie, voor jullie adviezen en steun in al deze jaren.

Arie en Corrie Huurman, de liefste schoonouders van de wereld, bedankt voor alle goede zorg en voor de vele dagen dat jullie op Elvira en Alex hebben gepast, zodat ik weer aan het onderzoek kon werken.

Draga **mama si tata,** fara dragostea voastra si educatia primita de la voi nimic nu ar fi fost posibil. Draga **tata,** ce rau imi pare ca nu esti azi cu mine!

Draga **Alexandru,** in sfirsit am reusit, multumesc pentru incredere si incurajari!

Elvira si Alex, de acum mama o sa fie mult mai des acasa!

Lieve **Ruud,** voor je onvoorwaardelijke liefde zal ik je nooit kunnen bedanken. Dit proefschrift, vanaf het boeken van tickets voor San Francisco tot de laatste pagina, was zonder jouw steun nooit tot stand gekomen. "No matter where you go, there you are!"